A review of theories of the L-H transition

2000 Plasma Phys. Control. Fusion 42 R1

(http://iopscience.iop.org/0741-3335/42/1/201)

Plasma Phys. Control. Fusion **42** (2000) R1–R74. Printed in the UK PII: S0741-3335(00)07020-2

REVIEW ARTICLE

A review of theories of the L–H transition

J W Connor and H R Wilson

EURATOM/UKAEA Fusion Association, Culham Science Centre, Abingdon, Oxon, OX14 3DB, UK

Received 19 August 1999, in final form 25 October 1999

Abstract. After a general discussion of the experimental characteristics of the L–H transition and consideration of basic theoretical principles underlying models for it, this paper reviews the various theories of the L–H transition available in the literature, providing some background information on each theory and expressing the transition criteria in forms suitable for comparison with experiment. Some conclusions on the relevance of these models for explaining the experimental data on the transition are drawn.

1. Introduction

The fusion capability of tokamaks, such as the proposed International Thermonuclear Experimental Reactor (ITER), will be greatly enhanced if they can access the high confinement operational regime known as the H-mode [1]. Although the H-mode can be realized in a wide variety of toroidal confinement systems, it is most clearly associated with divertor tokamaks possessing a separatrix. The H-mode of confinement is characterized by steep gradients in density, n, and temperature, T, at the plasma edge, figure 1 [2], indicating the presence of an edge transport barrier. This is associated with a drop in fluctuations and the transition from the low confinement regime, or L-mode, is a sharp one, which suggests a bifurcation between two plasma states.

Experimental evidence suggests that this L–H transition requires sufficient heating power, P_{Th}, to be deposited in the tokamak plasma. In general this power threshold appears to increase with density, magnetic field and the size of the tokamak, as represented by the empirical law proposed by the ASDEX team [3].

$$P_{\mathrm{Th}} = 0.04 \bar{n}_{\mathrm{e}} B S \,(\mathrm{MW}, 10^{20}\ \mathrm{m}^{-3}, \mathrm{T}, \mathrm{m}^2). \tag{1.1}$$

Here $\bar{n}_{\mathrm{e}}$ is the line-averaged electron density, B the magnetic field strength and S the plasma surface area. According to this scaling law, ITER as specified in the Final Design Review (ITER FDR) [4, 5], with parameters, $B = 5.7$ T, major radius $R = 8.1$ m, minor radius $a = 2.8$ m and elongation $k = 1.6$, would require ∼250 MW to achieve the H-mode at fusion relevant densities, $\bar{n}_{\mathrm{e}} \simeq 10^{20}\ \mathrm{m}^{-3}$, and it is important to establish confidence in such projections, either by using a multi-machine database to improve the empirical basis or by developing a theoretical foundation. Another issue is that of hysteresis: for example, in ITER it is anticipated that an operational scenario could be to access the H-mode at low density, $n_{\mathrm{e}} \sim 0.5 \times 10^{20}\ \mathrm{m}^{-3}$, where P_{Th} is lower, and then increase the density, relying on the alpha-heating power to be sufficiently strong to maintain the H-mode in the presence of hysteresis in P_{Th}. The robustness of this strategy depends on the experimental observation that approximately twice the power is

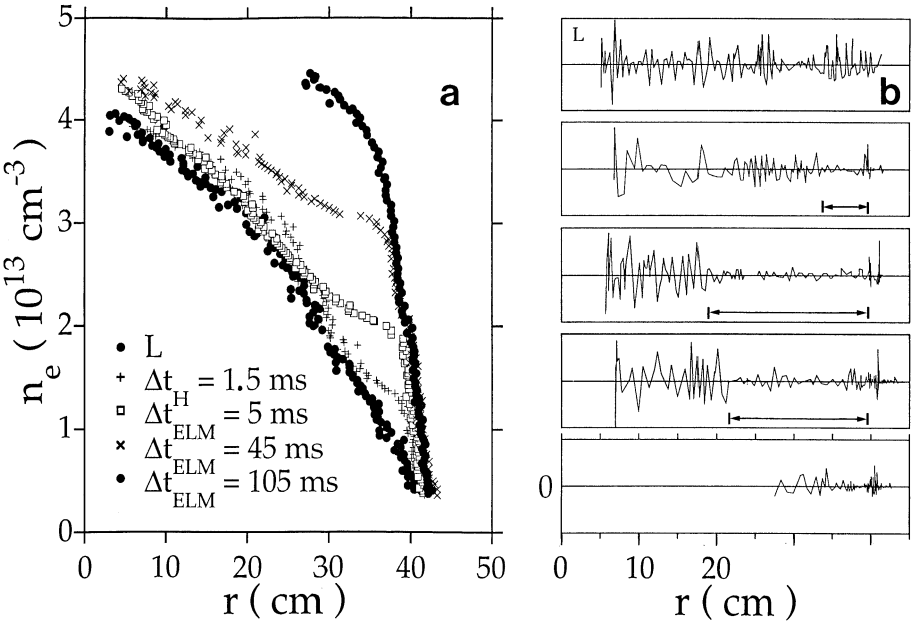

Figure 1. Evolution of density profiles and fluctuations following the L–H transition in ASDEX [2]: (a) development of edge density profiles (from reflectometry) from the L-mode phase, 0.5 ms after the transition and then in a quiescent phase which developed after an ELMy phase; (b) radial variation of edge fluctuations for the same time points.

needed to access the H-mode than is needed to remain there [6]. Recent observations on JET [7] and at high density in ASDEX Upgrade [8], for example, have cast doubt on the extent and universality of this hysteresis in $P_{\rm Th}$; however, a unified picture of such apparently different results has been proposed in a study of data from JET and DIII-D [9]. Another feature of the L–H transition is that it requires a lower value of $P_{\rm Th}$ when the magnetic field configuration is such that the ion-∇B drift direction is towards a single null formed by the divertor geometry, rather than away from it. This, and many other, experimental features of the H-mode are described in [10]. Theoretical understanding could shed light on all these issues.

Wagner [11] gave a simple argument for the result (1.1) which provides an illustrative example of the ingredients of L–H transition theories. He assumed the transition occurs when the ion diamagnetic velocity $V_{*\rm i} = -(1/neB)\,{\rm d}p_{\rm i}/{\rm d}r$ achieves a critical value, $V_{\rm crit}$. Expressing the pressure gradient length in terms of the power flux, using a thermal conduction equation at the plasma edge, yields

$$P_{\rm Th} = \frac{c}{2} e\chi \bar{n}_{\rm e} BSV_{\rm crit} \tag{1.2}$$

where c is a fitting parameter. If one sets the thermal diffusivity $\chi \simeq 1$ m^2 s^{-1} and takes $V_{\rm crit} \simeq 2\times 10^4$ m s^{-1} from the measured electron pressure gradient at the transition in ASDEX, then choosing $c = 0.27$ recovers the ASDEX law (1.1). However, it remains to explain $V_{\rm crit}$ and χ. This argument reveals a basic difficulty: even if one understands the criterion for transition, translating it into a power threshold requires a theory for confinement as well. In fact, the observed hysteresis in $P_{\rm Th}$ may merely reflect the fact that the improved confinement in the H-mode means some critical plasma parameter needed for the transition can be achieved with less power. We shall return to this later.

The explanation above relied upon using absolute values for $V_{\rm crit}$ and χ; in reality these quantities should be given by dimensionally correct expressions. If the phenomena responsible for determining the threshold power were pure plasma physics, then we would be able (following Connor and Taylor [12]) to express $P_{\rm Th}$ in the form

$$P_{\rm Th}L^{3/4} \propto (nL^2)^p (BL^{5/4})^q \tag{1.3}$$

where L is a macroscopic length, for example, major radius R. Clearly this is inconsistent with the scaling (1.1): choosing $p = q = 1$ to fit the indices on n and B leads to a size scaling $L^{2.5}$, rather than L^2 as in (1.1).

However, since the H-mode transition is an edge phenomenon it is quite possible that an additional atomic physics parameter is involved, for example, $\ell_n/L \propto 1/nL$ where ℓ_n is a neutral particle penetration length [13]. The involvement of atomic processes means one cannot scale plasma temperature T, as noted by Lackner [14], since characteristic atomic energy levels are introduced. This would generalize the result (1.3) to

$$P_{\rm Th}L^{3/4} \propto (nL^2)^p (BL^{5/4})^q (nL)^r \tag{1.4}$$

so that scaling (1.1) can be recovered by the choice $p = 1/2, q = 1, r = 1/2$. It is interesting to note that Kadomtsev [15] has observed that the scaling law (1.1) can be expressed as

$$\frac{\beta}{\beta_{\rm crit}} \sim \sqrt{M} \tag{1.5}$$

if the L-mode energy confinement time scaling

$$\tau_E \sim \frac{I}{P^{1/2}} Ra^{1/2} \tag{1.6}$$

is used to replace $P_{\rm Th}$ by $\beta = 2\mu_0 nT/B^2$, the ratio of plasma to magnetic energy. Here $\beta_{\rm crit} = gI/aB$ is the Troyon critical β for ideal magnetohydrodynamic (MHD) stability (g is a numerical coefficient $\sim$3), I is the plasma current and $M = nR/B$ is the Murakami number (closely related to the Hugill number $Hu = nRq/B$ which has been associated with atomic physics processes [16]).

Nevertheless, the ITER H-mode database working group has chosen to fit a multi-machine database for the H-mode threshold power with a form which satisfies the constraints of finite-β, collisional plasma physics

$$P_{\rm Th} = (0.45 \pm 0.10) B({\rm T}) \bar{n}_{\rm e_{20}}^{0.75} R({\rm m})^2 (0.6\bar{n}_{\rm e_{20}} R^2({\rm m}))^{\alpha} \tag{1.7}$$

where $|\alpha| \leqslant 0.25$ [17], see figure 2. Examination of figure 2 reveals departures from linearity at low n, where some devices (e.g. COMPASS-D [18, 19]) show that $P_{\rm Th}$ begins to increase as n decreases further. There is also considerable spread of data about the fit and the uncertainties in the exponent α lead to predictions for ITER FDR ranging from 50 to 200 MW, which is unacceptably wide, given that it was planned to have no more than 100 MW available. However, recent results from JET using H, D and T indicate a favourable isotope effect [20]

$$P_{\rm Th} \propto A_{\rm i}^{-1} \tag{1.8}$$

where $A_{\rm i}$ is the atomic mass number of the isotope involved, not included in the scaling (1.7). While this improves the situation for ITER, the uncertainties remain large, demonstrating the need for an improved understanding of the essential physics responsible for the threshold scaling.

In this paper we provide a comprehensive review of theories proposed to explain the H-mode transition, discussing briefly their ability to reproduce not only the scaling of $P_{\rm Th}$, but other key aspects of the experimental observations on this phenomena in order to evaluate their validity. These other observations may be grouped as follows:

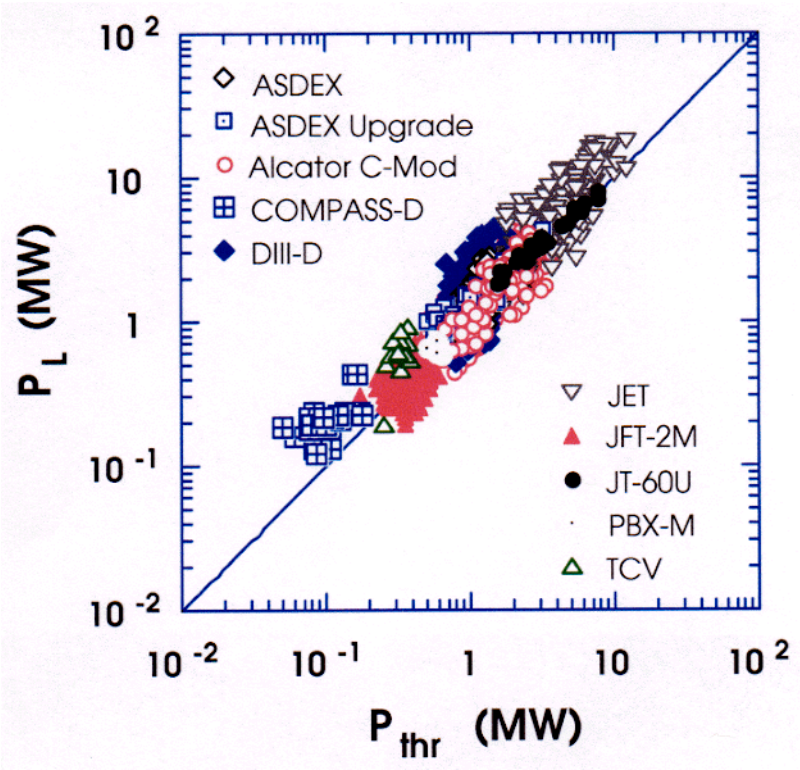

Figure 2. Comparison of experimental data for P_L, the power for the L–H transition, from ten tokamaks to a scaling $P_{\rm Th} = 0.45 B n_{20}^{0.75} R^2$ [17].

(i) *Local edge parameters*. Since the H-mode transition is an edge phenomena one would expect that the condition for it to occur can be expressed in terms of local parameters and scale lengths at the plasma edge, for example, n, T, $L_n = [\mathrm{d}(\ln n)/\mathrm{d}r]^{-1}$, $L_T = [\mathrm{d}(\ln T)/\mathrm{d}r]^{-1}$ etc, evaluated in the vicinity of the outer flux surface, $r = a$. Theoretical models are usually expressed in terms of such quantities, or equivalent dimensionless parameters such as the normalized ion Larmor radius, $\rho_* \equiv \rho_{\rm i}/a$, collisionality $\nu_* \equiv \nu R q / V_{\rm Th} \epsilon^{3/2}$ and β, together with geometrical ratios such as R/L_n, q etc. (Here ρ_j is the Larmor radius $\rho_j = (m_j T_j / e_j^2 B^2)^{1/2}$, ν_j the 90° Coulomb collision frequency, q the safety factor and $V_{{\rm Th}j} = (2T_j/m_j)^{1/2}$ the thermal speed of species j; theoretically, it is sometimes useful to define ρ_* in terms of $\rho_{\rm s}$, the ion Larmor radius evaluated with the electron temperature.) There is indeed evidence that a critical edge electron temperature is involved [8, 21–25]

$$T_{\rm ecrit} \sim B^{\alpha} n^{-\gamma} \qquad 1/2 < \alpha < 2, \quad 0 < \gamma < 2/3 \tag{1.9}$$

(see figure 3 which is from [23], for example). In terms of such local plasma parameters the existence of hysteresis is less obvious [8, 21] (reinforcing the idea that the hysteresis in $P_{\rm Th}$ results from changes in τ_E), but the critical temperature responds to the ion-∇B drift in the same way as $P_{\rm Th}$ [21, 25] and somewhat more weakly to $A_{\rm i}$ [26]. Although these measurements are difficult, their use obviates the need to have a theory of confinement, or edge transport, as well as a transition criterion.

(ii) *Spatial and temporal characteristics*. The H-mode is associated with the creation of an edge transport barrier, typically several centimetres wide. The region over which this exists, particularly how it scales with plasma parameters (e.g., figure 4 which is from JT-60U [27]) is one potential test of theories. The time scales associated with the H-mode transition (usually comprising a fast submillisecond or microsecond onset, followed by a slower evolution on a time scale of 1–10 ms) provide a further test. Another, is the temporal sequence of events occurring at the transition: the creation of steep electric field gradients, suppression of turbulence, steepening of density and temperature profiles at the plasma edge (see figure 1 which is from ASDEX and figure 5 which is from DIII-D [28]); invariably some of these are ingredients of theories to explain the transition. These events can be difficult to untangle experimentally, but their causal relationship helps to identify the mechanism that triggers the H-mode.

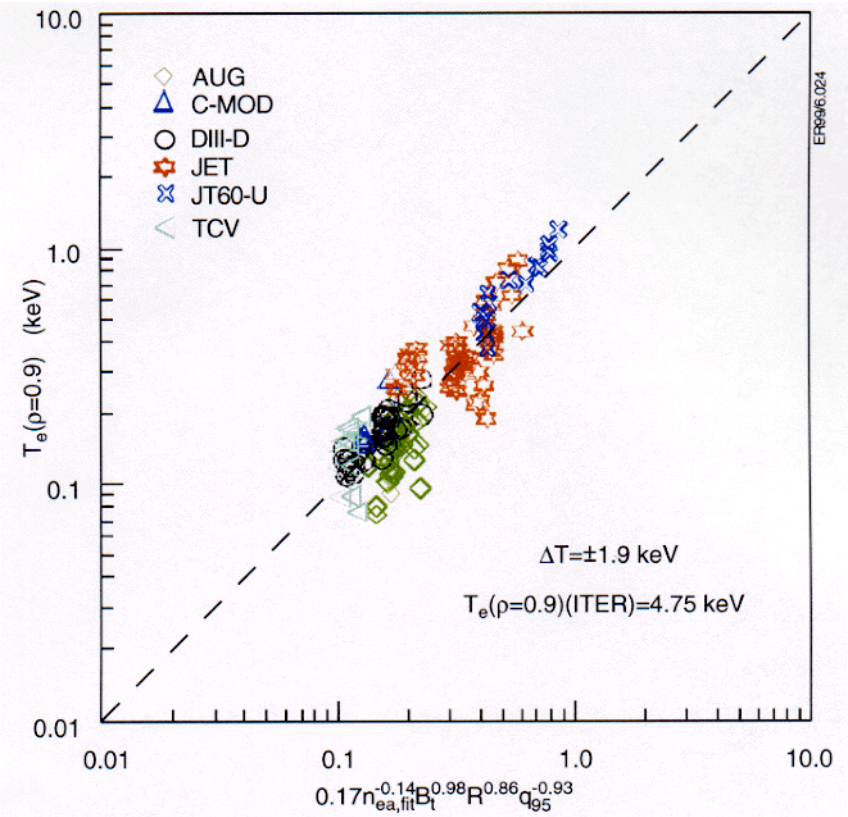

Figure 3. Comparison of experimental data for the edge electron temperature, T_e ($\rho = 0.9$), where $\rho = r/a$, from six tokamaks to a scaling $T_e = 0.17 n_{ea}^{-0.14} B^{0.98} R^{0.86} q_{95}^{-0.93}$ [23].

In section 2 we present some general theoretical tools and concepts that provide a background for theories. These general ideas are:

(i) dimensional analysis [12, 14, 29] which helps to characterize the types of plasma physics involved: collisions; electromagnetic effects, atomic physics, etc. However, this must be discussed in parallel with confinement properties if one wishes to understand the scaling

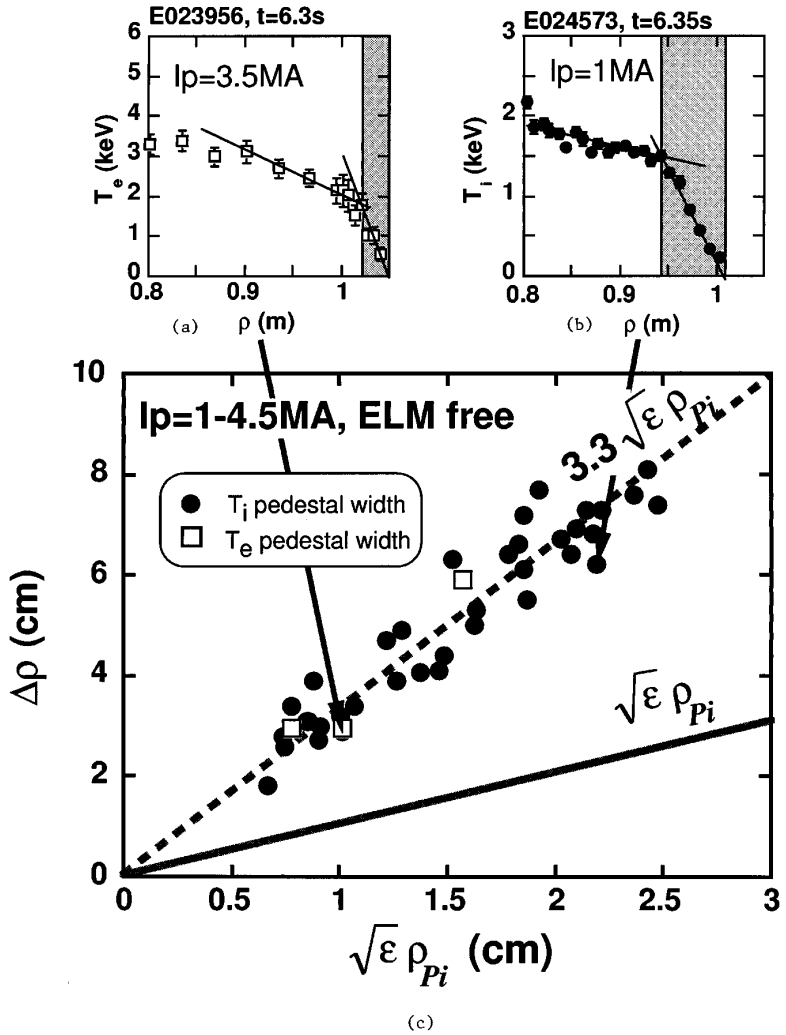

Figure 4. Comparison of experimental data for the pedestal width $\Delta\rho$ from JT-60U to a scaling $\Delta\rho = 3.3\sqrt{\epsilon}\rho_{\rm pi}$ [27]: (a) an example $T_{\rm e}$ profile; (b) an example $T_{\rm i}$ profile; and (c) the scaling for $\Delta\rho$, indicating where data from (a) and (b) lie.

of $P_{\rm Th}$. Therefore we also consider the energy balance at the plasma edge involving cross-field transport into the scrape-off layer (SOL) [30] which provides a link between edge parameters, including gradient lengths, and the power flow from the plasma and helps one to deduce a threshold power;

(ii) the stabilization of instabilities postulated to cause anomalous transport in L-mode, particularly the suppression of turbulent transport by sheared radial electric fields or plasma flows [31–34];

(iii) the mechanisms producing bifurcations in such electric fields and flows, and their consequences for the spatial localization and the temporal evolution of the edge transport barrier [35]; references [36] and [37] provide recent excellent reviews of these topics.

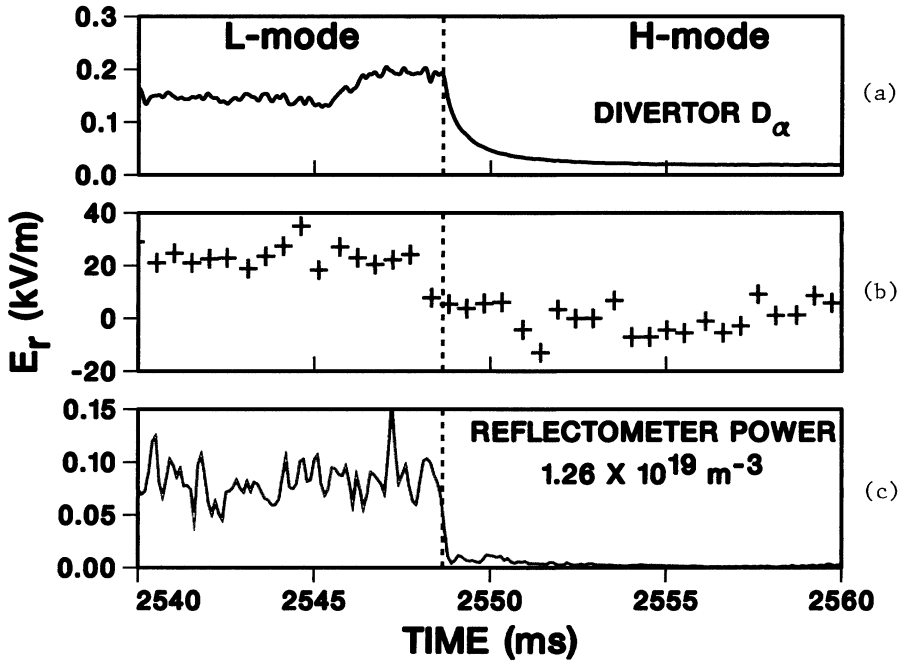

Figure 5. Temporal changes at the L–H transiation in DIII-D [28] showing: (a) the drop in D_α, signifying the transition; (b) the change in E_r; and (c) the associated drop in density fluctuations as measured by a reflectometer.

While the stabilization of some linear instability responsible for transport may be an element of a theory, in itself it is unlikely to account for the rapid changes usually observed at the L–H transition since stability criteria usually depend on parameters that change on a transport time scale (a similar situation prevails for sawtooth crashes [38]). However, linear instabilities may play a role by triggering some nonlinear process that leads to a rapid bifurcation between states of high and low confinement.

These general considerations lead to a classification of the specific theories which are addressed in sections 3–5. They allow us to divide these theories into three basic groups:

(i) in section 3 we consider those that rely on achieving the conditions on plasma parameters for the stabilization of particular instabilities or the suppression of the associated turbulence: these instabilities can be further subdivided into those in the edge of the core plasma (section 3.1A) and those in the SOL (section 3.2B);

(ii) in section 4 we describe those theories that rely on the suppression of turbulent transport by sheared radial electric fields or plasma flow; these are further classified by the physical processes that drive and limit these quantities, as identified in section 2.

(iii) in section 5 we discuss some miscellaneous mechanisms, such as effects arising from divertor action, neoclassical theory and particular transport models, which do not fit into the earlier categories: for example, the role of neoclassical drifts, which relates to the dependence of P_{Th} on the ion-∇B direction [39].

Nevertheless the categorization into these groups is not perfect; elements from one can appear in another.

The results of the various theories are summarized in tables 1 and 2 in a way that is convenient for comparison with experiment: table 1 covers theories leading to a criterion in terms of local edge parameters; table 2 those actually leading to a prediction for $P_{\rm Th}$.

In section 6 we provide an assessment of the extent to which theory provides an explanation of the experimental observations of the L–H transition, identifying the more promising candidates [40–44]. Finally, we draw some brief conclusions in section 7, indicating possible directions for future progress.

2. Theoretical considerations

In this section we discuss a number of general theoretical concepts that underpin many of the more detailed theories in sections 3–5, namely dimensional analysis, power balance at the plasma edge, the shear flow paradigm, radial electric fields and mechanisms for bifurcations.

2.1. A dimensional analysis

In terms of plasma physics variables one would expect to be able to represent the L–H transition condition by a relation of the form

$$\rho_* \propto \beta^x \nu_*^y \tag{2.1}$$

although geometric or compositional factors such as a/R, q, $T_{\rm e}/T_{\rm i}$, $A_{\rm i}$, $Z_{\rm eff}$, ... may also play a role. This can be re-expressed, for example, as a critical (invariant) temperature $T_{\rm crit}L^{1/2}$ [12]

$$T_{\rm crit}L^{1/2} \propto (nL^2)^{y_1}(BL^{5/4})^{y_2} \tag{2.2}$$

where

$$y_1 = 2(x+y)/(1-2x+4y) \tag{2.3}$$
$$y_2 = 2(1-2x)/(1-2x+4y).$$

Unfortunately, interpreting $T_{\rm crit}$ as a threshold power requires an understanding of confinement since

$$P \propto \frac{nTL^3}{\tau_E}. \tag{2.4}$$

Thus, using equations (2.2) and (2.4),

$$P_{\rm Th}L^{3/4} \propto \frac{(nL^2)^{1+y_1}(BL^{5/4})^{1+y_2}}{B\tau_E}. \tag{2.5}$$

Clearly, one cannot deduce y_1 and y_2 (or x and y) from (1.7) without first knowing the form of $B\tau_E$. Now expression (1.7) can be written as

$$P_{\rm Th}L^{3/4} \propto (nL^2)^r(BL^{5/4})^s \qquad r = \tfrac{3}{4} \pm \tfrac{1}{4}, \quad s = 1. \tag{2.6}$$

Then energy balance (2.4) can be used to write the scaling (2.5) as

$$T_{\rm crit}L^{1/2} \propto (nL^2)^{r-1}(BL^{5/4})^{s-1}B\tau_E \tag{2.7}$$

or, in terms of ρ_*, β and ν_*, as

$$\rho_*^{2r+\frac{3}{2}s-\frac{9}{2}}\beta^{-r-\frac{1}{4}s+\frac{7}{4}}\nu_*^{\frac{1}{4}s-\frac{3}{4}} > cB\tau_E. \tag{2.8}$$

With an L-mode energy confinement scaling law [7, 45]

$$B\tau_E \propto \rho_*^{-2}\beta^{-\epsilon}\nu_*^{-\delta} \qquad \epsilon, \delta < \tfrac{1}{4} \tag{2.9}$$

this becomes

$$\rho_*^{2r+\frac{3}{2}s-\frac{5}{2}}\beta^{-r-\frac{1}{4}s+\frac{7}{4}+\epsilon}\nu_*^{\frac{1}{4}s-\frac{3}{4}+\delta} > c'. \tag{2.10}$$

Introducing the specific values of r and s from (2.6), condition (2.10) has the form

$$\rho_*^{\frac{1}{2}\pm\frac{1}{2}}\beta^{\frac{3}{4}+\epsilon\mp\frac{1}{4}}\nu_*^{-\frac{1}{2}+\delta} > c' \tag{2.11}$$

indicating that the physics parameters β, probably ρ_* and possibly ν_* play a role in the transition criterion (2.1), thus suggesting electromagnetic phenomena may be involved. It is interesting to note that the condition (2.11) is compatible with a favourable isotope effect, as in the scaling (1.8). It also suggests that the condition becomes more difficult to meet in larger machines with small ρ_*. Furthermore, we see from (2.8) that maintenance of the H-mode with an H-mode confinement scaling law $\tau_E \propto \rho_*^{-3}$ [46] eventually becomes impossible at small ρ_* [47]. However, the transition criterion may be affected by atomic physics processes, as in (1.4), implying a role for the parameter ℓ_n/L in (2.1).

Perkins [48] has also demonstrated that the form (1.7) is definitely not consistent with a purely electrostatic phenomenon for the L–H transition. To relate a transition condition to a power threshold requires a transport model to be invoked as well, so this could introduce the β dependence. However, if we assume electrostatic gyro-Bohm transport, $\chi \sim \chi_{GB} \propto T^{3/2}/LB^2$, so that

$$\frac{P}{S} \propto \frac{nT^{5/2}}{B^2L^2} \tag{2.12}$$

and a transition which depends on β as in (2.1), then

$$\frac{P}{S} \propto \frac{n}{B^2L^2}[B^{1-2x}L^{y+1}n^{y+x}]^{5/(1-2x+4y)}. \tag{2.13}$$

The experimentally observed linear B dependence requires $x = -3y + 1/2$, so that

$$\frac{P}{S} \propto n^{3/4}B(nL^2)^{(1-3y)/4y} \tag{2.14}$$

implying $1/4 < y < 1/2$ (i.e. $-1 < x < -1/4$) in order to fit (1.7). In terms of dimensionless variables the transition occurs for

$$\rho_* \propto \left(\frac{\nu_*}{\beta^3}\right)^y \beta^{1/2} \tag{2.15}$$

or

$$T_{crit} \propto n^{-2/5}B^{6/5}L^{1/5}(nL^2)^{1/10y}. \tag{2.16}$$

Similar considerations for Bohm transport, $\chi \sim \chi_B \propto T/B$, yield $x = -2y + 1/2$ and

$$\frac{P}{S} \propto n^{3/4}B(nL^2)^{(1-y)/4y} \tag{2.17}$$

implying $1/2 < y$ (i.e. $x < -1/2$). Furthermore,

$$\rho_* \propto \left(\frac{\nu_*}{\beta^2}\right)^y \beta^{1/2} \tag{2.18}$$

or

$$T_{crit} \propto n^{-1/4}BL^{1/4}(nL^2)^{1/8y}. \tag{2.19}$$

Of course, ν_* and β dependences of the transport coefficient could modify these conclusions.

It is interesting to note that [49] has shown a correlation between the invariant threshold power and dimensionless edge parameters (measured at 95% of the poloidal flux)

$$P_{Th}L^{3/4} \propto \rho_*^{-2.3}\beta^{0.65}\nu_*^{-0.3} \tag{2.20}$$

although the edge temperature appearing implicitly on the right-hand side should be expressible in terms of P_{Th}.

2.2. Edge power balance

A more consistent approach to introducing the threshold power is to discuss the criterion (2.1) in terms of edge parameters, using a local edge power balance to determine the radial length scales; these lengths can be related to the SOL width, $\Delta_{\rm SOL}$. Thus one first relates the outflow of power into the SOL to a local model for the heat flux across the magnetic field, $q_\perp$, at the plasma edge

$$P \propto aRnq_\perp \sim aRn\chi_\perp T/\Delta_{\rm SOL} \tag{2.21}$$

where the edge temperature gradient length is given, assuming continuity between the core and SOL, by $\Delta_{\rm SOL}$. The power into the SOL must be transported along the field lines to the divertor plates

$$P \sim \frac{q_\parallel \Delta_{\rm SOL} a}{q} \tag{2.22}$$

where $q_\parallel$ is the heat flux parallel to the magnetic field and we take the length to the divertor plates to be proportional to the connection length, Rq. We require some knowledge about the perpendicular and parallel heat transport in the SOL [50]: for definiteness, we provide estimates when the perpendicular transport is either Bohm or gyro-Bohm and when the parallel transport is either dominated by collisional diffusion or by flow at the sound speed $C_{\rm s} = \sqrt{T_{\rm e}/m_{\rm i}}$. Balancing perpendicular and parallel heat flows in the SOL, i.e. neglecting energy sinks such as radiation, provides an expression for $\Delta_{\rm SOL}$

$$\Delta_{\rm SOL} \sim \left(\frac{nT\chi_\perp Rq}{q_\parallel}\right)^{1/2}. \tag{2.23}$$

Taking Bohm perpendicular transport, $\chi_\perp \sim T/B$, and collisional parallel transport, $q_\parallel \sim \chi_\parallel nT/Rq$ with $\chi_\parallel \propto T^{5/2}/n$, we obtain

$$P \propto \frac{n^{1/2}RI}{aB^{3/2}}T^{11/4} \tag{2.24}$$

while for flow at $C_{\rm s}$, $q_\parallel \propto nT^{3/2}$,

$$P \propto \frac{nRI^{1/2}T^{7/4}}{B}. \tag{2.25}$$

In the gyro-Bohm case we assume the transport is driven by gradients on the scale $\Delta_{\rm SOL}$: $\chi_\perp \propto T^{3/2}/B^2\Delta_{\rm SOL}$. Thus for collisional parallel transport

$$P \propto \frac{n^{1/3}RI^{4/3}T^{19/6}}{a^{5/3}B^2} \tag{2.26}$$

and for flow at $C_{\rm s}$

$$P \propto \frac{nRI^{2/3}T^{11/6}}{a^{1/3}B^{4/3}}. \tag{2.27}$$

More complex dependences of $\chi_\perp$ on β and ν_* would lead to different scalings.

It should be emphasized that the parameter $T_{\rm e}/T_{\rm i}$ can modify the results for $P_{\rm Th}$ if transport scalings in electron and ion channels differ significantly [51].

2.3. The shear flow paradigm

A leading generic paradigm for reducing turbulent transport in the H-mode transport barrier is based on sheared radial electric fields: either due to stabilization of linear modes (an example of an early reference is [52]) or through a reduction of turbulence amplitudes, correlation

lengths or a change in phases between the fluctuations responsible for the turbulent transport fluxes. However, it should be noted that while shear flow tends to be a stabilizing mechanism in linear theory, the effect of the curvature of the flow depends on its sign and it may be difficult to correlate experimental flow profiles with stability [53]. There is experimental evidence, particularly from DIII-D [54], that steep gradients in the radial electric field are generated at the L–H transition (figure 6). Hassam [33] has shown that a number of drift-wave instabilities can be stabilized when

$$V'_{\mathrm{E}} > \frac{C_{\mathrm{s}}}{R} \tag{2.28}$$

where V'_{E} denotes the radial derivative of the equilibrium $\boldsymbol{E} \times \boldsymbol{B}$ velocity, V_{E}. Biglari *et al* [34] investigated the effect of sheared rotation on turbulence, finding that in the limit $\omega_{\mathrm{s}} > \omega_{\mathrm{t}}$ (where $\omega_{\mathrm{s}} = k_\theta \Delta r V'_{\mathrm{E}}$, with Δr the radial correlation length and k_θ a characteristic poloidal wavenumber of the turbulence, and $\omega_t = 4D/(\Delta r)^2$ is the diffusive scattering rate of the turbulence, with D the turbulent diffusivity), Δr is reduced by a factor $(\omega_{\mathrm{t}}/\omega_{\mathrm{s}})^{1/3}$. Thus the turbulent eddies are torn apart by the differing $\boldsymbol{E} \times \boldsymbol{B}$ flows at different radial locations within the eddy, as shown in figure 7 which is from [37]. Analysis of a model equation describing the process showed that turbulence suppression occurs when

$$|\omega_{\mathrm{t}}| < |\omega_{\mathrm{s}}|. \tag{2.29}$$

This criterion, known as the Biglari–Diamond–Terry (BDT) criterion, could be written as

$$V'_{\mathrm{E}} > (\Delta r k_\theta \tau_{\mathrm{c}})^{-1} \tag{2.30}$$

where τ_{c} is the turbulent decorrelation time, say $\tau_{\mathrm{c}} \sim \omega_*^{-1}$ for drift waves, where the diamagnetic frequency $\omega_* \sim k_\theta \rho_{\mathrm{s}} C_{\mathrm{s}}/L_n$. A more complete expression for ω_{s} in toroidal geometry has been given by Hahm [55]

$$\omega_{\mathrm{s}}^2 = (\Delta r)^2 \left\{ \frac{1}{(\Delta\phi)^2} \left(\frac{\partial}{\partial r} \left(\frac{q V_{\mathrm{E}}}{r} \right) \right)^2 + \frac{1}{(\Delta\eta)^2} \left(\frac{\partial}{\partial r} \left(\frac{V_\parallel}{qR} \right) \right)^2 \right\} \tag{2.31}$$

where $\Delta\phi$ and $\Delta\eta$ are correlation angles for the turbulence around the torus and along the field line, respectively, and $V_\parallel$ is the parallel velocity. For flute-like fluctuations, $\Delta\eta \to \infty$, but generalizing the geometry, Hahm and Burrell [56] obtain

$$\omega_{\mathrm{s}} = \left(\frac{\Delta\psi}{\Delta\phi} \right) \frac{\partial^2}{\partial\psi^2} \Phi(\psi) \tag{2.32}$$

where ψ is the poloidal flux and ϕ is the toroidal angle. If the correlation 'lengths' of the fluctuations, as well as the electrostatic potential Φ, are constant on a flux surface, this reduces to

$$\omega_{\mathrm{s}} = \frac{R^2 B_\theta^2}{r B_\phi} \left(\frac{\Delta r}{\Delta\theta} \right) \frac{\partial^2 \Phi}{\partial\psi^2} \propto R^3 \tag{2.33}$$

for fixed Δr and $\Delta\theta$ (where $\Delta\theta$ is the correlation angle in the poloidal direction), so that it is significantly higher on the outboard midplane. When the turbulence is isotopic ($\Delta r \sim r\Delta\theta$), ω_{s} can be written in the form

$$\omega_{\mathrm{s}} = \frac{R B_\theta}{B} \frac{\partial}{\partial r} \left(\frac{E_r}{R B_\theta} \right). \tag{2.34}$$

Curvature of E_r does not have a generic effect on turbulence, but can affect specific instabilities [57–59]. A reduction in Δr is also predicted in the linear theory of toroidal mode structure [60]

$$\Delta r \propto \left(\frac{V_{\mathrm{Th\,i}}}{r V'_{\mathrm{E}}} \right)^{1/2} \rho_{\mathrm{i}}. \tag{2.35}$$

The transport coefficients are taken to be suppressed by the presence of ω_s:

$$D = \frac{D_0}{1 + c(\omega_s/\omega_t)^\gamma}. \tag{2.36}$$

Thus Biglari *et al* [34] use $c = 1$, $\gamma = 2/3$, while Shaing *et al* [61] take $c = 1/4$, $\gamma = 2$. Hinton justifies the choice $\gamma = 2$ [62], as do Itoh *et al* in their current diffusive ballooning mode model [63]. The validity of such assumptions has been explored in [64]. Turbulence simulations find that ω_t can be approximated by the maximum linear growth rate, γ_{max} [65]. It is interesting to note that the relative velocity between particle guiding centres and the average phase velocity of turbulence can suppress test particle transport [66]:

$$D = D_0 \left(1 + \frac{\omega_*^2}{\omega^2}\right)^{-3/2} \tag{2.37}$$

where ω is a typical mode frequency of the turbulence. Another mechanism for reducing transport is the effect of V_E on the cross-phase of the fluctuations contributing to the transport flux [67], even when V_E' does not affect the amplitude of the fluctuations.

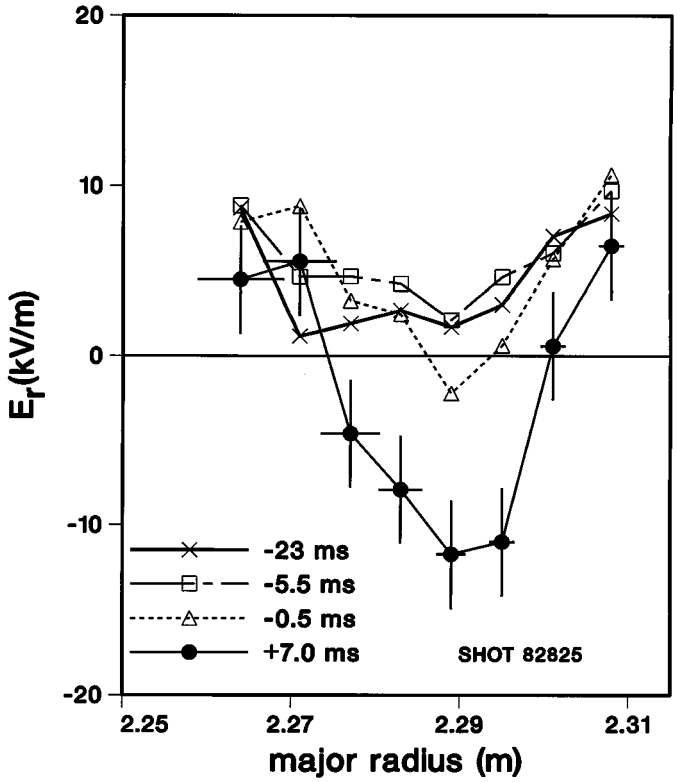

Figure 6. Temporal evolution of steep gradients in the radial electric field, E_r, for shot 82825 from DIII-D [54]; times are measured relative to the L–H transition.

2.4. Radial electric fields

In section 4 we consider L–H transition theories in which V_E' plays a role. These theories show that the plasma admits a bifurcation to a state of larger V_E' and consequently reduced transport.

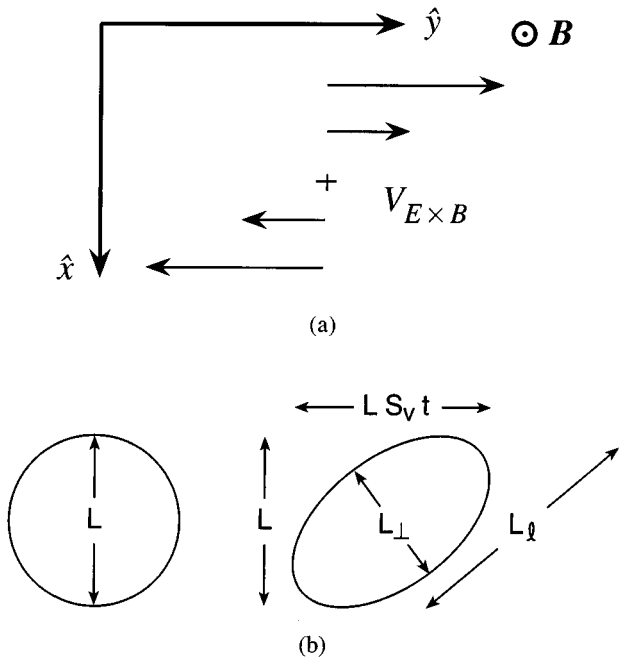

Figure 7. The effect of sheared flow on the perpendicular correlation length of a turbulent eddy (see p 226 in [37]): (a) sheared $\boldsymbol{E}\times\boldsymbol{B}$ flow in the y-direction varying in the x-direction; (b) the anisotropic eddy of scale length L is distorted into an elliptical shape by the sheared flow. If $V_y = S_v x$, then $L_\ell \simeq \sqrt{L^2 + (LS_v t)^2}$ after time t. Since area is preserved, $L_\perp \equiv L/\sqrt{1+S_v^2 t^2}$.

$V_{\rm E}$ is determined by the radial electric field, E_r, which in turn can be deduced from the radial force balance for any plasma species j

$$E_r = -\frac{1}{n_j e_j}\frac{{\rm d}p_j}{{\rm d}r} + V_{\theta j}B_\phi - V_{\phi j}B_\theta \tag{2.38}$$

where e_j, p_j, n_j, $V_{\theta j}$ and $V_{\phi j}$ are the charge, pressure, density and poloidal and toroidal velocities of species j. Thus, changes in E_r can be associated with changes in $V_{\phi j}$, $V_{\theta j}$ or p_j', where prime again refers to a radial derivative. Those in $V_{\theta j}$ correspond to bifurcations in the solutions of the poloidal momentum balance equation. The various models correspond to different sources and sinks in this equation. Typically a model involves a momentum source, or torque (e.g. ion-orbit loss [68, 69], non-ambipolar electron loss [69], Stringer spin-up due to poloidal asymmetries in turbulent transport [70] (related to an effect in neoclassical theory [71]), Reynolds stress from the turbulence present [72]) and a sink (e.g. ion parallel neoclassical viscosity, charge exchange on neutral particles). Such models are discussed in section 4.1. Models involving p_j' or $V_{\phi j}$ depend on sources of particles (e.g. neutral particles surrounding the plasma, or neutral beams), energy (additional heating) or toroidal momentum (neutral beams) driving E_r' until a transport bifurcation takes place; these are discussed in section 4.2. It is interesting to note that if one balances $\omega_{\rm s}$ from (2.34), using E_r derived from the p' contribution in (2.38), then the criterion $\omega_{\rm s} = \gamma_{\max}$ from [65] reduces to

$$\rho_{*\rm s} > \rho_{*\rm s\,crit} \tag{2.39}$$

where $\rho_{*\mathrm{s\,crit}}$ depends on the scaling of $\gamma_{\max}$. Thus, if we assume $\gamma_{\max} \sim C_\mathrm{s}/(R^\alpha L_T^{1-\alpha})$ (where $0 < \alpha < 1$), as might be expected for ion temperature gradient driven turbulence [65], then

$$\rho_{*\mathrm{s}} > \epsilon_T^{1+\alpha}/\epsilon. \tag{2.40}$$

where $\epsilon_T = L_T/R$. Sometimes these theories are generic model systems constructed to have the necessary ingredients, sometimes they are derived from the basic plasma dynamical equations.

2.5. Bifurcations

Bifurcations in some quantity, such as the radial particle flux, Γ, heat flux, q_r, or radial electric field, E_r, can take place when the equation which determines it has multi-valued or non-monotonic solutions as a function of an 'order' variable, such as the density or temperature gradients, n' and T', respectively. The nature of these solutions allows a categorization of bifurcations. When these are multivalued solutions, as in figure 8(a), one has a 'hard' bifurcation [35]. When it is merely non-monotonic, as in figure 8(b), it is a 'soft' bifurcation, sometimes called a 'first-order phase transition'. A milder transition, in which the solution remains monotonic but undergoes a change of slope, is sometimes called a 'second-order phase transition'. By considering such diagrams in the space of the order parameter and an additional 'control' parameter, the topology can change as the control parameter varies, as in figure 8(c). Such a 'cusp-type' surface has been obtained from experimental studies of the L–H transition in JET and DIII-D [9].

The poloidal torque balance has the potential to lead to a bifurcation in poloidal flow, and hence E_r: this equation can admit multi-valued solutions for these quantities, as discussed by Itoh [35]. For singly charged ions, this equation can be written in the form

$$\frac{\epsilon_0\epsilon_\perp}{e}\frac{\partial E_r}{\partial t} = \Gamma_{\mathrm{e-i}}^{\mathrm{anom}} - \Gamma_\mathrm{i}^{\mathrm{lc}} - \Gamma_\mathrm{i}^{\mathrm{bv}} - \Gamma_\mathrm{i}^{\mathrm{v\nabla v}} - \Gamma_\mathrm{i}^{\mathrm{neo}} + \Gamma_\mathrm{e}^{\mathrm{neo}} - \Gamma_\mathrm{i}^{\mathrm{cx}} \tag{2.41}$$

with $\epsilon_\perp \sim n_\mathrm{i} m_\mathrm{i}/\epsilon_0 B^2$ the perpendicular dielectric constant, where the right-hand side represents a number of sources of non-ambipolar particle flux which balance that due to the polarization current on the left-hand side; alternatively one can consider that the net radial current corresponding to the right-hand side produces a $\boldsymbol{j} \times \boldsymbol{B}$ force which drives a poloidal $\boldsymbol{E} \times \boldsymbol{B}$ flow.

The terms on the right-hand side represent the following processes. The first one, $\Gamma_{\mathrm{e-i}}^{\mathrm{anom}}$, is the contribution of the non-ambipolar part of the anomalous cross-field flux (i.e. the excess flux of electrons relative to that of ions). The second one, $\Gamma_\mathrm{i}^{\mathrm{lc}}$, is that from an ion-loss cone. The third, $\Gamma_\mathrm{i}^{\mathrm{bv}}$, is from the collisional bulk plasma viscosity, i.e. due to the inhomogeneity of the magnetic field. The fourth, $\Gamma_\mathrm{i}^{\mathrm{v\nabla v}}$, originates from the Reynolds stress due to the plasma flow. The fifth and sixth, $\Gamma_\mathrm{i}^{\mathrm{neo}}$ and $\Gamma_\mathrm{e}^{\mathrm{neo}}$, are the contributions of other collisional processes, such as ripple diffusion. The last, $\Gamma_\mathrm{i}^{\mathrm{cx}}$, is the contribution of the loss of ions from charge exchange processes. In order to provide a perspective, qualitative dependences of these terms are [35]

$$\Gamma_{\mathrm{e-i}}^{\mathrm{anom}} = nC_\mathrm{s}\hat{D}(\lambda - X) \tag{2.42}$$

$$\Gamma_\mathrm{i}^{\mathrm{lc}} = f_{\mathrm{lc}}\nu_\mathrm{i}\rho_{\mathrm{pi}}n_\mathrm{i}\exp(-\xi_{\mathrm{lc}}X^2) \tag{2.43}$$

$$\Gamma_\mathrm{i}^{\mathrm{bv}} = f_{\mathrm{bv}}\nu_\mathrm{i}\rho_{\mathrm{pi}}n_\mathrm{i}\frac{X + X_0}{1 + X^2} \tag{2.44}$$

where $X = e\rho_{\mathrm{pi}}E_r/T_\mathrm{i}$ is the normalized radial electric field (X_0 is a reference value) and λ is a normalized gradient, $\lambda = -\rho_{\mathrm{pi}}(n'/n + cT'/T)$ with c a constant, ν_i is the ion–ion collision frequency, ρ_{pi} is the ion poloidal gyro-radius and the coefficients f_{lc} and f_{bv} are functions of

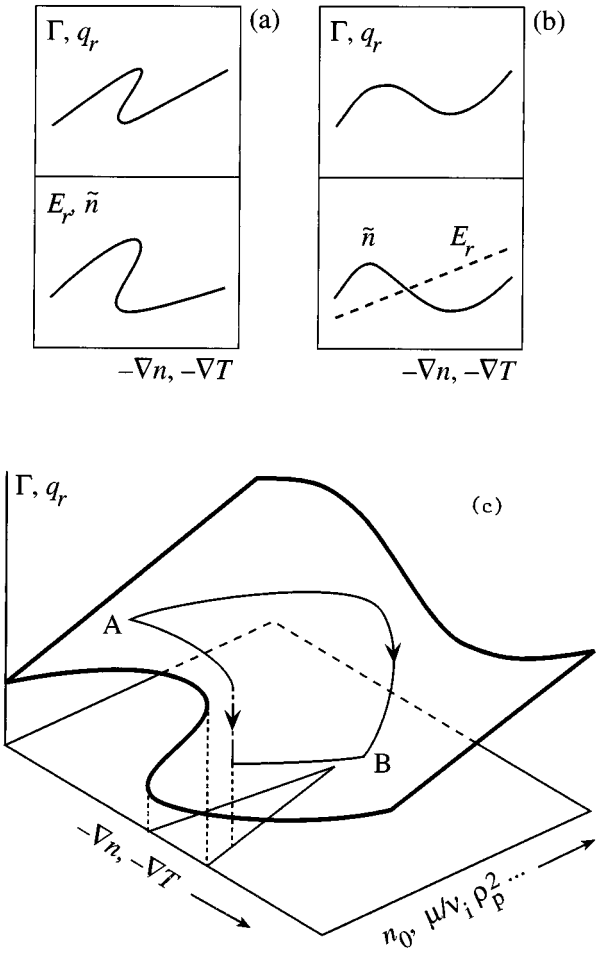

Figure 8. Bifurcation diagrams: (a) a 'hard' transition in particle flux, Γ, and heat flux, q_r, radial electric field, E_r, and fluctuation level, $\tilde{n}$, as functions of the 'order' parameters, i.e. the density and temperature gradients, $-\nabla n$ or $-\nabla T$; in this case quantities exhibit multiple values; (b) as in (a), but a 'soft' transition; in this case quantities are non-monotonic but single-valued; and (c) a cusp-type bifurcation surface can be obtained when an additional 'control' parameter, such as the neutral density, n_0, or viscosity, $\mu_\perp$, is introduced: a change from a state with large flux, A, to one with low flux, B, can occur by a route involving a hard or a soft transition (see p 248 in [37]).

$\epsilon = a/R$. The coefficients $\hat{D}$ and $\xi_{\rm lc}$ can be affected by the electric field gradients as discussed in [34]. From (2.41)–(2.44) one sees that the flux has a nonlinear dependence on the radial electric field.

Combining various terms, a variety of bifurcations can be predicted. The first bifurcation model was made by balancing $\Gamma_{\rm e-i}^{\rm anom}$ and $\Gamma_{\rm i}^{\rm lc}$ [69]; another model balances $\Gamma_{\rm i}^{\rm lc}$ and $\Gamma_{\rm i}^{\rm bv}$ [68]; while a third $\Gamma_{\rm i}^{\rm bv}$ and $\Gamma_{\rm i}^{\rm v\nabla v}$ [70].

The simplest models for the bifurcation physics are local in radius; however, one can introduce effects to determine the radial structure of the bifurcation layer. If the bifurcation in E_r arises from V_θ, then one can expect the layer width Δ to be given by a combination of the width over which the nonlinear drives in (2.41) exist, say $\rho_{\rm pi}$ for ion-orbit loss, and that set

by viscosity and drag terms appearing in the transport equation for poloidal flow. Thus, for example,

$$\Delta \sim \left(\rho_{\rm pi}^2 + c\frac{\mu_\perp}{\nu_{\rm i}}\right)^{1/2} \tag{2.45}$$

where $\mu_\perp$ is the, possibly turbulent, cross-field viscosity (strictly momentum diffusivity), c is a constant of order unity and $\nu_{\rm i}$ represents poloidal flow damping [35].

On the other hand, the width may be set by the transport equations for density or temperature when the gradients in these drive E_r. For the paradigmatic bifurcation diagram shown in figure 8(b), the barrier location can be determined by the Maxwell construction [73, 74]. Introducing a small dissipative term to resolve the spatial structure of the transition layer, one finds that the position of the barrier is determined by an 'equal areas' rule, as shown in figure 9; in the case of L–H transitions driven by density gradients one can then derive a width comparable to the neutral particle fuelling depth $\ell_{\rm n}$ [75].

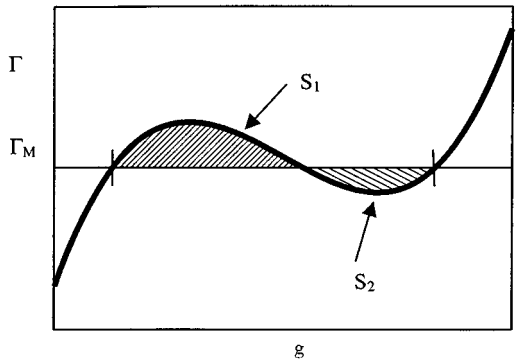

Figure 9. Maxwell's rule of equal areas at a phase transition determines the position of the transport barriers; it occurs where the flux $\Gamma = \Gamma_{\rm M}$, the Maxwell flux, such that the areas S_1 and S_2 between $\Gamma(g)$ and $\Gamma_{\rm M}$, where g is the driving gradient, are equal.

However, a recent treatment of such bifurcation models, in which the contribution to E_r shear arising from second-order derivatives of n, implied in (2.38), are properly retained, indicates a weakness in the paradigm represented by figure 8(b). In figure 8(b), which we refer to as 'first-order' transport, the flux-gradient relation is unique; it can be defined locally and has a built-in potential for bifurcation between high and low transport regimes. With 'second-order' transport, i.e. when we include the second derivatives, the flux–gradient relation cannot be described locally; it depends on the global distribution of sources [76]. More importantly, even with a given source distribution, the relation between flux and plasma gradients is not unique; there is a family of possible flux–gradient relations (see figure 10 which is from [76]). The appropriate one depends on a boundary condition at the plasma edge (such as might emerge from a model of the SOL). The boundary condition plays a crucial role in determining the overall plasma profile and demonstrates the dominant effect of the plasma edge on tokamak profiles and on confinement. It is a condition that is not required, indeed is not admissible, with first-order transport, where it would over-determine the problem. However, if the transport equation with second-order transport is to have a stationary solution it must place the edge gradient within prescribed limits. This argument suggests that bifurcations in E_r due to ones in V_θ or V_ϕ are more consistent. Thus a bifurcation transport model for V_ϕ would exhibit the characteristics of a first-order theory since E_r' only depends on the first-order derivative V_ϕ'; bifurcations in V_θ arise from ones in poloidal momentum balance, rather than transport fluxes.

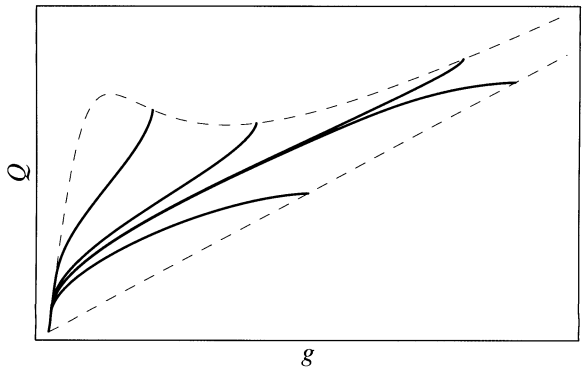

Figure 10. The relation between flux, Q, and gradient, g, is not unique with 'second-order' transport (full curves), in contrast to the first-order ('local') theory (upper dashed curve) [76] (the lower dashed curve corresponds to the lower 'H-mode' level of transport); depending on an additional boundary condition, say at the plasma edge, many solutions are admissible.

The time scale of the transition is also set by equations such as (2.41). Taking a typical term on the right-hand side of (2.41), say the ion-orbit-loss term (2.43), one finds that the time scale for a bifurcation is

$$\tau_{\rm tr} \sim \frac{\epsilon^{5/2}}{\nu_{\rm i} q^2} \tag{2.46}$$

i.e. a 'microscopic' time scale; similar microscopic time scales would result for other contributions to (2.41). Although scalings such as (2.46) hold numerically, $\tau_{\rm tr}$ could become very long if the plasma parameters were such that the transition threshold was only marginally exceeded. In this discussion we have emphasized the role of bifurcations in E_r arising from poloidal flow. However, for models in which E_r is controlled by density and temperature gradients, the width and time scales are set by transport processes. Thus, if the transition occurs within a region Δ, say controlled by edge refuelling of particles so that $\Delta \sim \ell_{\rm n}$, then $\tau_{\rm tr} \sim \Delta^2/D$ where D is an anomalous diffusion coefficient; again one recovers a microscopic time scale.

3. Instabilities and turbulence at the plasma edge

In this section we consider models for the L–H transition involving instabilities and turbulence in the plasma edge region: either the edge of the core plasma or the SOL. Such models invoke either the stabilization of a particular mode, hence removing the drive for an associated turbulent flux, or the reduction of a turbulent transport flux as some parameter (e.g. collisionality) passes a critical value. When this occurs the plasma can make a sudden bifurcation to a state supporting the same transport flux but with lower residual transport coefficients and hence steeper profiles: an L–H transition. We shall note some cases where the reduction in transport fluxes results from self-consistent generation of sheared flows, although such models strictly belong to the next section. The various models will be discussed in turn, separating them into core and SOL instabilities.

3.1. Edge region of the core

3.1.1. Ideal MHD modes. Bishop [77] proposed that ideal MHD ballooning mode stability plays a part in the L–H transition, investigating the role of separatrix geometry and an edge plasma current, $j_{\|}$. He concluded that the stability properties become progressively better in a separatrix configuration in which the X-point position moves into the region of favourable curvature and that a finite edge current allows the possibility of complete stability to both ballooning and interchange modes for surfaces close to the separatrix. This is partly due to the fact that regions of zero local magnetic shear are moved into the region of favourable curvature. As a result, a picture for L- and H-regimes in a divertor tokamak emerges. In the L-mode the edge temperature and hence the current density are relatively low and the edge pressure gradient is ballooning limited. A sufficient increase in edge temperature, and therefore current, allows access to a second stability regime over a region near the separatrix surface, as in figure 11 which is from [78] (values of $T_{\text{edge}} \sim 350$ eV suffice). This picture is consistent with older data from PDX, but more recent data from DIII-D and ASDEX Upgrade [24, 79] suggest the L–H transition occurs well below the simple ballooning limit

$$\alpha = -2\mu_0 p' q^2 R/B^2 \leqslant \alpha_{\text{crit}} \tag{3.1}$$

where α_{crit} is the critical value of α for instability and the prime denotes a radial derivative. In [78] it was shown how these ballooning stability criteria could be combined with a simple transport model involving marginal stability [80] to construct global L- and H-mode profiles. The appearance of the H-mode requires the power to exceed a threshold value; above this value there is a bifurcation so that both L- and H-mode profiles can occur.

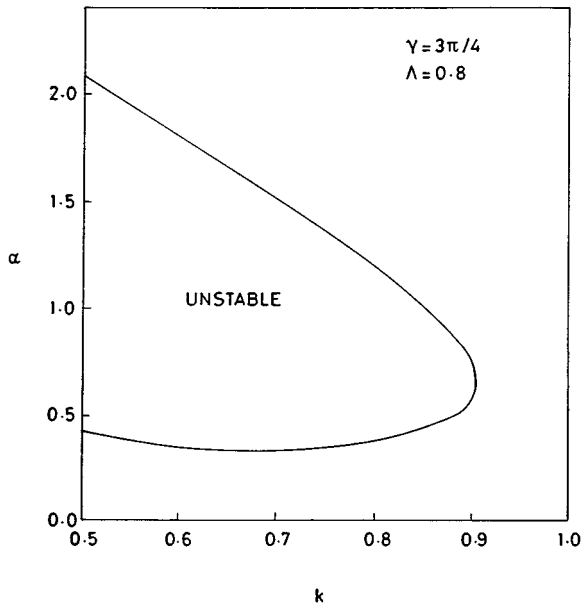

Figure 11. Marginally stable pressure gradient parameter, α, as a function of shaping parameter, k (representing proximity to the plasma edge), for X-point angle $3\pi/4$ and finite edge current measured by Λ [78].

However, an edge plasma current can also drive instabilities. The peeling mode occurs when a resonant surface for an ideal external kink mode lies just outside the plasma surface. In

cylindrical geometry this mode, which is localized at the plasma surface, is destabilized by a finite plasma current at the edge of the plasma. In toroidal geometry it is found that favourable Mercier stability permits a finite edge current [81, 82] (see figure 12). Thus, to $O(\epsilon^2)$, one finds a stability criterion

$$\alpha\left\{\frac{r}{R}\left(1-\frac{1}{q^2}\right)+s\Delta'_{\mathrm{Shaf}}\right\} > \mu_0 Rqs\frac{j_\parallel}{B} \tag{3.2}$$

where all terms are evaluated at the plasma edge. In this condition, Δ'_{Shaf} is the radial derivative of the Shafranov-shift parameter and $s = \mathrm{d}(\ln q)/\mathrm{d}(\ln r)$ is the magnetic shear. The first term on the left represents the Mercier contribution while the second term results from the Pfirsch–Schlüter current; $j_\parallel$ contains only the contributions from the inductive current and the bootstrap current. Written in this form the criterion illustrates the stabilizing effect of the Pfirsch–Schlüter current, whereas both the inductive and bootstrap currents are destabilizing. The overall effect of the pressure gradient depends on the bootstrap current. While the term on the left of (3.2) is stabilizing, the bootstrap current is also proportional to α and this will be destabilizing. However, the edge of a tokamak is typically collisional, $\nu_{*\mathrm{e}} > 1$, in the L-mode and this will suppress the bootstrap current so that one might expect that increasing α is generally stabilizing; a comparison of these conditions on α and $\nu_{*\mathrm{e}}$ with COMPASS-D data [19] is shown in figure 13. Measurements on DIII-D [83] show that ν_* can be in the range 5–50, so that different mechanisms may pertain in different regimes and devices; alternatively, stability to the peeling mode may only be a necessary condition for the L–H transition and a complete theory would require an additional ingredient.

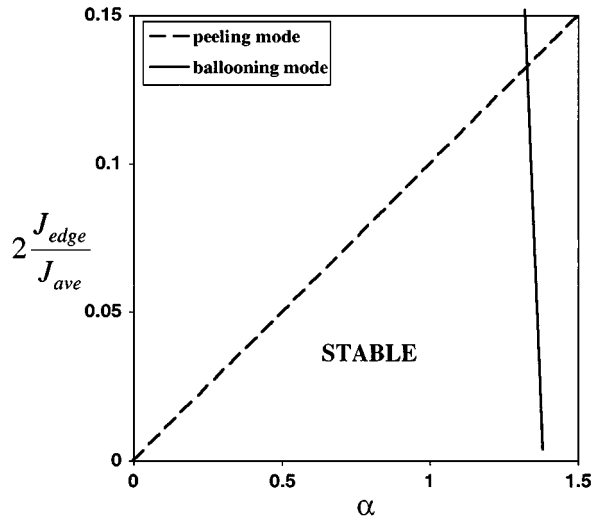

Figure 12. Stability diagram in the $J_{\mathrm{edge}}/J_{\mathrm{ave}}$–$\alpha$ (edge current-edge pressure gradient; J_{ave} is the average of J over the plasma cross section) plane for peeling and ballooning modes [81]; the full line relates to high-mode number ballooning modes, the dashed line to peeling modes.

These properties of the peeling mode suggest the following picture of the L–H transition. The L-mode is considered to be unstable to the peeling mode, resulting in a high level of magnetic fluctuations at the tokamak edge and therefore an enhanced thermal diffusivity. As the heating power is increased, α will rise and eventually pass beyond the critical value required for stability. The peeling mode will then switch off and the edge confinement will improve. This can be interpreted as a necessary condition for the H-mode. Of course, the edge

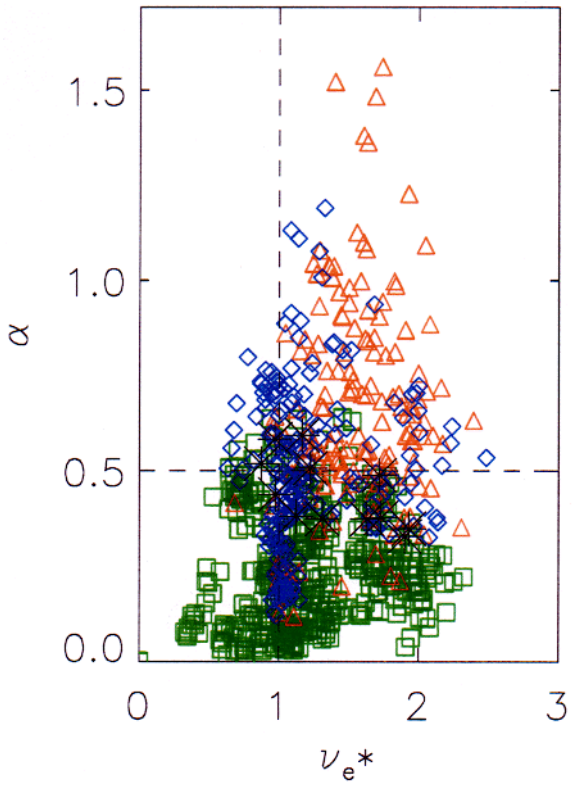

Figure 13. Comparison of COMPASS-D data at the L–H transition with the peeling mode stability condition involving the pressure gradient and collisionality parameters, α and ν_{*e}, respectively [23]: red triangles are ELM-free H-modes, blue diamonds, ELMy H-modes and green squares, L-modes. The theory predicts that H-modes lie in the top right quadrant of this diagram.

temperature will also rise with heating power and this will raise the plasma conductivity and decrease ν_* and therefore increase the edge current. Whether the peeling mode is stabilized as the power is increased therefore depends on the competition between the rise in α and the rise in temperature, and consequently on the relative time scales of current and pressure diffusion, providing a possible explanation for differences observed in L–H transitions between large and small tokamaks. Certain other experimental observations of H-mode characteristics are reproduced by the peeling mode stability criterion: (i) the mechanism exhibits 'hysteresis', in that once the peeling mode has been stabilized by sufficient input power, the edge confinement improves and α can be maintained above the critical value with a lower power; (ii) an H-mode cannot be accessed by increased heating power if the X-point is on the outboard (low field) side because the relevant average of the Pfirsch–Schlüter current is destabilizing; (iii) low edge collisionality discharges may experience difficulty entering the H-mode because of the high edge bootstrap current: this may provide an explanation of the observation on COMPASS-D that it is not possible to access the H-mode if the line-averaged density is below a critical value [18, 19] (see figure 14 which is from [19]); (iv) an H-mode can be accessed by reducing the edge current, as demonstrated on COMPASS-D [18] and JIPP T-IIU [84] by current ramp-down and on TUMAN-3 by pellet injection at the plasma edge [85] (this decreases the edge temperature, thus enhancing the resistivity).

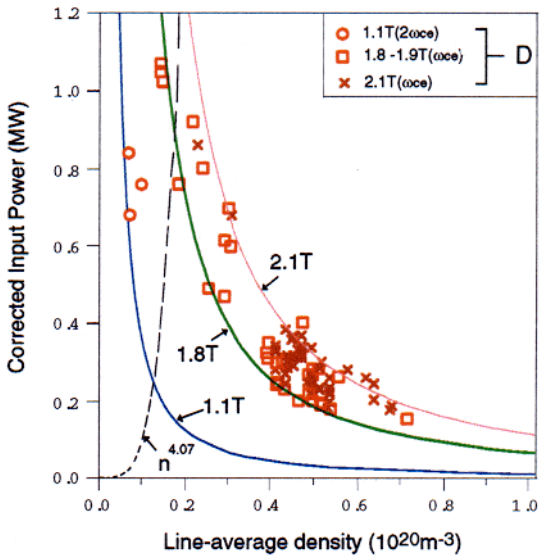

Figure 14. The L–H threshold power for COMPASS-D as a function of line-averaged density, showing an increase at low density, for several magnetic field strengths [19]. The dashed curve, $P \propto n^{4.01}$, is the threshold power corresponding to a critical collisionality for the L–H transition, using L-mode confinement scaling.

3.1.2. Resistive ballooning modes. A number of studies of resistive ballooning modes have been carried out. A model in which diamagnetic stabilization causes a bifurcation has been given by Drake and coworkers in a series of papers [86–90]. The first paper [86] developed a model for edge turbulence due to electrostatic resistive ballooning modes with high toroidal mode number, n, such that $n^2/S \sim 1$, where S is the Lundquist number; this implies the modes are strongly ballooning in character. The condition that they are stabilized by diamagnetic effects is $\omega_{*\mathrm{i}} > 2\gamma_0$, where $\omega_{*\mathrm{i}}$ is the ion diamagnetic frequency defined with respect to a 'resistive' wavelength, $L_0 = 2\pi q(\nu_\mathrm{e} R\rho_\mathrm{s}/2\Omega_\mathrm{e})^{1/2}(2R/L_n)^{1/4}$, with Ω_e the electron gyro-frequency, and γ_0 is the ideal ballooning mode growth rate in the absence of such effects. A threshold criterion for this stabilization is given by

$$\frac{V_{\mathrm{The}}}{\pi\nu_{\mathrm{ei}}qR} > 2\pi q\left(1+\frac{T_\mathrm{i}}{T_\mathrm{e}}\right)\left(\frac{L_n^2}{RL_p}\right)^{1/2}\left(\frac{m_\mathrm{e}}{m_\mathrm{i}}\right)^{1/2} \tag{3.3}$$

equivalent to

$$\hat{\nu}_{*\mathrm{e}} < \frac{1}{\pi}\left(\frac{m_\mathrm{i}}{m_\mathrm{e}}\frac{RL_p}{L_n^2}\right)^{1/2}\frac{1}{2\pi q}\left(\frac{T_\mathrm{e}}{T_\mathrm{i}+T_\mathrm{e}}\right) \tag{3.4}$$

where $\hat{\nu}_{*\mathrm{e}} = \nu_{\mathrm{ei}}Rq/V_{\mathrm{The}}$ and L_p is the pressure scale length which would need to be evaluated just inside the last closed flux surface (LCFS). (For shaped plasmas the connection length $L_\mathrm{c} = 2\pi Rq$ must be generalized to reflect the magnetic geometry.)

A bifurcation model involving the density evolution with a diffusion coefficient depending on the fluctuation intensity, which in turn is governed by the competition between the pressure gradient drive and diamagnetic stabilization, was derived; condition (3.3) yields the condition for the onset of the bifurcation. The model considers that the transition results from a steepening of the pressure gradient which stabilizes the ballooning mode and reduces the transport. It does not require $\boldsymbol{E}\times\boldsymbol{B}$ velocity shear, V'_E, and for present experiments, where $V_{*\mathrm{i}} \sim V_\mathrm{E}$,

this mechanism is expected to be more important. The transition will be accompanied by a suppression of turbulence, which is predominantly electrostatic. The L–H cycle shows hysteresis in this model. This work has been supported by extensive numerical calculations.

In a subsequent paper, Drake *et al* [87] carried out three-dimensional (3D) nonlinear simulations of drift resistive ballooning modes at the plasma edge for a finite β, toroidal equilibrium with shifted circular surfaces, so that the Shafranov shift can reduce the local magnetic shear. Such calculations are parametrized by α and a 'diamagnetic' parameter $\alpha_{\rm dia} = (1/2\pi q)(m_{\rm i}/2m_{\rm e})^{1/4}\ (V_{{\rm Th\,e}}/\nu_{\rm ei}\sqrt{RL_n})^{1/2}$. For low values of $\alpha_{\rm dia}$ these calculations, which self-consistently evolve p', exhibit a bifurcation in β when $\alpha = 1.2$, so that the local shear on the outside of the torus reverses; they also display hysteresis. The fluctuations are essentially unchanged at the L–H transition but decrease rapidly as α increases further and the original, radially extended, resistive ballooning modes develop shorter radial correlation lengths. This model can really only apply to shaped plasmas when the ideal MHD ballooning mode stability limit $\alpha = \alpha_{\rm crit}$ exceeds $\alpha = 1.2$. In later work [88], the inclusion of electromagnetic effects (necessary for self-consistency when $\alpha \sim 1$) and velocity shear was considered. It was found that long wavelength modes are strongly destabilized and the transport fluxes increase rapidly with α for $\alpha < \alpha_{\rm crit}$, although this can be mitigated by plasma shaping. However, velocity shear was found to be very effective in reducing transport due to its effect on long wavelength modes and a bifurcation, producing a transport barrier, occurs when

$$V'_\theta > \frac{sC_{\rm s}}{\sqrt{RL_p}}. \tag{3.5}$$

For the case of Stringer spin-up ($V_\theta \sim C_{\rm s}a/Rq$) and $L_p \sim L_v$, the velocity gradient length, this can be written as a purely geometrical condition

$$L_p < a^2/q^2s^2R \tag{3.6}$$

whereas, using $V_\theta \sim V_{\rm E}$ derived by balancing E_r and p',

$$L_p < (R\rho_{\rm i}^2/s^2)^{1/3} \tag{3.7}$$

or

$$\rho_{*{\rm s}} > s\left(\frac{L_p}{a}\right)^{3/2}\left(\frac{a}{R}\right)^{1/2}\left(\frac{T_{\rm e}}{T_{\rm i}}\right)^{1/2}. \tag{3.8}$$

This approach has been taken further [89, 90] with 3D simulations of ideal and drift-resistive ballooning modes including the ion temperature gradient and electron drift modes. These simulations showed the formation of a transport barrier when $\alpha \lesssim 0.5$ and $\alpha_{\rm dia} \geqslant 0.75$, due to the generation of sheared poloidal flows by a nonlinear Kelvin–Helmholtz instability: only for $\alpha \gtrsim 0.5$ are the flows generated by the ballooning modes sufficiently long-lived to suppress the turbulence and the Kelvin–Helmholtz instability is enhanced when $\alpha_{\rm dia} \sim 1$. The latest version of these 3D nonlinear simulations with the Braginskii fluid model for the plasma edge region, carried out in shifted-circle geometry, including self-consistent magnetic fluctuations and neoclassically-correct shear-flow damping [90], leads to a 'phase space diagram' in the n–T plane for tokamak edge turbulence with regions which correspond to L-mode, H-mode and a sub-L-mode region which may be related to the density limit. The H-mode is identified with the spontaneous appearance of a transport barrier as the pressure gradient is increased at sufficiently high values of $\alpha_{\rm dia}$. Several features consistent with experiments appear in the simulations, including formation of mini-barriers which may correspond to 'dithering' L–H transitions. While more work is clearly required, particularly the inclusion of a more realistic magnetic geometry, the agreement between experiment and theory is encouraging: thus the conditions for L–H transitions in Alcator C-Mod correlate well with these two parameters

[21], as shown in figure 15. However, comparisons with the theory and DIII-D data show that while the parameter α, suitably generalized to realistic geometry, separates out L-modes about to undergo an L–H transition, there is no correlation with $\alpha_{\rm dia}$. Furthermore, while evidence from COMPASS-D suggests a critical value of α, there is no evidence for a correlation with $\alpha_{\rm dia}$ (although $\alpha_{\rm dia} > 0.75$ always appears to be satisfied) [91].

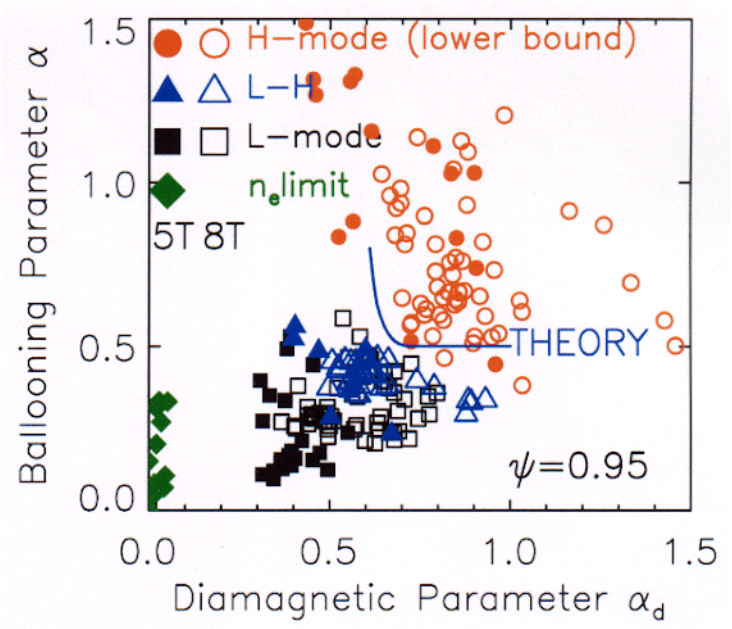

Figure 15. A comparison of the drift ballooning theory of Rogers and Drake, involving the pressure gradient parameter, α, and the diamagnetic parameter, $\alpha_{\rm d}$, with L–H transition data from Alcator C-Mod [21]; the full symbols are at 5 T, the open ones at 8 T.

Guzdar and Hassam [92] have carried out nonlinear simulations of resistive ballooning modes in a torus, retaining only one toroidal mode number, but self-consistently evolving the profiles. The turbulent Reynolds stress and Stringer spin-up from the poloidally asymmetric L-mode transport fluxes, drive poloidal flows which lead to reduced transport and a transition to the H-mode; the poloidal flows convect the transport reduction from the outside of the torus, where it first appears, to make the transport poloidally symmetric in the H-mode. For DIII-D parameters they find $V_\theta \sim 5$ km s^{-1} and a transition time ~80–160 μs. The transition results from the heating power accentuating the in–out asymmetry through the Shafranov shift and occurs when

$$\frac{D\Delta'_{\rm Shaf}}{\epsilon L_n^2} > \gamma_{\rm damp} \tag{3.9}$$

where D is the anomalous diffusivity and $\gamma_{\rm damp}$ is poloidal flow damping due to magnetic pumping and charge exchange; this formula therefore represents an interplay between core and edge. If one assumes that D is Bohm-like, $D \sim \rho_{\rm s} C_{\rm s}$, $\Delta'_{\rm Shaf} \sim \epsilon\beta_{\rm pol}$, where $\beta_{\rm pol}$ is the value of β referred to the poloidal magnetic field, and $\gamma_{\rm damp} \propto \nu_{\rm ii}$, the ion–ion collision frequency, then this takes the form

$$\rho_{*\rm s}\left(\frac{T_{\rm e}}{T_{\rm i}}\right)^{1/2}\frac{R^3q^3}{L_n^2 a}\beta > \hat{\nu}_{*\rm i} \tag{3.10}$$

or, taking $L_p \propto a$, a critical temperature scaling as

$$T_{\mathrm{e\,crit}} \propto \frac{B^{6/7}a^{8/7}}{(Rq)^{4/7}}. \tag{3.11}$$

In a series of papers [93–96], Zeiler and coworkers have performed 3D nonlinear simulations of drift resistive ballooning modes in toroidal geometry. Their results are characterized by the ratio $\delta = \omega_*/\gamma$, where ω_* again has a poloidal wavelength corresponding to the 'resistive' width, L_0, and γ is an ideal ballooning mode growth rate, $C_s\sqrt{2/RL_n}$. For $\delta \leqslant 1$ they observe resistive ballooning mode turbulence with in–out asymmetry and weak diamagnetic propagation. For $\delta \sim 2$ these modes are stabilized, leaving a weakly ballooning, nonlinearly destabilized drift wave with $\omega \sim \omega_{*\mathrm{e}}$ and larger radial correlation lengths Δr. The results in this region depend on the parameter $\hat{\rho}^2 = \epsilon_n(\delta s)^{4/3}(1 + T_\mathrm{i}/T_\mathrm{e})$, where $\epsilon_n = L_n/R$, and the thermal diffusivity drops rapidly with $\hat{\rho}$. The 'transition' condition $\delta > 1$ can be expressed as

$$\hat{\nu}_{*\mathrm{e}} < \frac{1}{2^{5/2}\pi^2 q}\left(\frac{T_\mathrm{e}}{T_\mathrm{e}+T_\mathrm{i}}\right)^2\left(\frac{m_\mathrm{i}}{m_\mathrm{e}}\right)^{1/2}\left(\frac{R}{L_n}\right)^{1/2} \qquad \text{i.e. } T_{\mathrm{e\,crit}} \propto (aR)^{1/4}n^{1/2}q \tag{3.12}$$

similar to (3.4) of course, whereas the condition $\hat{\rho} > 1$ corresponds to

$$\hat{\nu}_{*\mathrm{e}} < \frac{s^2}{2\pi^2 q(1+\tau)^{1/2}}\left(\frac{m_\mathrm{i}}{m_\mathrm{e}}\right)^{1/2}\epsilon_n \tag{3.13}$$

where $\tau = T_\mathrm{e}/T_\mathrm{i}$, and a similar scaling for $T_{\mathrm{e\,crit}}$. The regime with $\delta \leqslant 1$ can be identified with ohmic and L-mode transport, those in the L-mode being higher than in ohmic because $T_\mathrm{i} \gg T_\mathrm{e}$. A rise in edge temperature increases δ, stabilizing the resistive ballooning mode. Near the separatrix, $\hat{\rho}$ is low and transport is high, but further in ($\sim$1 cm) $\hat{\rho}$ is higher ($\hat{\rho}^2 \sim 0.12$), fluctuations are suppressed and a transport barrier forms. These values of δ are found to correlate with ohmic, L-mode and H-mode regimes in ASDEX. In [96] these authors included ion temperature gradient dynamics and found that it can strongly enhance the resistive ballooning mode transport.

The effects of separatrix geometry, discussed by Bishop in the context of ideal MHD ballooning modes, have been investigated for resistive modes by Hahm and Diamond [97], since the turbulent transport due to resistive ballooning and rippling modes provides a plausible description of edge transport in ohmic and L-mode plasmas. The effect on such resistive modes is more dramatic than in the ideal case: for these resonant modes the radial correlation length scales as

$$\Delta r \sim a/k_\theta Rqs. \tag{3.14}$$

Thus the divergences in q and s near the separatrix lead to a strong reduction in mixing length estimates of turbulent transport there; indeed this reduction is significant for $r \geqslant 0.9a$, consistent with the location of observed edge transport barriers. In particular, transport arising from stochastic magnetic fields due to resistive ballooning mode turbulence is a candidate for explaining thermal transport at the edge; the reduction in mixing length magnetic fluctuation levels due to the decrease in Δr, is consistent with improved runaway electron confinement in the H-mode. Also, resistive impurity gradient driven turbulence provides an explanation of particle transport at the edge. The inverse dependence on temperature of the transport coefficients corresponding to both these resistive fluid models allows one to envisage scenarios for the build up of steep pressure profiles in separatrix geometry. Furthermore, the increased shear also allows the plasma to remain stable to resistive kink modes driven by large current gradients in the edge region.

3.1.3. Tearing modes. An instability proposed by Ohyabu *et al* [98], to explain early Doublet III measurements of edge fluctuations at the transition, is the micro-tearing mode, which has been analysed in slab geometry by Gladd *et al* [99] and has a stability criterion given approximately by

$$\nu_{\mathrm{ei}} \leqslant \eta_{\mathrm{e}}\omega_{*\mathrm{e}}. \tag{3.15}$$

When this is satisfied there will be a reduction in both magnetic and electrostatic fluctuations with $\omega \sim \omega_{*\mathrm{e}}$. This criterion can be written

$$\hat{\nu}_{*\mathrm{e}} \leqslant m\rho_{*\mathrm{s}}\sqrt{\frac{m_{\mathrm{e}}}{m_{\mathrm{i}}}}\frac{Rq}{L_{T_{\mathrm{e}}}} \tag{3.16}$$

where m is the poloidal mode number and $L_{T_{\mathrm{e}}}^{-1} = |\mathrm{d}(\ln T_{\mathrm{e}})/\mathrm{d}r|$.

If the poloidal mode number can be treated as a constant, independent of the temperature, then this condition can be expressed as

$$T_{\mathrm{e}} \gtrsim T_{\mathrm{e\,crit}} \propto [naBL_{T_{\mathrm{e}}}]^{2/5}. \tag{3.17}$$

It is noteworthy that this suggests a power threshold which increases with density and magnetic field. However, if we assume $k_\theta \rho_{\mathrm{s}} \sim 1$, then no magnetic field scaling results from (3.15). We should also add that the analytic result given in (3.15) is an over-simplification and the mode stability also depends on the ratio L_n/L_s (where $L_s = Rq/s$ is the shear length), with larger values corresponding to greater stability. This may explain why it is generally easier to obtain an H-mode in a diverted plasma than in a limiter case. Equation (3.15) is therefore too simple to test an equilibrium for stability to the microtearing mode and a full numerical calculation is required. This has been attempted by Lau [100] who found that for typical DIII-D discharges the H-mode actually tends to be *less* stable than the L-mode. However, Lau considered a 'local shear length' which is much larger than the actual shear length when one is close to the separatrix. Such an approximation is only valid if the mode has a strong ballooning nature, away from the X-point, but then the slab approximation is not good. Strictly the model requires a full toroidal stability calculation in order to be tested rigorously.

The microtearing modes discussed above have a high poloidal mode number and instability occurs as a result of the thermal force. Strauss [101] considered lower m tearing modes which are driven by magnetic forces, determined by the tearing mode stability index Δ'. These are unstable when Δ' exceeds some critical value Δ'_{crit}, which represents the stabilizing effects determined by the non-ideal 'electron' layer around the resonant surface. The value of Δ'_{crit} depends on the dominant physics. For example, when the drift effects are the major stabilizing mechanism, the tearing mode is stable when

$$\Delta' < \Delta'_{\mathrm{crit}} = 0.7\left(\frac{m_{\mathrm{i}}}{m_{\mathrm{e}}}\right)\frac{C_{\mathrm{s}}^3}{C_{\mathrm{A}}^2 L_T^2 \nu_{\mathrm{e}}}\left(\frac{L_T}{L_s}\right) \tag{3.18}$$

where C_{A} is the Alfvén speed. This corresponds to a critical collisionality scaling as

$$\hat{\nu}_{*\mathrm{e\,crit}} \propto \beta_{\mathrm{e}}\left(\frac{m_{\mathrm{i}}}{m_{\mathrm{e}}}\right)^{1/2}\frac{s}{L_T\Delta'} \tag{3.19}$$

or a temperature

$$T_{\mathrm{e\,crit}} \propto (RqB^2)^{1/3}. \tag{3.20}$$

For Δ'_{crit} determined by sound waves, a different threshold pertains, corresponding to

$$\hat{\nu}_{*\mathrm{e\,crit}} \propto \left(\frac{m_{\mathrm{i}}}{m_{\mathrm{e}}}\right)^{1/2}\frac{L_s}{L_n}\frac{\beta_{\mathrm{e}}^2}{\rho_{*\mathrm{s}}}\frac{k_\theta a}{(a\Delta')^2}Z\left(\frac{T_{\mathrm{e}}}{T_{\mathrm{i}}}\right)^{3/2} \tag{3.21}$$

where Z is the ionic charge, or

$$T_{\mathrm{e\,crit}} \propto B^{6/7}/n^{2/7}. \tag{3.22}$$

Stabilization of the tearing mode is postulated to lead to an improvement in confinement, and (3.20) and (3.22) correspond to a power threshold for the L–H transition. In this theory, any radial electric field appearing results from the reduction in transport due to the collapse of the tearing mode island (alternatively, the reduction in island size could lead to unlocking of the island from the wall and a consequent spin-up of the plasma). As the electrons are expected to be most affected, the resulting radial electric field (required to maintain plasma neutrality) is expected to be more negative in the H-mode than the L-mode, as is observed.

3.1.4. Drift waves. Collisional drift wave turbulence has been investigated by Scott *et al* [102]. In the electrostatic limit this provides a model for the L–H transition as collisions are reduced with increasing T_{e}; this is seen in 2D and 3D simulations where a nonlinear instability, insensitive to curvature, is found. However, the results are strongly modified when electromagnetic effects are incorporated, leading to the finite-β universal mode. The finite β removes the long wavelength sink in the electrostatic model, introducing drift-Alfvén modes which are only weakly Landau-damped. Thus increasing β leads to more long wavelength activity as the instability source exceeds the sink, but also the coherence of $\tilde{\phi}$, $\tilde{n}$ and $\tilde{T}$ (the electrostatic potential, density and temperature fluctuations, respectively) reduces. This suggests a maximum in the flux occurs when

$$\beta > m_{\mathrm{e}}/m_{\mathrm{i}} \qquad \text{i.e. } T_{\mathrm{crit}} \propto B^2/n. \tag{3.23}$$

This allows an L–H bifurcation; the theory has been compared with ASDEX Upgrade data. Later calculations indicate this result may be misleading but a bifurcation does appear for warm ion simulations when [103]

$$\mathrm{d}(\ln T)/\mathrm{d}(\ln p) > 1/2. \tag{3.24}$$

The code used by Scott *et al* includes the drift-resistive ballooning modes invoked by Drake and co-workers. Recent modifications to the code [104] show that it can produce a similar dependence of transport on β to that found by Rogers and Drake. However, detailed comparison with edge parameters at the L–H transition in ASDEX Upgrade, using realistic magnetic geometry, indicates these lie in a region of β, near the ideal ballooning limit, where the predicted transport fluxes are increasing with β, which is not consistent with a transport bifurcation (it should be remarked that calculations of ideal ballooning stability can be very sensitive to equilibrium properties at the plasma edge, such as inclusion of the bootstrap current). As a result, Scott envisages that the externally imposed sheared radial electric field arising from matching that in the core, which balances the ion pressure gradient as in (2.38), to that determined by sheath boundary conditions in the SOL, $E_r' \sim (3\text{–}4)T_{\mathrm{e}}'/e$, suppresses the turbulence and leads to the L–H transition.

Drift-Alfvén turbulence has been studied analytically by Kerner and co-workers [105, 106], stimulated by experimental data that suggests the L–H transition is related to β and the presence of electron drift wave turbulence at the plasma edge. Using a gyro-kinetic model for ions and a dissipative fluid electron model, quasi-linear estimates of the resulting turbulent diffusivities have been made. These are expressed in terms of the five relevant dimensionless edge parameters: η_{e}, $\tau = T_{\mathrm{e}}/T_{\mathrm{i}}$, $\hat{\beta} = (m_{\mathrm{i}}/m_{\mathrm{e}})\beta$, $\hat{\nu} = \nu_{\mathrm{e}} L_p/C_{\mathrm{s}}$ and $\mu = k_{\parallel} V_{\mathrm{Th\,e}} L_p/C_{\mathrm{s}}$, where $k_{\parallel}$ is the parallel wavenumber. Thus

$$D \sim \frac{D_{\mathrm{GB}}}{\sqrt{\mu}} f(\beta_n, \nu_n) \tag{3.25}$$

where $\beta_n = \hat{\beta}/\mu$, $\nu_n = \hat{\nu}/\mu^{1/2}$, $D_{GB} \sim \rho_s^2 C_s/L_p$ and

$$f = \frac{\nu_{cr}^{1/3}[1 + (\nu_n/\nu_{cr})^2]^{1/2}}{[1/\nu_{cr}^2 + (\nu_n/\nu_{cr})^{4/3}]^{1/2}} \tag{3.26}$$

with $\nu_{cr} = (1 + \beta_n^2)^{-3/2}$. The parameters β_n and ν_n are essentially equivalent to α and α_{dia}, respectively, of the model of Rogers and Drake ($\nu_n \propto 1/\alpha_{dia}$). Analysis of the behaviour of f shows that there is a transition to lower transport, i.e. an L–H transition, when

$$\beta_n > 1 + \nu_n^{2/3} \tag{3.27}$$

as shown in figure 16. To express this in terms of plasma parameters, one needs to determine L_p; this can be assumed to be continuous across the separatrix and hence determined by the SOL width, Δ_{SOL}, with different scalings for a collisionless and collisional SOL. For example, in the collisionless limit ($\nu_n < 1$, collisionless SOL)

$$\beta\left(\frac{Rq}{\rho_s}\right)^{4/7}\left(\frac{m_i}{m_e}\right)^{5/7} \gg 1 \tag{3.28}$$

or

$$T_e \geqslant T_{e\,crit} \propto \frac{B^2}{n^{7/5}(Rq)^{4/5}A_i^{3/5}} \tag{3.29}$$

while in the collisional limit ($\nu_n > 1$, collisional SOL)

$$\beta\left(\frac{Rq}{\rho_s}\right)^{4/5}\left(\frac{V_{Th\,e}}{\nu_e Rq}\right)^{6/5}\left(\frac{m_i}{m_e}\right)^{1/3} \gg 1 \tag{3.30}$$

or

$$T_e \geqslant T_{e\,crit} \propto n^{1/15}(Rq)^{2/15}B^{2/5}A_i^{1/45}. \tag{3.31}$$

These results have been compared with DIII-D data by Carlstrom *et al* [83]: while β_n has the correct order of magnitude it does not discriminate between L-modes in general and those about to undergo a transition, and there is no correlation of the transition criterion with ν_n.

Kerner *et al* [107] have built on the idea that drift wave transport relative to the magnetic surfaces in the collisionless regime, is only effective for fluctuations with $k_\perp \delta_e > 1$, where δ_e is the collisionless skin depth. Since typically $k_\perp \rho_s \sim 1$, transport is suppressed for $\rho_s/\delta_e > 1$, or

$$\beta_e > m_e/m_i. \tag{3.32}$$

To translate this into a power threshold they use the local energy balance at the plasma edge, assuming n and T have similar profiles,

$$\frac{P}{Sn} \sim \frac{\chi_\perp T}{L_n} \tag{3.33}$$

with $\chi_\perp$ assumed to be Bohm-like (since the edge transport is assumed to be due to electron drift wave turbulence with $k_r \sim (L_n\rho_s)^{-1/2} \gg k_\theta \sim \rho_s^{-1}$). Consideration of electron and neutral particle balances at the edge, assuming recycling is of order unity, yields an expression for L_n

$$L_n \sim (D_0/n_e\langle\sigma_{ion}v\rangle)^{1/2} \tag{3.34}$$

where the neutral particle diffusion coefficient is estimated as

$$D_0 \sim \frac{T}{m_i n_e \langle\sigma_{cx}v\rangle} \tag{3.35}$$

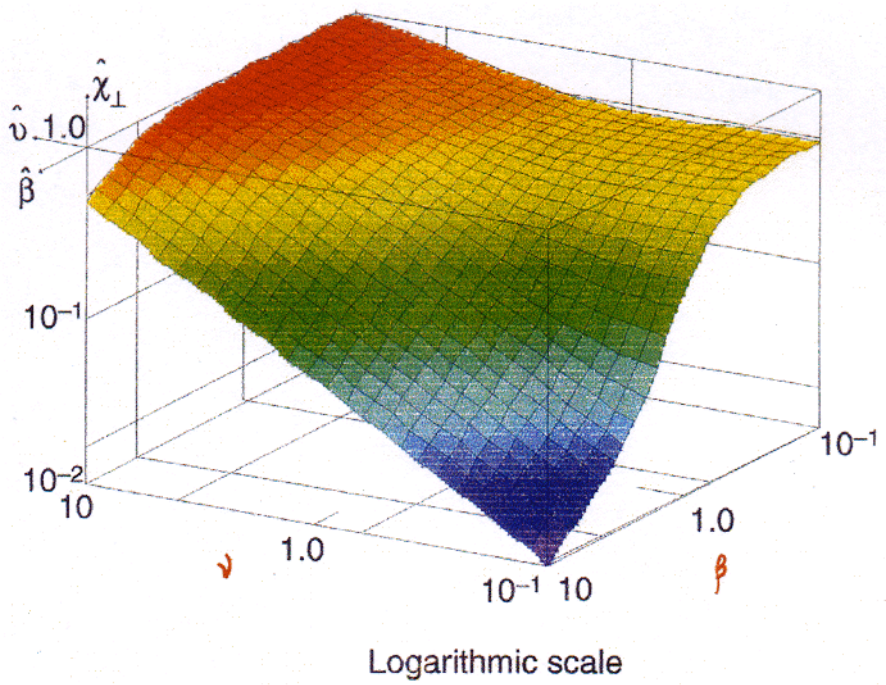

Figure 16. The normalized thermal diffusivity, $\hat{\chi}_\perp$, arising from the drift-Alfvén turbulence theory of Pogutse and Igitkhanov [106], as a function of the normalized β and collisionality parameters, $\hat{\beta}$ and $\hat{\nu}$, respectively.

and $\langle\sigma_{\rm ion}v\rangle$ and $\langle\sigma_{\rm cx}v\rangle$ are ionization and charge exchange rates, respectively. Assuming

$$\langle\sigma_{\rm ion}v\rangle = \frac{C_{\rm ion}}{\sqrt{T}}\phi_{\rm ion}\left(\frac{E_0}{T}\right) \qquad \langle\sigma_{\rm cx}v\rangle = \frac{C_{\rm cx}}{\sqrt{m_{\rm i}}}\phi_{\rm cx}\left(\frac{E_0}{T}\right) \tag{3.36}$$

where $C_{\rm ion}$ and $C_{\rm cx}$ are constants and $\phi_{\rm ion}$ and $\phi_{\rm cx}$ are weak functions of E_0/T with E_0 an ionization energy, (3.32)–(3.36) lead to

$$P_{\rm Th} \propto \frac{Sn_{\rm e}^{3/4}B^{3/2}}{A_{\rm i}}\phi\left(\frac{E_0 n A_{\rm i}}{B^2}\right) \tag{3.37}$$

where $\phi = \sqrt{\phi_{\rm ion}\phi_{\rm cx}}$ is a slowly varying function. A similar result,

$$P_{\rm Th} \propto \frac{Sn_{\rm e}^{1/2}B^2}{A_{\rm i}^{5/4}}\phi_{\rm cx}^{1/2}\left(\frac{E_0 n A_{\rm i}}{B^2}\right) \tag{3.38}$$

follows if it is instead assumed that $\langle\sigma_{\rm ion}v\rangle$ is approximately constant. These scalings of $P_{\rm Th}$ with S, $n_{\rm e}$, B and $A_{\rm i}$ are similar to the experimental observations; the more fundamental relation (3.32) is also broadly consistent with observations of edge parameters at the L–H transition.

Drift wave instabilities driven by neutral particle effects have been considered by Rogister [108]. These are hybrid drift/Kelvin–Helmholtz instabilities due to the steep radial gradients at the edge and they are assumed to generate an associated magnetic island belt. This offers a picture for the L–H transition: the magnetic island belt (with $m = q_a$, the edge value of q, and $n = 1$) provides a path for dumping the confined plasma onto the separatrix, implying a

plateau in the density profile. Consideration of particle and energy balances and the instability criterion at the plasma edge leads to a prediction for the separatrix temperature $T_{\mathrm{e\,sep}}$

$$T_{\mathrm{e\,sep}} = 2.0[A_{\mathrm{i}}^{-1} P_{\mathrm{con}} B^{-1} I^3 T_0^{1/2} \bar{n}^{-2} a^{-5} R]^{2/5} \tag{3.39}$$

where A_{i} is the ion mass in AMU, T_0 is the neutral temperature, P_{con} is the convected power and units are 10 eV, m, MW, T, MA, 10^{20} m^{-3}. The magnetic fluctuation level, $\tilde{b_r}$, needed to exhaust the power by transport along the perturbed magnetic fields is

$$\tilde{b_r}/B = (0.53/Nq)10^{-5} Z_{\mathrm{eff}} A_{\mathrm{i}}^{7/5} T_0^{-7/10} (q/a)^{12/5} Hu^{14/5} P_{\mathrm{con}}^{-2/5} \tag{3.40}$$

where N is the number of collector plates around the poloidal cross section and $Hu = \pi a^2 n_{\mathrm{e}}/I$ is the Hugill parameter. If the power increases, then the value of $\tilde{b_r}$ needed to exhaust the power falls, so that the island chain no longer reaches the separatrix. The neutral particle source is then removed, the related magnetic fluctuations and transport vanish and a transition to the H-mode occurs. This transition criterion scales as

$$\rho_{*\mathrm{s}} \propto \left(\frac{\ell_{\mathrm{n}}}{a\hat{\nu}_{*\mathrm{e}}}\right)^{1/2} \qquad \text{or} \qquad T_{\mathrm{e\,crit}} \propto (n/B)^2 (Rq/a) \tag{3.41}$$

where ℓ_{n} is the neutral particle mean free path. Radial electric fields play no causal role in this mechanism.

3.2. Scrape-off layer region

3.2.1. Resistive interchanges. Pogutse and coworkers [109, 110] have studied the nonlinear evolution of the resistive flute-like interchange instability in the SOL and found it can lead to a bifurcation in transport there, as shown in figure 17. In the stability analysis of these modes parallel dissipation along the field lines to the divertor plates is included. Due to the lack of closed flux surfaces, instabilities in the SOL are basically two dimensional, having the characteristics of flute-like instabilities in open systems. Since the destabilizing curvature is not averaged over a surface in the SOL, these modes may be more unstable than those within the LCFS. However, the parallel conductivity provides an additional stabilizing effect and the final result is determined by the balance of these two effects. The nonlinear equations governing this electrostatic instability are the vorticity equation, a parallel Ohm's law with a parallel pressure gradient and the continuity equation with diffusion coefficients $D_{\parallel}$ and $D_{\perp}$; an isothermal approximation is used. Assuming that β is below the ideal threshold in the SOL ($\beta < \epsilon/(\pi q)^2$), there remains a slower dissipative linear instability. 2D nonlinear simulations of these resistive interchange modes show that the resulting turbulence drives poloidal flows, which on dimensional grounds scale as $V_\theta \sim C_{\mathrm{s}}(\Delta_{\mathrm{SOL}}/R)^{1/2}$, and leads to a cross-field diffusion which can be estimated as

$$D_\perp \sim \frac{L_\parallel^2}{C_{\mathrm{A}}^2} \frac{C_{\mathrm{s}}^2 D_{\mathrm{M}}}{\Delta_{\mathrm{SOL}} R} \qquad D_M = \frac{1}{\mu_0 \sigma} \tag{3.42}$$

where σ is the plasma conductivity and $L_\parallel$ is the distance to the divertor plates. The electrostatic potential fluctuations, $\tilde{\phi}$, at the edge are found to satisfy $e\tilde{\phi}/T_{\mathrm{e}} > \tilde{n}/n$, unlike drift waves, and propagate in the $\omega_{*\mathrm{i}}$ direction. The authors also derived a simplified set of model equations for the nonlinear evolution of the spatially averaged shear flow, density gradient and fluctuation level; these were shown to represent successfully the results of simulations of the full nonlinear system. An alternative simplification, namely a truncation with five modes which produces a Lorenz model system, was also considered; this too leads to equilibrium flow generation above

a threshold value of a certain parameter which increases with temperature. This condition can be written as

$$\beta > 10\frac{\Delta_{\rm SOL}R}{L_\parallel^2}\frac{\mu_\perp}{D_{\rm M}}. \tag{3.43}$$

If one assumes the cross-field viscosity, $\mu_\perp$, is due to banana ion-orbit loss, i.e. $\mu_\perp \sim \epsilon^{1/2}\nu_{\rm ii}\rho_{\rm pi}\Delta_{\rm SOL}$, this threshold condition becomes

$$\rho_{\rm ps} > 10\left(\frac{m_{\rm i}}{m_{\rm e}}\right)^{1/2}\frac{\Delta_{\rm SOL}^2}{R\epsilon^{3/2}}\frac{T_{\rm e}}{T_{\rm i}}. \tag{3.44}$$

When the divertor end-plate sheath resistivity dominates the volume resistivity (i.e. $\nu_{\rm ei} \to (V_{\rm Th\,e}/L_\parallel)(m_{\rm i}/m_{\rm e})^{1/2}$ in $D_{\rm M}$), as is likely in higher temperature plasmas, and one takes the corresponding gyro-Bohm estimate for $\mu_\perp$ with $\mu_\perp \sim D_\perp$, i.e.

$$\mu_\perp \sim D_\perp \sim \frac{L_\parallel}{R}\frac{C_{\rm s}\rho_{\rm s}^2}{\Delta_{\rm SOL}} \tag{3.45}$$

it is found that condition (3.43) is replaced by

$$\Delta_{\rm SOL} < 0.1\rho_{\rm s}\left(\frac{R}{\rho_{\rm s}}\right)^{1/3}. \tag{3.46}$$

This work has been carried forward by Cordey *et al* [110] who have made dimensional estimates of resistive MHD drift/interchange turbulence in the SOL. The theory ignores electron temperature gradients but allows unequal electron and ion parallel currents. The steep radial gradients in the SOL ($\Delta_{\rm SOL} \sim$ few $\rho_{\rm s}$) lead to stabilization, a drop in cross-field diffusivity and a L–H bifurcation. The resistive interchange branch is found to be stable if

$$\frac{\rho_{\rm s}}{\Delta_{\rm SOL}} > C_1\sqrt{\frac{\Delta_{\rm SOL}}{R}} \tag{3.47}$$

which is similar to result (3.46), and the drift branch is stable if

$$\frac{\rho_{\rm s}}{\Delta_{\rm SOL}} > C_2\left(\frac{\Delta_{\rm SOL}}{L_\parallel}\right)^{1/3}. \tag{3.48}$$

In order to account for short wavelength modes and nonlinear effects these conditions are replaced by more robust estimates such as

$$\rho_{\rm s} > C_1\Delta_{\rm SOL} \qquad \rho_{\rm ps} > C_2\Delta_{\rm SOL} \tag{3.49}$$

corresponding to

$$T_{\rm e} \geqslant T_{\rm e\,crit} \propto \Delta_{\rm SOL}^2 B^2. \tag{3.50}$$

Allowing for SOL energy balances they find that, for the resistive interchange mode,

$$\frac{P_{\rm Th}}{nS} \propto B^3 f(n, R, L_\parallel) \tag{3.51}$$

in the collisionless limit. In the collisional case for a single-null divertor (SND)

$$\frac{P_{\rm Th}}{nS} \propto \frac{n^3}{B}\left(\frac{L_\parallel^2}{R}\right)^4 \tag{3.52}$$

and for a double-null configuration (DND)

$$\frac{P_{\rm Th}}{nS} \propto \left(\frac{L_\parallel^2}{R}\right)^{8/5} n^{3/5}L_\parallel^{-2/5}B^{3/5}. \tag{3.53}$$

For the drift wave branch

$$\frac{P_{\mathrm{Th}}}{nS} \propto B^3 L_{\parallel}^3 \tag{3.54}$$

in the collisionless case and

$$\frac{P_{\mathrm{Th}}}{nS} \propto n^{1/2} L_{\parallel}^{3/2} B \tag{3.55}$$

in the collisional one.

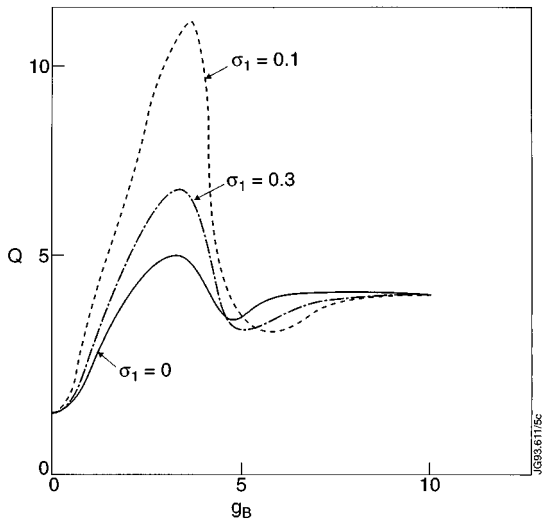

Figure 17. Dependence of the time-averaged particle flux at the boundary, Q, on the parameter g_{B} (labelling the curvature of the magnetic field) for different values of the conductivity, σ_1, from Pogutse *et al* [109].

The influence of the ion-∇B drift direction has been addressed in two publications. Chankin and Stangeby [111] have shown that when this drift is towards a SND X-point, the poloidal variation in pressure drives a radial current inwards which helps the L–H transition. This is significant for $\Delta_{\mathrm{SOL}} \sim \rho_{\mathrm{pi}}$ and increases with inverse aspect ratio, ϵ. Cordey *et al* [112] have shown that the direction of parallel current, $j_{\parallel}$, in the SOL affects the sheath resistance for interchange modes in a SND. As a result, the predicted $\chi_{\perp}$ increases with $j_{\parallel}$ by a factor of two to four. Experimentally $j_{\parallel}$ is found to be positive for ion-∇B drifts away from the X-point. Thus, in this situation Δ_{SOL} increases and it is found that the threshold power can be up to five times greater than for the other ion-∇B drift direction. More precisely, it is found that

$$P_{\mathrm{Th}}/nS \propto f(u)^{8/5} n^{3/5} B^{3/5} q^3 R \tag{3.56}$$

where $u = j_{\parallel}/enC_{\mathrm{s}}$ and f increases by a factor $\sim$2 when u varies between -1 and +1. For detached discharges there is less asymmetry in $j_{\parallel}$ and less dependence on the ion-∇B drift direction.

3.2.2. Electron temperature gradient modes. The electron temperature gradient instability and associated turbulent transport in the SOL have been considered by Berk and co-workers [113, 114]. Cohen and Xu [115] have considered the stabilizing influence of increased radial wavenumbers on the related conducting plate, drift-curvature modes in the SOL; this effect arises from the polarization current. If these modes determine the cross-field transport in the

SOL, their stabilization reduces $\Delta_{\rm SOL}$; the increased drive resulting from the steeper gradients does not change this result. Consideration of SOL energy balances with a mixing length estimate for the turbulent transport due to these modes leads to two solutions for $\Delta_{\rm SOL}$—one, $\Delta^{\rm L}_{\rm SOL}$, stable (the L-mode), one unstable. Inclusion of more physics (finite-β, finite parallel wavenumber, parallel velocity shear) can lead to suppression of transport at higher electron temperatures and the appearance of a third stable solution, $\Delta^{\rm H}_{\rm SOL}$ (the H-mode). Typically $\Delta^{\rm H}_{\rm SOL} \sim (1/4\text{–}1/2)\Delta^{\rm L}_{\rm SOL}$. The condition for this to occur is

$$K \equiv \beta^{1/2}(L_\parallel/L_{T_{\rm e}})^{1/3} > K_{\rm crit} \tag{3.57}$$

and corresponds to a power threshold scaling as

$$P_{\rm Th} \propto A_{\rm i}^{-0.99} B^{0.74} n^{0.75} R L_{\rm pol}^{0.68} \tag{3.58}$$

where $L_{\rm pol}$ is the poloidal length of the separatrix. Simulations in 2D have supported these results. This picture allows both SOL and core to provide a trigger: a steeper radial electric field in the SOL can cause turbulence suppression in the core; the heat flux from the core can affect the SOL. The model predicts that E_r is more positive in the SOL and more negative in the core than is found from most other models.

When $L_{T_{\rm e}}$ in (3.57) is estimated from SOL power balance using the cross-field $\chi_{\rm e}$ arising from the electron temperature gradient turbulence [114], one finds that this condition can be expressed as a critical β

$$\beta_{\rm crit} \propto \rho_{*\rm s}^{2/5}\left(\frac{a}{L_\parallel}\right)^{2/5}\left(\frac{T_{\rm e}}{T_{\rm i}}\right)^{2/15}\left(\frac{m_{\rm e}}{m_{\rm i}}\right)^{1/10}. \tag{3.59}$$

3.2.3. Drift waves. A wide ranging discussion of instabilities and transport in the SOL has been given by Chankin [116] making use of dimensional analysis. One expects transport to be impeded when the skin depth is less than the perpendicular wavelength, $k_\perp$, of the drift waves. In the collisional regime, appropriate to the SOL at medium to high densities, this occurs when

$$k_\perp^{-1} > \sqrt{\frac{2}{\mu_0 \sigma \omega_*}} \tag{3.60}$$

or

$$\beta > \frac{\nu_{\rm ei}}{\omega_*}(k_\perp \rho_{\rm s})^2 \frac{m_{\rm e}}{m_{\rm i}}. \tag{3.61}$$

Using a self-consistent model for SOL transport and $k_\perp \rho_{\rm s} =$ constant, this yields the condition

$$\frac{A_{\rm i}^{1/8} T_{\rm e}^{13/8}(T_{\rm e}+T_{\rm i})^{3/8}}{Z_{\rm eff}^{3/4} B (qR)^{1/4}} > \text{constant} \tag{3.62}$$

i.e.

$$\beta_{\rm e} > \beta_{\rm e\,crit} \propto \hat{\nu}_{*\rm e}\rho_{*\rm s}^{2/3}\left(\frac{\epsilon}{q}\right)^{2/3}\left(1+\frac{T_{\rm i}}{T_{\rm e}}\right)^{-1/2} A_{\rm i}^{-1/2}. \tag{3.63}$$

At this point the corresponding anomalous diffusivity begins to decrease, allowing a bifurcation; this represents a temperature of 10–85 eV for JET. The predicted threshold power can be written

$$P_{\rm Th} = F_{\rm p} n B R^\gamma \tag{3.64}$$

where the form factor $F_{\rm p}$ is given by

$$F_{\rm p} = R^{2-\gamma}\left[\frac{(T_{\rm e}+\alpha T_{\rm i})^{0.6}(T_{\rm e}+T_{\rm i})^{0.3} T_{\rm e}^{0.2}}{B(qR)^{0.4}}\right]^{5/3} \tag{3.65}$$

where the ratio of heat flow in the ion to the electron channels is $\alpha T_i/T_e$. Invoking the transition criterion (3.62) and some plausible arguments about T_e and T_i, Chankin concludes that this theory requires $\gamma \simeq 1.75$ to make F_p independent of R (for the alternative assumption $k_\perp \rho_s \sim (\rho_s/a)^{1/2}$, he obtains $\gamma = 1.5$).

A more general result, avoiding the assumptions about SOL transport, is [117]

$$T^3_{e\,crit} \propto \frac{B^2 \Delta_{SOL} Z_{eff}}{A_i^{1/2}} \tag{3.66}$$

or

$$\beta_e > \beta_{e\,crit} \propto \hat{\nu}_{*e} \left(\frac{m_e}{m_i}\right)^{1/2} \frac{\Delta_{SOL}}{Rq}. \tag{3.67}$$

This scaling possesses a positive feedback through Δ_{SOL}, leading to a bifurcation possibility, as in the work of Scott [103].

At low densities a collisionless skin-depth treatment is appropriate, leading to the transition criterion

$$\beta_e > (k_\perp \rho_s)^2 \frac{m_e}{m_i} \tag{3.68}$$

resembling (3.23) and (3.32). With a self-consistent treatment of the SOL transport, this provides a low density limit

$$n_{crit} \propto A_i^{-15/16} Z_{eff}^{-3/8} \left(\frac{T_e}{T_e + T_i}\right)^{13/16} \frac{B^{3/2}}{(qR)^{1/8}} \tag{3.69}$$

but tends to be much lower than observed in experiments. Equation (3.68) provides a more stringent critical temperature than (3.61) or (3.67).

In a more direct treatment in a later paper [118], it was noted that the suppression occurred when the collisional skin depth δ_e was less than a typical perpendicular wavelength of the drift waves, i.e. ρ_s, corresponding to the interaction of drift and Alfvén waves. The condition $\delta_e < \rho_s$ leads to (3.32) again.

4. Models involving sheared radial electric field and flows

It is possible to classify the models involving the suppression of turbulence by sheared radial electric fields, E_r, according to the processes generating E_r: poloidal flow drives and damping, toroidal flows and transport processes. In addition, one can separate models according to whether or not they treat the evolution of gradients and fluctuations on the same footing, i.e. whether they introduce dynamical equations for the fluctuation levels which then control the transport coefficients.

4.1. Poloidal torque balance

These theories involve a balance of torques driven by radial currents (arising from non-ambipolar fluxes or ion-orbit loss, Stringer spin-up, ion thermal forces as in neoclassical theory and Reynolds stresses) against poloidal viscosity or damping (arising from neoclassical theory, turbulence or charge exchange collisions with neutral particles). The balance of these torques can lead to multiple solutions for the poloidal flow (or radial electric field); these solutions can be associated with situations of high and low transport, i.e. L- and H-modes.

4.1.1. Ion-orbit loss theories. The earliest model which predicts a bifurcation in E_r as the tokamak heating power is increased is due to Itoh and Itoh [69]. They appealed to ion-orbit loss at the tokamak edge and balanced this against a non-ambipolar electron diffusion to derive an expression for the equilibrium radial electric field, as illustrated in figure 18 which is from [37]. The electron diffusion is calculated on the basis that it results from microturbulence, although the specific origin of this turbulence is not addressed in this first work. (The non-ambipolarity results from the emission of wave momentum which is not absorbed in the plasma but lost to the SOL.) The balance of the non-ambipolar fluxes results in a nonlinear equation for the electric field which has a variety of solutions depending on the value of the parameter λ_e, where

$$\lambda_e = -\frac{T_e}{T_i}\rho_{pi}\left(\frac{n_e'}{n_e} + c_e\frac{T_e'}{T_e}\right) \tag{4.1}$$

with c_e an O(1) constant whose actual value depends on the nature of the microturbulence. For $\lambda_e < \lambda_c$ (where $\lambda_c \simeq \rho_{pi}^2\nu_{ii}/\epsilon^{1/2}D_e$ and D_e is the electron diffusion coefficient) only one solution exists and this corresponds to a low (negative) electric field. As λ_e is increased so that $\lambda_e \simeq \lambda_c$, two new solutions exist with higher E_r; finally, for $\lambda_e > \lambda_c$, only the highest E_r solution exists. Thus, as λ_e increases beyond λ_c, the plasma is forced to jump to the high E_r solution so that the threshold condition corresponds to

$$\lambda_e = \lambda_c \qquad \text{i.e. } \frac{\epsilon^{1/2}D_e\tau}{\nu_{ii}\rho_{pi}L_n}(1 + c_e\eta_e) \gtrsim 1. \tag{4.2}$$

In general, this is equivalent to ν_{*i} being below a critical value. It should be noted that when this threshold is exceeded, the resulting radial electric field is positive, which is at odds with experimental measurements. Typically, λ_c is of order unity so that a more direct necessary condition for the bifurcation is

$$\rho_{pi}/L_n \gtrsim 1 \tag{4.3}$$

where L_n is the density gradient length; this is similar to an earlier result by Ohkawa and Hinton [119]. A later theory [120] included the effects of the radial derivative of the radial electric field and then the agreement with experimental observation is improved, although the above scalings for the threshold criterion are not significantly affected. It was found that for a negative radial electric field, E_r, its radial derivative, E_r', flips from being small and positive in the L-mode to large and negative in the H-mode. It is the jump in E_r' which is responsible for the confinement improvement and there is an associated reduction in the turbulence level predicted at the time of the transition. The theory also exhibits a 'hysteresis' effect, in which the back transition, H–L, occurs at lower threshold power than the forward transition. A net poloidal flow of plasma does not necessarily result from this theory, although it is not excluded.

In a subsequent paper [121] the generation of toroidal flow by ion-orbit loss was considered, but the results were similar (the paper also considered the role of neutral particles and impurities—this will be discussed below in subsection 4.1.2). A result for the threshold power in the absence of neutrals was derived using a SOL power balance

$$P_{Th} \propto Z^{1.5}B^{1.4}R^{1.2}a^{0.5}n^{0.5}A_i^{-1.2}I^{-0.7}. \tag{4.4}$$

An extension of the theory to a situation where additional heating generates energetic electrons, which are then lost due to magnetic field ripple trapping, has been made [122]. A bifurcation condition

$$\frac{n_h}{n_i}\left(\frac{T_h}{T_i}\right)^{7/2} > 0.17\frac{\epsilon^3}{\lambda_h\delta^{3/2}}\left(\frac{m_i}{m_e}\right)^{1/2}\nu_{*i}^2 \tag{4.5}$$

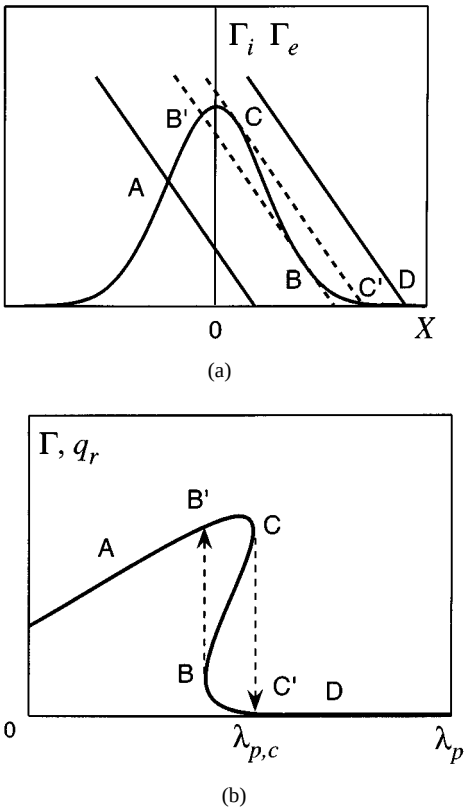

Figure 18. An example of a hard transition arising from the balance between ion-orbit loss and the bipolar electron fluxes, Γ_i and Γ_e, respectively, as functions of the normalized radial electric field $X = e\rho_{pi}\, E_r/T_i$. In (a) the 'Gaussian-shaped' curve is Γ_i and the straight lines are Γ_e. When gradients are weak, as measured by λ_p in (b), these lines cross at A, corresponding to a large flux; as the gradient increases the solution moves from A through B′ to C. At the critical point C a transition to C′ occurs and the solution moves to D with further increase of gradients. When gradients are decreased, the solution moves from D to C′ to B, with a back transition from B to B′ (see p 250 in [37]).

where $\lambda_h = \rho_{pi} n_h'/n_h$, is found, corresponding to a power threshold

$$P_{Th} = 10\epsilon^2 \frac{T_h}{T_i} \frac{\rho_{pi}}{a} \nu_i n_i T_i V. \tag{4.6}$$

Here h labels the hot electrons, δ is the ripple amplitude and V the plasma volume.

A specific transport model, the current diffusive ballooning mode (CDBM) model, to determine D_e has been examined by Itoh *et al* [63, 123, 124]. The model, which is based on a 'resistive' ballooning mode turbulence, but where dissipation arises from renormalized viscosity and current diffusion coefficients associated with electron inertia (and is supported by a numerical simulation of the turbulence [125, 126]), includes a reduction in the transport for larger E_r', independent of its sign. Using the results from this transport model, the threshold for the L–H transition is [127]

$$\left(\frac{a}{m_i}\right)^{1/2} \frac{m_e}{e^2 B^2} \frac{a_0 q^2}{f(s)} \frac{|dT/dr|^{5/2}}{\rho_{pi}\nu_{ii} T} = 1 \tag{4.7}$$

where a_0 is a numerical coefficient and $f(s)$ is a function of the magnetic shear, s, which depends on the mode structure. In terms of dimensionless variables, this condition also corresponds to $\nu_{*\mathrm{i}}$ falling below a critical value. It is interesting that when this model is incorporated in a transport code which models the self-consistent evolution of p' and E_r', it can produce a stable edge transport barrier [128], as shown in figure 19.

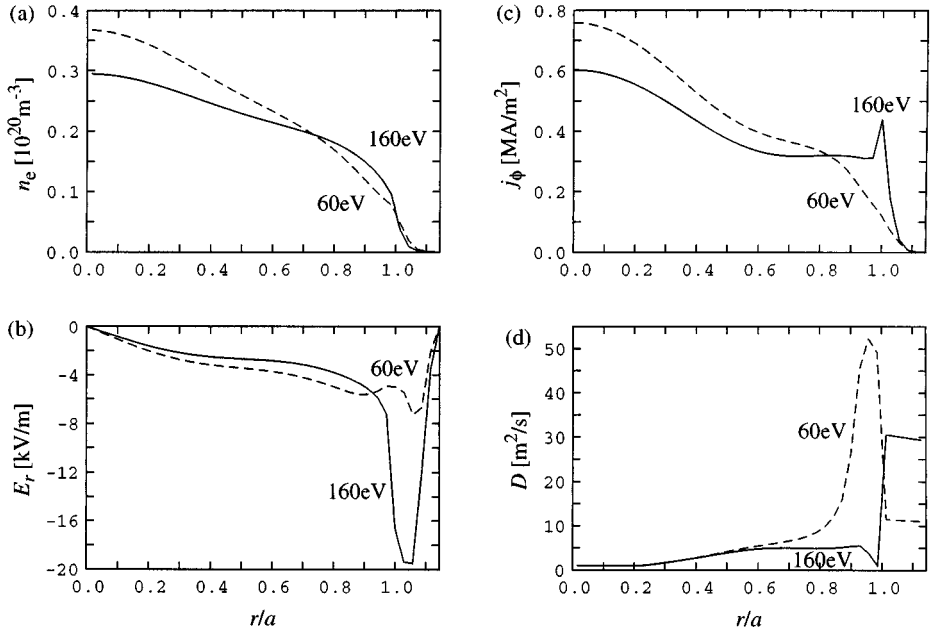

Figure 19. Radial profiles from simulations with the CDBM transport model: (a) electron density, n_e, (b) radial electric field, E_r, (c) toroidal current, j_ϕ, (d) diffusivity, D. The full curves are for the case of high edge temperature $T_\mathrm{edge} = 160$ eV, the dashed curves for low edge temperature $T_\mathrm{edge} = 60$ eV (see p 293 in [37]).

The model of Shaing and Crume [68] also appealed to ion-orbit loss for the generation of a radial electric field. These authors balanced the change in poloidal momentum, resulting from loss of the faster ions in the tail of a Maxwellian velocity distribution, against the neoclassical poloidal viscous damping ('magnetic pumping'), which is dominated by the slower thermal ions. The resulting equation yields solutions for the poloidal flow velocity which exhibit a bifurcation as the temperature is increased: a low velocity (L-mode) solution and a high velocity (H-mode) solution. The improvement in confinement is assumed to result from the effect of the sheared flow on the correlation length of the turbulence. The threshold conditions correspond to the point at which the bifurcation occurs, which can again be expressed as falling below a critical ion collisionality, $\nu_{*\mathrm{i}}$, or

$$\frac{nRq}{\epsilon^{3/2}T_\mathrm{i}^2} < c \tag{4.8}$$

where c is a constant. Predictions of the theory include a poloidal spin-up of the plasma and an associated negative radial electric field within a region at the plasma edge of width $\epsilon^{1/2}\rho_\mathrm{pi}/\sqrt{s}$; a hysteresis effect is also predicted. The original theory was based on the assumption that the ions take up a Maxwellian velocity distribution, which therefore predicts that high collisionality plasmas, $\nu_{*\mathrm{i}} \gtrsim 1$, should not exhibit an H-mode. However, in the presence of a fast ion

source (e.g. neutral beams) the Maxwellian assumption is no longer valid. The same threshold criterion as (4.8) holds, although the parameters are now to be interpreted as those of the fast ions, not the bulk (Shaing and Christenson [129]).

Shaing and Zhang [130] have modified the ion-orbit-loss model of Shaing and Crume to include the stress arising from the interaction of a magnetic field perturbation, b_r, with the vacuum vessel, in the equation for the ion poloidal velocity. Relative to the orbit-loss term they find an effective stress

$$\pi_{\rm eff} = \frac{C_{\rm A}^2 a\omega\tau_{\rm w}(r_{\rm s}/r_{\rm w})^{2m}(b_r/B)^2}{V_{\rm Th\,i}^2 w(1+(\omega\tau_{\rm w})^2[1-(r_{\rm s}/r_{\rm w})^{2m}]^2)} \tag{4.9}$$

which can remove the possibility of a bifurcation in poloidal flow leading to sheared radial electric fields. Here w is the magnetic island width arising from b_r, ω is the laboratory frame frequency, $\tau_{\rm w}$ is the wall time constant, $r_{\rm s}$ is the resonant surface for the island and $r_{\rm w}$ the wall radius. This expression has the consequence that increasing b_r increases $P_{\rm Th}$ for the L–H transition; conversely, for a given b_r, increasing n or $T_{\rm i}$ assists the transition. Furthermore, the bifurcated flow is smaller (the poloidal Mach number is $M_{\rm p} \sim 0.3$, rather than $\sim$1.0). These effects are significant when $\pi_{\rm eff} \geqslant 1$, which can occur typically for $b_r/B \sim 4\times10^{-4}$.

A number of other contributions to ion-orbit-loss theories have been made. Hinton and Kim [131] have demonstrated theoretically how to link E_r from the SOL to the core across the separatrix, where a radial current, j_r, must flow; this allows divertor biasing to affect the core. Miyamoto [132] has considered ion-orbit loss in a divertor/separatrix geometry and demonstrated that bifurcations in electrostatic potential are possible. In a complementary study, Krasheninnikov and Yushmanov [133] have shown that a potential step can increase ion-orbit loss, allowing an unstable growth of potential and an L–H transition. Kim *et al* [134] and Hinton *et al* [135] have noted that orbit squeezing, due to electric field gradients comparable with the ion poloidal Larmor radius (i.e. when $S = 1 - m_{\rm i}E_r'/eB_\theta^2 > 1$), can increase ion poloidal flows (i.e. $V_{\theta{\rm i}} \sim V_{*{\rm i}}$, the ion diamagnetic velocity, which is reasonably consistent with observations on DIII-D), thus modifying the effect of poloidal flow damping; in addition, the same effect reduces the bootstrap current so that radial electric field shear can inhibit the bootstrap current drive for MHD instabilities at the plasma edge. Chang has examined ion-orbit loss at the X-point, where it is most effective since the poloidal field vanishes there [136]. He finds a critical collisionality depending on details of the X-point geometry and the conditions (e.g. neutral density) there, and a layer width $\Delta \sim \bar{\rho}_{\rm pi}$ where $\bar{\rho}_{\rm pi}$ is an average over the flux surface; thus control of these quantities could influence the transition.

4.1.2. The effects of neutral particles. Neutral particles can influence ion-orbit-loss theories in two ways: increasing both poloidal flow damping and ion-orbit losses through charge exchange collisions with ions can modify the predictions of the theories above, which only consider poloidal viscous damping. Itoh and Itoh introduced poloidal flow damping due to momentum losses from charge exchange collisions with neutral particles into their theories in [121]. This modifies the bifurcation condition (4.2), to yield

$$\frac{\lambda_{\rm e}}{\lambda_{\rm c}} = 1 + d_{\rm n}\lambda_{\rm i} \tag{4.10}$$

where

$$\lambda_{\rm i} = -\rho_{\rm pi}\left(\frac{n_{\rm i}'}{n_{\rm i}} + \frac{c_{\rm i}T_{\rm i}'}{T_{\rm i}}\right) \tag{4.11}$$

($c_{\rm i}$ is a constant of order unity) and

$$d_{\rm n} = \sqrt{\epsilon}\frac{n_{\rm o}\langle\sigma_{\rm cx}v\rangle}{\nu_{\rm ii}F}\frac{\ell_{\rm n}}{\rho_{\rm pi}} \tag{4.12}$$

with n_o the neutral density, ℓ_n the neutral penetration length, σ_{cx} the charge exchange cross section and F a form factor of order unity. This effect increases the value of λ_c needed for a bifurcation; indeed, no bifurcation is possible when

$$n_o > \frac{c\nu_{ii}}{\sqrt{\epsilon}\langle\sigma_{cx}v\rangle}\frac{\rho_{pi}}{\ell_n} \tag{4.13}$$

where $c \sim O(1)$. The two conditions (4.10) and (4.13) provide limits on both electron and neutral particle densities

$$\bar{n}_{e_{19}} > 0.029\frac{qB}{\epsilon^2\sqrt{A_i}}\frac{n_{o16}}{T^{5/12}(\mathrm{eV})} \tag{4.14}$$

$$\bar{n}_{e_{19}} \geqslant \frac{0.031\epsilon^{1/4}}{A_i^{1/4}}\frac{B_p^{1/2}(\mathrm{T})}{Z}T^{19/24}(\mathrm{eV})n_{o16}^{1/2} \tag{4.15}$$

where $\bar{n}_e$ is in units 10^{19} m^{-3}, n_o in units 10^{16} m^{-3} and B_p is the poloidal magnetic field. Neutrals were also found to increase the time for the transition to take place. This paper also considered the effects of an impurity ion (of mass m_I and charge Z_I), both in increasing ν_i through Z_{eff} and from supersonic impurity flow. The result is to increase the right-hand side of (4.10), which becomes

$$Z_{eff} + \frac{n_I m_I Z_I}{n_i m_i Z_i} + d_n\lambda_i. \tag{4.16}$$

Itoh and Itoh [137] have also related the neutral population to the nature of the wall materials, showing that the condition for the H-mode can be written

$$P(v_f)r_f < \left[\frac{\langle\sigma_{ion}v\rangle n_e + \langle\sigma_{cx}v\rangle n_i}{\langle\sigma_{recomb}v\rangle n_e + (\nu_i\rho_{pi}/\ell_{recomb})}\right]\frac{\nu_i}{\langle\sigma_{cx}v\rangle n_i}\frac{\rho_{pi}}{\ell_{recomb}} \tag{4.17}$$

where r_f is the reflection coefficient of fast neutral particles at the wall, $P(v_f)$ the probability that the neutral particle has velocity v_f, σ_{ion}, σ_{cx} and σ_{recomb} the cross sections for ionization, charge exchange and recombination of neutral particles, respectively, and ℓ_{recomb} is the mean free path for recombination. Since r_f is higher for wall materials with high atomic number, this could explain why these mitigate against the H-mode.

In a later paper [138] a more detailed investigation of the effects of neutrals near the X-point was made. Their presence was found to lead to an increase in the effective collision frequency for ion-orbit loss. Thus, for a given set of parameters, there is a critical value for the neutral density near the X-point for an L–H transition: thus 'condensed' neutrals can trigger the H-mode, which is consistent with experimental results. This neutral density can be written

$$\xi < \frac{d_o\left(\frac{1}{2}+\sqrt{\nu_{*i}}\right)^3\exp\left(\frac{1}{2}+\sqrt{\nu_{*i}}\right)}{2\left(\frac{1}{4}+\sqrt{\nu_{*i}}\right)^{3/4}\left(\frac{3}{2}+\sqrt{\nu_{*i}}\right)} \equiv \xi_c \tag{4.18}$$

where $\xi = \nu_{in_o}(X)/\omega_{bi}$, with $\nu_{in_o}(X)$ being the ion–neutral collision frequency at the X-point and ω_{bi} the ion bounce frequency, and $d_o = n_o^{main}\langle\sigma_{cx}v\rangle(1+2q^2)/(\sqrt{\epsilon}\omega_{bi}q^2)$: the factor $1+2q^2$ accounts for toroidal effects.

Shaing and Hsu [139] have considered the effect of charge exchange losses of poloidal momentum in the ion-orbit-loss model. They find that the critical parameter is $\hat{\nu} \equiv \nu_{eff}Rq/V_{Thi}$ with $\nu_{eff} = n_o\langle\sigma_{cx}v\rangle$. For example, with $\epsilon = 0.25$, $\nu_{*i} = 1.85$ and $q = 3$, the possibility of bifurcation in the poloidal flow vanishes if $\hat{\nu} = 0.014$. Thus, for a hydrogen plasma with $T_e = 100$ eV, $T_i = 400$ eV and $R = 1.67$ m, the critical value of n_o is 10^{16} m^{-3}; conversely, if n_o and ν_{*i} are held fixed this provides a critical value of T_i. Neutral particles can lead to low values of ν_{*i} being required for a bifurcation to the H-mode.

Finally, the effect of charge exchange collisions on ion orbits has been investigated by Xiao *et al* [140]. They found that a negative value of E_r produces an inward ion mobility so that a positive bias helps the H-mode. The opposite bias is less helpful, relying on detrapping and compressing of passing particle orbits. For TEXT-U parameters ($T \sim 30$ eV, $n_e \sim 2 \times 10^{18}$ m^{-3}, dn_e/d$r \sim 10^{20}$ m^{-4}), the mobility flux $\Gamma_{mob} \sim \Gamma_{an}$, where Γ_{an} is the anomalous flux.

4.1.3. Stringer spin-up. Pfirsch–Schlüter transport can drive a poloidal spin-up of the plasma (Stringer [71]). This mechanism is damped by the magnetic pumping which, for typical tokamak parameters, exceeds the drive, so that no spin-up is predicted in neoclassical theory. However, transport in tokamaks is observed to be much greater than the predictions of neoclassical theory, and this has led Hassam *et al* [70] to propose a 'spontaneous poloidal spin-up' associated with anomalous transport which is not constant on a flux surface (see figure 20 which is from [141]). Balancing this drive against the damping from magnetic pumping gives the threshold condition

$$\frac{1}{nr}\frac{\partial}{\partial r}(nr\tilde{v}_r) + \epsilon\frac{1+2q^2}{q^2}\gamma_{MP} < 0 \tag{4.19}$$

where γ_{MP} represents the magnetic pumping and $\tilde{v}_r = v_r - \langle v_r \rangle$, with v_r the radial particle flow velocity and angled brackets representing a flux surface average. In a simple model with v_r represented by a diffusive term of the form $-D(1 + \delta\cos\theta)/L_n$ and a pinch term which is constant on a flux surface (and therefore does not enter the above equation), a simplified threshold condition for the onset of the poloidal flow instability can be deduced. Furthermore, if we assume $\gamma_{MP} \propto \nu_{ii}$, this threshold condition becomes

$$\frac{\epsilon}{q^2}(1+2q^2)\nu_{ii} \lesssim \delta D\left(\frac{n''}{n} + \frac{n'}{nr}\right). \tag{4.20}$$

Confinement is assumed to improve as a result of this flow but a specific mechanism is not addressed. Hassam and Antonsen [142] have extended the original calculation to include toroidally directed, poloidally asymmetric momentum sources, but did not include diamagnetic flows or gyro-viscosity.

An analytic and numerical investigation of the Stringer spin-up mechanism within a fluid model was carried out by McCarthy *et al* [143], who noted that if turbulent velocities are comparable to diamagnetic ones, then the Stringer spin-up effect is greater than the Reynolds stress (section 4.1.5) by a factor $L_n^3/R\rho_s^2$. Their geometry was toroidally axisymmetric but included a primitive SOL model with a particle sink; a flux consisting of a poloidally asymmetric diffusive part and a pinch, and flow damping from magnetic pumping, were also used in the model. With a diffusion coefficient scaling like that from drift-resistive ballooning modes, it transpires that the self-consistent L_n scales as $A_i^{1/6}$ and the diffusion coefficient as $A_i^{-1/6}$, so that the particle flux $\Gamma \propto A_i^{-1/3}$. The L-mode is taken to correspond to strong magnetic pumping, when it is found that poloidal flow balances the diamagnetic velocity, as in neoclassical theory. For the case of low magnetic pumping, large flows in the opposite direction to the diamagnetic velocity develop, with a shear flow scale length

$$L_v \sim \left(\frac{a\rho_e}{L_n\lambda_{e\,mfp}}\right)^{1/4} L_n \tag{4.21}$$

where $\lambda_{e\,mfp}$ is the electron mean free path and ρ_e the electron Larmor radius. The L–H transition would therefore be expected to relate to a change of collisionality. It is interesting that suitable choices of the poloidal location of particle sources can be used to control the

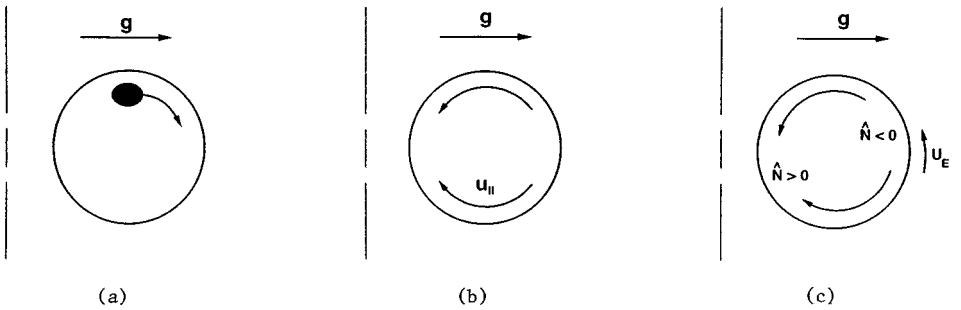

Figure 20. (a) Poloidal cross section of tokamak showing the direction of the effective gravity, g, and the pendulum-like response of a localized density enhancement in the absence of equilibrium parallel flows; (b) poloidal cross section with projection of equilibrium parallel flows, $u_{\|}$; (c) poloidal cross section with flow perturbation, u_{E}, showing the convection of parallel flows and density perturbations. A poloidal flow perturbation causes the parallel flows to shift poloidally. The convergence of these flows causes an enhancement of the density ($\hat{N} > 0$) in the lower half-plane and the divergence of these flows causes a corresponding reduction of the density ($\hat{N} < 0$) in the upper half-plane. The outward gravitational force then drives the high-density region towards the outside of the torus and the low-density region towards the inside of the torus, amplifying the 'seed' rotation [141].

character of this shear flow region, either assisting its formation or arranging for an outward radial electric field in order to exclude impurities.

The effects of a divertor X-point geometry have been considered by Strauss [144], using a dissipative reduced MHD model with viscous stresses in which poloidal variations are opposed by sound wave propagation. He found that the condition for spin-up was

$$\frac{\chi_\perp}{L_p^2}\tilde{G} > \frac{B_{\mathrm{p}}}{B}\frac{C_{\mathrm{s}}}{r} \tag{4.22}$$

where $\chi_\perp$ is the thermal diffusivity, and $\tilde{G}$ is a form factor representing the poloidal variations of the geometry ($\tilde{G} = (R^2 B_{\mathrm{p}}^2/\langle R^2 B_{\mathrm{p}}^2\rangle) - 1$, where B_{p} is the poloidal magnetic field, $\langle\rangle$ is a flux surface average and the tilde signifies the poloidal variation). For a Bohm-like diffusivity this corresponds to a critical value of ρ_*.

4.1.4. Neoclassical flows. Poloidal viscous forces in neoclassical theory produce a poloidal ion flow proportional to the ion temperature gradient

$$V_{\theta \mathrm{i}} = \frac{k}{eB}\frac{\mathrm{d}T_{\mathrm{i}}}{\mathrm{d}r} \tag{4.23}$$

where k depends on the ion collisionality, $\nu_{*\mathrm{i}}$. This results in a negative E_r, as is observed experimentally. Plasma microturbulence is expected to produce an 'anomalous' viscosity and inertia and this might be expected to affect the poloidal momentum balance equations. Rozhansky and Tendler [145] have taken these effects into account to derive an equation for the poloidal flow which balances the neoclassical viscosity with the anomalous viscosity and inertia. Their model excludes the presence of a toroidal flow. The neoclassical terms dominate for low edge temperature gradients, in which case the equation has a low poloidal flow solution (L-mode). For higher edge temperatures the poloidal flow is described by the anomalous terms which predict a much higher flow velocity; this is interpreted as the H-mode. The transition occurs when

$$\frac{\mathrm{d}^2 T_{\mathrm{i}}}{\mathrm{d}r^2} \gtrsim \sqrt{\pi}\epsilon q \frac{n(a) C_{\mathrm{s}} \tau_{\mathrm{p}}}{\bar{n} a^2 (1+2q^2)}\frac{\mathrm{d}T_{\mathrm{i}}}{\mathrm{d}r} \tag{4.24}$$

where τ_p is the particle confinement time and $n(a)$ and $\bar{n}$ are the edge and average densities, respectively.

The role of the sheared radial electric field associated with the flow (4.23) in suppressing the particle diffusivity has been investigated by Rozhansky *et al* [146, 147]. In their model there is a steep drop in the diffusion coefficient when the shear suppression parameter, as determined from the neoclassical expression for the radial electric field in terms of the density profile (ignoring $T_{\rm i}'$),

$$\kappa = \rho_{\rm pi}^2 \frac{{\rm d}^2(\ln n)}{{\rm d}r^2} \tag{4.25}$$

reaches a critical value, i.e. there is a critical value of ρ_*. Clearly this is most easily satisfied at the edge, where n is smallest. The resulting continuity equation is completed by a condition on the flux from the core and a boundary condition at the separatrix, which can represent the effect of the SOL. They solved the resulting diffusion equation and found that a L–H transition can be triggered by a change in the core density gradient; the flux must exceed a critical value which increases with $T_{\rm i}$ and decreases with n. The transition front propagates faster than a diffusion time, as shown in figure 21 which is from [148], and hysteresis is displayed. Introducing time scales τ_1 for core changes due to the formation of the transport barrier and τ_2 for the response of the SOL, this model can cause 'dithering'. The sensitivity of κ in (4.25) to the density profile means that the L–H transition can be triggered in a variety of ways: pellet injection, adiabatic compression and changes in the SOL [148].

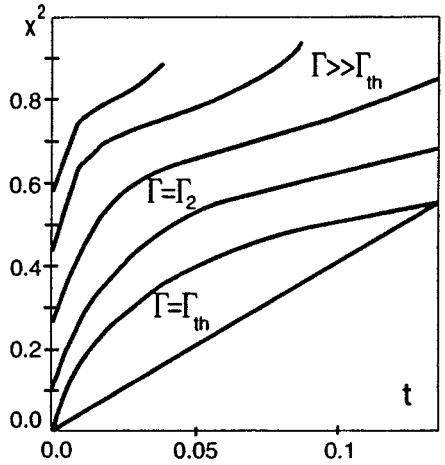

Figure 21. Propagation of the position of the front of the transport barrier, x, normalized to the barrier width, as a function of time, t (ms), parametrized by the incident particle flux, Γ. The straight line, corresponding to diffusion, $x^2 \propto t$, occurs when Γ is at the threshold value for the transition, $\Gamma_{\rm Th}$; the upper curves correspond to increasing values of Γ [148].

The velocity (4.23) has been invoked by Hinton [149] to develop a bifurcation model for the L–H transition by retaining the collisionality dependence of μ, the parallel viscosity, in the Pfirsch–Schlüter regime and keeping only contributions to $V_{\theta{\rm i}}'$ (and hence E_r') from $T_{\rm i}'$. He used a transport model

$$\chi = \chi_0 + \frac{\chi_1}{1 + \alpha V_{\theta{\rm i}}'^{\gamma}} \tag{4.26}$$

where there is a residual H-mode thermal diffusivity, χ_0, and the L-mode diffusivity, χ_1, can be suppressed by velocity shear (compare (2.36)). The value of α can be chosen to reflect

the BDT criterion, equation (2.30), for, say, drift wave turbulence and γ is a parameter. This form leads to a transport flux which exhibits a maximum as a function of $T_{\rm i}'$ when the heat flux, q_r, reaches a critical value, $q_{r\rm crit}$: this allows a bifurcation to an 'H-mode' state with higher $T_{\rm i}'$ when $q_r > q_{r\rm crit}$. Global solutions of the transport equations yield an edge region of steep gradients whose radial extent is determined by where the heat flux from the core just continues to exceed $q_{r\rm crit}$. The corresponding solutions for the energy confinement time, τ_E, display hysteresis. The model is considered to be generic; detailed predictions would require specific models for χ. However, with a model in which $\chi \propto n^2$, the corresponding threshold power for the L–H transition increases with n and B, $P_{\rm Th} \propto n^4 B$, and has a favourable isotope effect, but also inhibits a low n (and B) threshold transition.

4.1.5. Turbulent Reynolds stress and viscosity. The turbulence itself can drive flows through the Reynolds stress as first shown by Hasegawa and Wakatani [150]; an alternative derivation of the turbulent torque from the view point of the MHD dynamo is given in [151]. Indeed, the non-ambipolar electron transport in [69] can be considered from such a point of view, since it corresponds to a radial current which can produce a torque on the plasma. Diamond and Kim [72] calculated the effects of the turbulent Reynolds stress in a cylindrical geometry (see figure 22 which is from p 244 in [37]). In particular, they found that only turbulence which supports radially propagating waves is able to drive rotation (e.g. drift wave turbulence). However, since flow shear itself can lead to such propagation, this can be amplified for other types of turbulence such as resistive interchanges [152]. Another essential feature of the turbulence is that it should be radially inhomogeneous, which tends to limit rotation to the plasma edge where either (a) density and temperature gradients are sufficiently steep that they have a significant variation across a radial correlation length of the turbulence, or (b) the radial correlation length is cut off by the plasma boundary. No detailed calculations of the resulting steady-state flow are performed and no bifurcation condition is evident. The authors acknowledge that more physics would be required to explain the velocity profiles observed in the H-mode, where turbulence is suppressed and yet the $\boldsymbol{E} \times \boldsymbol{B}$ flow is *larger*, although the $p_{\rm i}'$ contribution may provide a significant part of this.

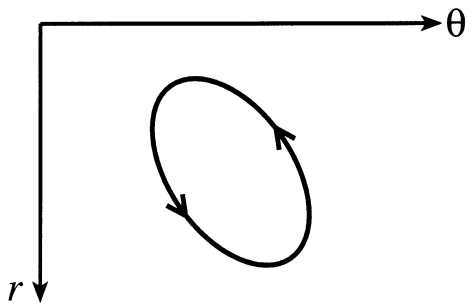

Figure 22. A flow pattern in the r–θ plane which shows a correlation between poloidal momentum, $\tilde{P}_\theta$, and radial velocity, $\tilde{V}_r$, fluctuations; these produce a net momentum flux $\langle \tilde{P}_\theta \tilde{V}_r \rangle$ (see p 244 in [37]).

The directional nature of the turbulence needed to generate a Reynolds stress means that it occurs most readily at the plasma edge (it has been measured in experiments, see figure 23 which is from [153]) and will exist over a width, Δ, related to the radial mode structure of the turbulence, although this estimate may be modified in the presence of high edge fluctuation levels. Whereas this width is likely to be on a microscopic scale, such as $\rho_{\rm i}$, in the cylindrical

approximation of the theories above, the theory of edge ballooning modes [81] shows that it could be over a larger width in toroidal geometry. In particular, for drift wave or ion temperature gradient turbulence one expects $\Delta \sim \rho_{\rm i}^{2/3} a^{1/3}$ [154, 155]. Indirect measurements of Δ on JET, based on the pedestal height and the assumption that the steep edge gradient is at the ideal MHD ballooning limit, are broadly consistent with this [156–158]; furthermore, it offers an explanation of the isotope scaling of the pedestal temperature, $T_{\rm ped}$, observed on JET [20].

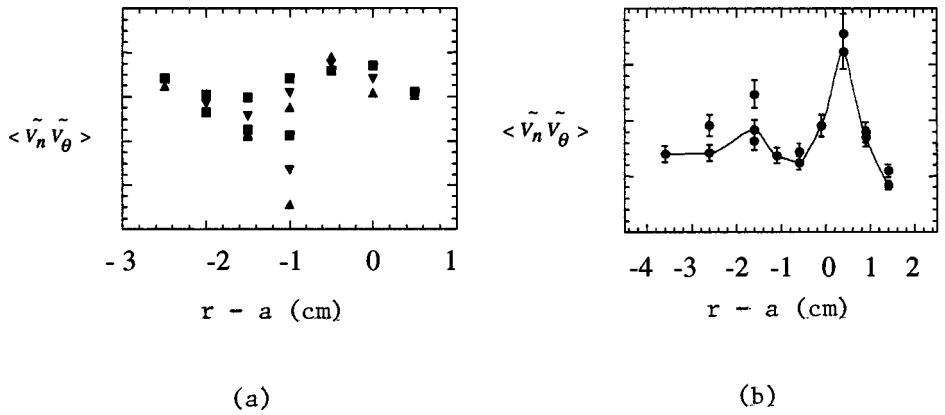

Figure 23. Experimental measurements of Reynolds stress, measured by the gradient in $\langle \tilde{V}_{\rm n} \tilde{V}_\theta \rangle$ ($\tilde{V}_{\rm n}$ is a velocity fluctuation normal to the magnetic surface, $\tilde{V}_\theta$ is in the poloidal direction), show a correlation with the velocity shear location near the plasma edge, $r = a$: (a) the tokamak ISTOK; (b) the helical device TJ-1U [153].

The $\eta_{\rm i}$ or ion temperature gradient driven mode is a strong candidate for the instability responsible for the L-mode anomalous transport [159]. Considering a slab model of the tokamak plasma, Staebler and Dominguez [160] have demonstrated that a radial electric field gradient has a strong stabilizing influence on the $\eta_{\rm i}$ mode and this might explain the improvement in transport which is observed in the H-mode, although it could not explain the origin of the radial electric field. In a later work, Staebler and Dominguez [161] calculated the turbulent viscosity resulting from the nonlinearly saturated $\eta_{\rm i}$ instability. They obtained the interesting result that this anomalous viscosity increases with radial electric field shear, to some critical value beyond which it falls. This allows the following picture of the H-mode. Some drive (i.e. a momentum source from, for example, the ion-orbit-loss mechanism discussed earlier) spins the plasma up in a continuous way, to give an equilibrium flow determined by the balance between the drive and the anomalous viscous damping. At some critical value of the drive, the radial electric field derivative reaches the critical value, $E'_{r\rm crit}$, where the viscous damping is a maximum. A prediction for $E'_{r\rm crit}$ is

$$E'_{r\rm crit} = 2.02 \times 10^4 B (T_{\rm e}/A_{\rm i})^{0.5} \tau^{-0.77} L_n^{0.7} L_{T_{\rm i}}^{-0.26} L_s^{-1.44} \ {\rm V\ m^{-2}} \tag{4.27}$$

where B is in T, $T_{\rm e}$ in eV and lengths are in m. Staebler and Dominguez postulate a smaller 'background' viscous damping, which increases linearly with the electric field gradient and does not possess a maximum. Figure 24 which is from [161] shows the resulting viscous stress. At the critical point, the plasma jumps to the part of the curve representing the background viscosity, which then determines the radial electric field in the H-mode. The result (4.27) corresponds to a flow shear scaling like that of Hassam, equation (2.28). The improvement in confinement results from the stabilization of the $\eta_{\rm i}$ mode with the sudden increase of the electric field gradient. The power threshold then corresponds to the point at which the critical

electric field is reached, and a value for this is estimated as follows. Two mechanisms may be considered for the momentum input to balance the turbulent viscosity: ion-orbit loss as predicted by Shaing and Crume [68] and a neutral beam injection source. The balance of the momentum source, M, and the turbulent viscosity then gives rise to the expression

$$M \sim \frac{nT_{\mathrm{e}}V\rho_{\mathrm{s}}}{L_n^2}H \tag{4.28}$$

where V is the plasma volume and the form factor H is assumed to be a function of E_r' only and represents the variation of the turbulent viscosity with E_r'. Neglecting the poloidal rotation (so that the $\boldsymbol{E}\times\boldsymbol{B}$ poloidal flow is balanced by the diamagnetic poloidal flow) and assuming M to be given by the ion-orbit-loss mechanism, then gives the condition

$$f\nu_{*\mathrm{i}}^{1/2} \gtrsim \frac{\rho_{\mathrm{s}}a}{L_n^2} \tag{4.29}$$

corresponding to a minimum collisionality, $\nu_{*\mathrm{i}} \propto \rho_*^2$. This results in a power threshold if one assumes forms for the scalings of temperature and the fraction of fast particles, f, with power. An alternative, for neutral beam heated plasmas, is to consider the momentum source from the beam itself. In this case we assume $M \propto P$ and obtain

$$P \gtrsim P_{\mathrm{Th}} \sim \frac{nTV\rho_{\mathrm{s}}C_{\mathrm{s}}}{L_n^2} \tag{4.30}$$

which could be manipulated to give a power threshold scaling for a given confinement time scaling.

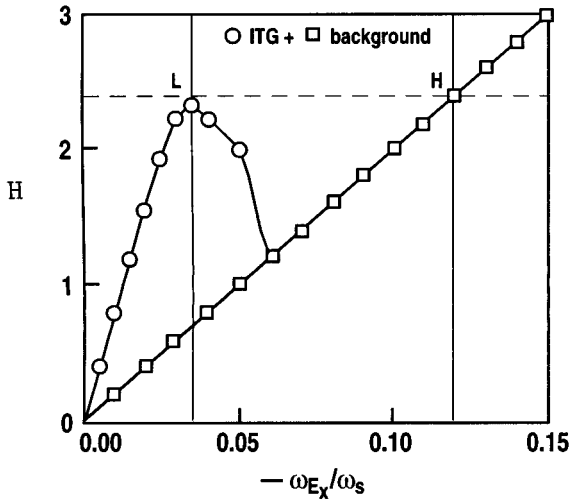

Figure 24. Viscous stress weighting function, H, as a function of normalized radial electric field shear, $-\omega_{\mathrm{E}_x}/\omega_{\mathrm{s}}$, obtained by adding the effect of a constant 'background' turbulent viscosity to the ion temperature gradient mode weighting function [161].

In principle, this theory also allows for a smooth transition into the H-mode. If the η_{i} mode is completely stabilized by E_r' before the maximum in the anomalous viscosity is reached, then no spontaneous spin-up of the plasma occurs and the threshold power corresponds to that power which provides sufficient radial electric field gradient to stabilize the η_{i} mode. In the opposite case, a bifurcation-type H-mode with spontaneous creation of radial electric field is predicted.

4.2. Transport bifurcation theories

In transport bifurcation theories the transport suppression from V_{E}', as in equation (4.26), is determined by E_r' arising from p_{i}' through radial force balance. In practice these are closely related to the theory of Hinton [149] where E_r' is driven by the neoclassical $V_{\theta\mathrm{i}}$, equation (4.23), which is itself dependent on T_{i}', since in both cases the appropriate gradients are determined by transport processes. Bifurcation becomes possible when the sources of energy and particles can drive sufficient gradients.

When the poloidal and toroidal flows can be neglected, the $\boldsymbol{E} \times \boldsymbol{B}$ velocity is given by

$$V_{\mathrm{E}} = -\frac{1}{n_{\mathrm{i}} e B}\frac{\mathrm{d}p_{\mathrm{i}}}{\mathrm{d}r}. \tag{4.31}$$

This expression is correct if standard neoclassical theory is valid at the plasma edge and when the ion temperature gradient is neglected. However, inclusion of orbit squeezing effects which result from the existence of a radial gradient in the radial electric field can lead to significant poloidal rotation, as was discussed by Hinton *et al* [135]. In this case V_{E} would be suppressed by the factor $S = 1 - m_{\mathrm{i}} E_r'/e B_\theta^2$ describing the orbit squeezing, and this simply leads to a modification of the parameters α and γ in equation (4.26).

Using equation (4.31), the particle and energy fluxes can be expressed solely in terms of the density and pressure gradients (and the parameters α and γ). Particle and energy conservation then yield expressions for the fluxes in terms of the heat and particle sources [162]. The resulting system can then be solved to determine the pressure and temperature profiles. For a given particle flux, Γ, and heat flux, q, less than a critical value q_{crit} (both fluxes are per unit area), only one solution exists for the ion density and pressure gradient pair, both of which are low—this is interpreted as the L-mode solution. When $q > q_{\mathrm{crit}}$ the solution jumps to the higher gradient solution, which is to be interpreted as the H-mode (figure 25(a)). It is easiest to access this H-mode solution at the plasma edge where Γ is largest, while further into the plasma core, the L-mode solution is the only one. This leads to density and temperature profiles with steep edge gradients and flat core gradients, as observed experimentally. A threshold condition is given which corresponds to the product of the particle and energy fluxes exceeding a critical value

$$(q\Gamma)_{\mathrm{crit}} = \frac{9}{16}\frac{D_1\chi_1}{(3\alpha)^{1/2}}\left(1 + \frac{4}{3}\frac{D_0}{D_1}\right)\left(1 + \frac{4}{3}\frac{\chi_0}{\chi_1}\right) \tag{4.32}$$

where D_0 and D_1 are H-mode and L-mode particle diffusivities, respectively, and χ_0 and χ_1 the corresponding thermal diffusivities (see figure 25(b)); (4.32) is in convenient normalized variables. Applying this condition close to the edge for the L–H transition, then q is the total input power per unit area and Γ can be calculated from the source resulting from the neutrals diffusing in from the plasma edge and becoming ionized inside the plasma. Interpreting D_0 and χ_0 as neoclassical diffusivities and D_1 and χ_1 as anomalous diffusivities having an assumed scaling (e.g. Bohm), equation (4.32) results in a rather complicated scaling for a power threshold, even in the limit that the neoclassical diffusivities are neglected. The prediction also depends on the particular model which is chosen for the recycling. (It is interesting to note that bifurcations are only possible provided $\gamma > 1/2$ and $D_1/D_0 > 2\gamma(\gamma - 1/2)^{-2}$.) Thus a bifurcation transition is expected in tokamaks where the edge transport is dominated by turbulent processes, while a smooth transition would occur when there is a higher proportion of neoclassical transport.

This work has been extended to incorporate poloidal and toroidal flows, as well as density and temperature gradients [62, 163]. The reduction in drift wave transport is modelled as

$$D = D_0 + \frac{D_1}{1 + \alpha|S_\perp|^\gamma} \tag{4.33}$$

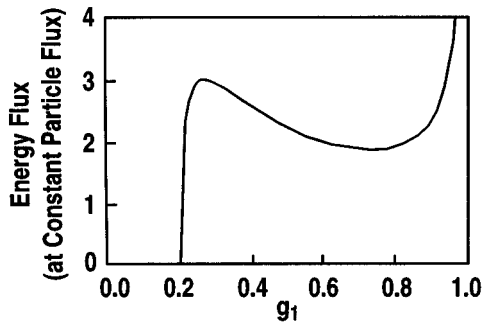

(a)

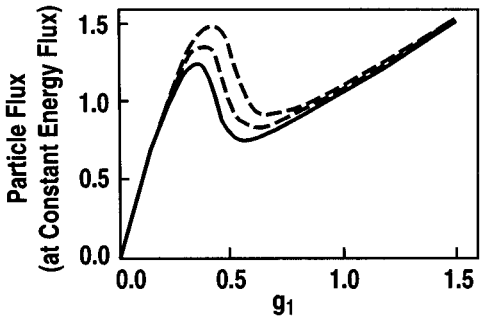

(b)

Figure 25. (a) Energy flux as a function of the density gradient, g_1, for a given particle flux Γ; (b) particle flux as a function of the density gradient for three given values of energy flux, q. The larger particle fluxes correspond to smaller energy fluxes: it is the product of q and Γ that is important [162].

(see equation (2.36)) for the particle diffusivity D, with similar forms for the heat and toroidal momentum diffusivities, $\chi_\perp$ and $\mu_\perp$, respectively; here

$$S_\perp = \frac{B_\phi}{B} V'_\theta + \frac{B_\theta}{B} \frac{\Pi_\phi}{\mu_\perp} + \frac{q\Gamma}{eB\chi_\perp D_\perp} \tag{4.34}$$

which allows for stabilizing influences of V'_{E} and $V'_{\|\mathrm{i}}$ (for ion drift waves) and q, Γ and Π_ϕ are heat, particle and toroidal momentum fluxes, with diffusivities $\chi_\perp$, $D_\perp$ and $\mu_\perp$, respectively. This model is intended to describe L-, H- and VH-modes. For L–H transitions q and Γ are important and, if Γ is expressed in terms of the edge recycling particle flux, then $r < 0.98$ is needed for a transition, where r is the recycling coefficient. The width of the edge transport barrier is $\Delta \propto \ell_{\mathrm{ion}} \ln P$, i.e. proportional to the neutral ionization depth ℓ_{ion} and only weakly varying with additional power P. The barrier forms in a few milliseconds: $\Delta\tau \sim (\Delta/a)^2\tau_{\mathrm{p}}$ where τ_{p} is the particle confinement time. The theory also addresses the generation of poloidal flows, for example, by biased probes or ion-orbit-loss mechanisms. The threshold power reduces when $B_\phi(\mathrm{d}V_\theta/\mathrm{d}r) > 0$; this case is to be expected for ion-orbit loss [163]. The influence of orbit squeezing has been considered by Hinton *et al* [164]. The condition for it to produce a large poloidal flow, $\rho_{\mathrm{pi}}/L_n > 1$, typically exceeds that needed for an L–H transition arising from the normal pressure gradient contributions to $S_\perp$ in (4.34), i.e. $\rho_{\mathrm{pi}}/L_n > (L_n q/a)$.

Garbet and Waltz [165] have given a simplified generic model for the L–H transition based on ion temperature gradient turbulence and allowing for rotational shear stabilization.

It is the increase of this latter term with temperature gradient, or heat flux, which allows for a bifurcation at a normalized power

$$P_{\rm Th} L^{3/4} \propto \rho_*^{-7/2} \beta^{7/4} \nu_*^{-3/4}. \tag{4.35}$$

Vojtsekhovich *et al* [166] considered situations with radiofrequency electron heating where the preferential loss of hot electrons can generate sheared radial electric fields. Two cases, corresponding to thermalized and suprathermal electrons, respectively, were investigated using transport modelling and both led to L–H transitions, but the theory had no specific predictions to compare with experiment other than a positive sign of E_r.

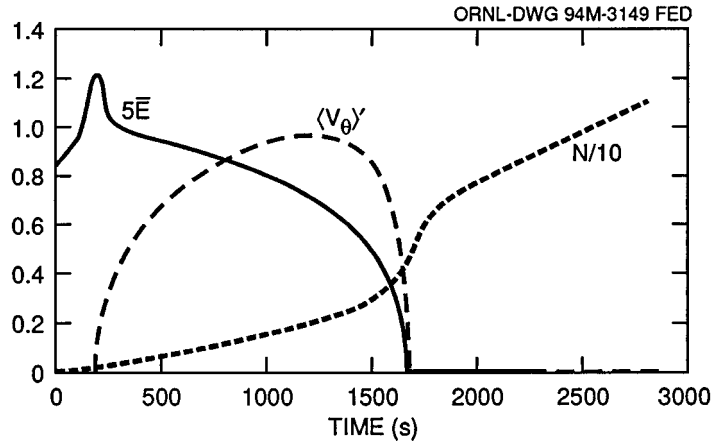

Figure 26. The time evolution of the fluctuation level, $\bar{E}$, poloidal flow shear, $\langle V_\theta \rangle'$, and density (representing ion pressure) gradient, N, as the flux increases in a phase-transition model [170].

4.3. Phase-transition models

So-called 'phase-transition' models evolve in time a set of spatially-averaged, coupled equations for the turbulence level, the driving gradients and the consequent radial electric field, with the transport coefficients responding to the fluctuation level and the radial electric field (or flow) shear as discussed in [120]. (If the turbulence dynamics time scale is removed from those models, they collapse to the transport bifurcation type so that they can be considered as a more complete form of the latter, rather than as a totally different class.) A turbulent dynamo effect amplifies the flow shear until the fluctuations are self-regulated as the flow shear suppression exerts itself. This system of equations allows a L–H bifurcation; the threshold power follows from the condition that the energy input rate in the absence of flow shear exceeds neoclassical or charge exchange poloidal flow damping. The seminal treatment of Diamond *et al* [167, 168] investigated the interaction between flows and turbulence in a generic system of model equations. The fluctuation energy, $E = |\tilde{n}_k/n|^2$ satisfies

$$\frac{1}{2}\frac{{\rm d}E}{{\rm d}t} = \gamma_0 E - \alpha_1 E^2 - \alpha_2 U E \tag{4.36}$$

where γ_0 is the linear growth rate, α_1 represents nonlinear damping due to coupling to other helicities and $\alpha_2 U$, where $U \equiv V_{\rm E}^{'2}$, represents the effect of a sheared $\boldsymbol{E} \times \boldsymbol{B}$ flow in stabilizing the instability. The sheared $\boldsymbol{E} \times \boldsymbol{B}$ flow itself is governed by the competition between the

Reynolds stress drive due to the fluctuations and the damping due to the parallel viscosity, μ, since

$$V_{\rm E} = -\frac{E_r}{B} = V_\theta - \frac{\rho_{\rm s} C_{\rm s}}{p_{\rm i}} \frac{{\rm d}p_{\rm i}}{{\rm d}r}. \tag{4.37}$$

Thus

$$\frac{1}{2}\frac{{\rm d}U}{{\rm d}t} = -\mu U + \alpha_3 U E \tag{4.38}$$

where the ion pressure gradient contribution has been dropped from the expression for $V_{\rm E}$ for simplicity. The quantities α_i can be estimated for different types of turbulence (note energy conservation requires $\alpha_2 = \alpha_3(\Delta r)^4/C_{\rm s}^2\rho_{\rm s}^2$, where Δr is the radial width of the instability). This system forms a 'predator–prey' model (where the fluctuation intensity, E, is the prey to the shear flow predator, U) which depends only on the parameters $a = \alpha_3/\alpha_1$ and $b = \mu/\gamma_0$. There are two fixed points: $E = \gamma_0/\alpha_1$, $U = 0$ and $E = \mu/\alpha_3$, $U = (\gamma_0 - \alpha_1\mu/\alpha_3)/\alpha_2$. The first is stable if $\gamma_0 < \alpha_1\mu/\alpha_3$ and can be identified with the L-mode (high fluctuations and no flow). The second is stable if $\gamma_0 > \alpha_1\mu/\alpha_3$ and can be identified with the H-mode (lower fluctuations and finite flow). For a generic drift wave model, we have $\gamma_0 \sim k_\theta \rho_{\rm s} C_{\rm s}/L_T$. Power balance at the edge implies $L_T^{-1} \sim P/(nTaR\chi)$, so that the bifurcation condition becomes

$$P_{\rm Th} = \frac{\alpha_1}{\alpha_3}\frac{\chi}{k_\theta \rho_{\rm s} C_{\rm s}}\mu n T a R. \tag{4.39}$$

A scaling for α_1 can be obtained by assuming a decorrelation frequency of order ω_* and a radial mode width of order $\rho_{\rm s}$, in which case

$$P_{\rm Th} = \frac{1}{\alpha_3}\mu n T C_{\rm s} a R \tag{4.40}$$

if one takes $\chi \sim C_{\rm s}\rho_{\rm s}^2/L_n$. Furthermore, Diamond *et al* [167, 168] also state that $\alpha_3 \sim C_{\rm s}/L_s$ for generic drift wave turbulence, so that finally

$$P_{\rm Th} = \mu n T L_s a R \tag{4.41}$$

where (μnT) is to be evaluated for the L-mode edge parameters, prior to the transition, for example, in the banana/plateau regime we have

$$\mu = \frac{0.78\epsilon^{1/2}\nu_{\rm ii}}{1 + 0.44\nu_*}. \tag{4.42}$$

A more direct estimate of the bifurcation condition [167, 169] leads to a critical value of the local quantity

$$\lambda = \frac{V_{\rm Thi}}{L_s \mu}\left(\frac{\Delta r}{L_n}\right)^2 \tag{4.43}$$

where $\Delta r \sim \rho_{\rm i} L_s/L_n$ is typically 2 cm. This provides a critical value of $\nu_{*\rm i}(\propto\rho_*^2)$ in the banana region (where $\nu_* < 1$ in (4.42)) and ρ_* in the plateau regime (where $\nu_* > 1$), and is more easily satisfied in a divertor configuration where L_s is smaller. The model has also been extended to include an equation for the evolution of the ion pressure gradient and its contribution to $V_{\rm E}$ as given in (4.37) [170]. This leads to an L–H transition (which is a first-order phase transition) in $V_{\rm E}'$ and E_r as a function of applied heat flux, q. However, there is a second, later transition to zero fluctuations. The time evolution of the fluctuation level, poloidal flow shear and pressure gradient is illustrated in figure 26 which is from [170]. The inclusion of the ion pressure gradient, $p_{\rm i}'$, leads to a preferred direction for a seed radial electric field gradient, E_r'. Near the L–H transition the V_θ contribution to E_r dominates that due to $p_{\rm i}'$ and conversely for $P \gg P_{\rm Th}$; thus $P_{\rm Th}$ is unaffected. After the L–H transition the fluctuations are quenched, and

therefore the drive for V_θ' vanishes so that only the p_i' contribution remains. A rapid power ramp compresses the time duration of the sheared flow generation phase, which may then be unobservable. On the other hand, the transition time becomes logarithmically singular at the transition point, $P \sim P_\mathrm{Th}$, which is like a second-order phase transition, i.e. there are jumps in temporal gradients of quantities, not in the quantities themselves [169].

An elaboration of the model [171] is to introduce an external torque T_ext to drive V_θ; this can represent a biased limiter, a probe or radiofrequency waves. The result is a reduction in the critical power

$$P_\mathrm{Th} = P_\mathrm{Th}^0 - K T_\mathrm{ext}^{2/3} \tag{4.44}$$

where it is found that a 10% change in the critical parameter for the transition due to the torque can produce a 20% change in the threshold power.

The model has been extended further [169, 172] to describe the radial propagation of the L–H transition front, which may be relevant to the global transition observed in JET, by including radial diffusion effects in the equations for fluctuation energy and poloidal velocity shear. The velocity of propagation is given by

$$V_\mathrm{f} = \frac{2D_1}{L_p}\left(\frac{P}{P_\mathrm{Th}} - 1\right)^{1/2} \tag{4.45}$$

where D_1 is the diffusion coefficient and L_p the pressure gradient length in the L-mode prior to the transition. With the three-equation model described above, one obtains a propagating form for $P \gtrsim P_\mathrm{Th}$, but for $P \gg P_\mathrm{Th}$ there is no propagation and the fluctuations collapse uniformly everywhere.

Carreras *et al* [173] have introduced neutral particles into the model, which increase the effective damping of V_θ by charge exchange, decrease the effective energy flux through charge exchange and ionization, and provide a particle source. The local particle and heat fluxes (Γ, q) act as order parameters. In a simple model which neglects q and V_θ, the bifurcation condition is symmetric in particle flux per unit area from the core, Γ_c, and the neutral influx, Γ_o:

$$\Gamma_\mathrm{c} + \Gamma_\mathrm{o} > \frac{n k_\theta \rho_\mathrm{s}}{4} C_\mathrm{s} \tag{4.46}$$

where, for drift wave turbulence, $k_\theta \rho_\mathrm{s} \leqslant 1$. The more complete model has four parameters, one of which is $g_1 = q/T\Gamma$. It is found that the threshold particle flux, equation (4.46), decreases with q in the absence of neutral particles but increases in their presence. If the energy losses in the edge due to ionization and charge exchange compete with q_core, the heat flux from the core (i.e. $g_1 < 1$), then increasing the neutral particle density lowers the threshold because n' dominates E_r and the neutral particle source increases n'. This case is like the simple model (4.46) and could be relevant to smaller devices. It has the implication that H-modes with $L_T > L_n$ are more stable against changes in Γ_o inducing a back transition. For the case $g_1 \sim 1$ the n' and T' contributions to E_r cancel and there is a maximum in the threshold. Finally the threshold is raised if $T_\mathrm{i}/T_\mathrm{e}$ is decreased, so that edge electron heating is unfavourable.

The phase-transition model can be elaborated to obtain a position and width for the barrier. The location of the transition can be obtained from the Maxwell construction [75] and in a time-dependent calculation, x, the radial position of the barrier at time t, propagates as

$$x = \sqrt{Dt(\Gamma - \Gamma_\mathrm{M})/\Gamma_\mathrm{M}} \tag{4.47}$$

where D is the diffusion coefficient, Γ is the flux and Γ_M is the Maxwell flux (see figure 9). In the case of an edge neutral particle source, one can deduce [174] that the barrier (or pedestal) width is

$$\Delta_\mathrm{ped} = \sqrt{\frac{D}{\nu_\mathrm{ion}}} F\left(\frac{\Gamma_\mathrm{o}}{\Gamma_\mathrm{M}}\right) \tag{4.48}$$

where $\nu_{\rm ion}$ is the ionization rate for neutral atoms at the plasma surface and F is a weak function of the incident neutral particle flux, $\Gamma_{\rm o}$, that provides an ionization source at the plasma edge. Thus, as examples, for a purely neoclassical D, $\Delta_{\rm ped} \sim 3$ mm for Alcator C-Mod and $\leqslant 1$ cm for DIII-D, while for an empirical D in the range 0.1–1 m^2 s^{-1}, they lie in the ranges 1–3 cm and 4–10 cm, respectively.

The basis for these phase-transition models has been investigated using nonlinear simulations of resistive pressure gradient driven turbulence [175]. It is found that a strong cancellation between the turbulent Reynolds stress drive for V_θ and damping due to the turbulent viscosity means that the L–H transition can only be realized at low fluctuation amplitudes near marginal stability. The reduction in transport in the resulting H-mode is partly caused by the changed phase relationship between fluctuations.

The possibility of active control of the L–H transition is raised by the investigation in [176], where it is shown that low-frequency poloidal flows are more weakly damped by neoclassical viscosity than are static ones; this could allow the driving of stabilizing oscillating poloidal flows.

In parallel to the series of papers described above, Horton and co-workers have pursued related ideas. In [177] they developed a dynamical model to describe electrostatic resistive pressure gradient driven turbulence in slab geometry. This consists of three ordinary differential equations describing the evolution of electrostatic potential, plasma flow and fluctuation energy, derived from energy balance by modelling the transfer and dissipation terms, with the energy input as an order parameter (unlike the above work, where p' plays this role). The L–H transition is triggered by an increase in $T_{\rm i}$, leading to a decrease in the neoclassical poloidal viscosity that opposes the Reynolds stress; the condition that there is a transition requires that the edge diffusivity exceeds the viscosity (i.e. $T_{\rm i} \geqslant$ 50–100 eV), implying a threshold for the power injected into the edge:

$$P_{\rm Th} = 6\pi^2 c_T a R D_p \frac{{\rm d}p}{{\rm d}x} \tag{4.49}$$

where $c_T \sim {\rm O}(1)$, D_p is the pressure diffusivity and units kW, m, eV m^{-3} are used. The time for the transition is typically $\sim$50 μs. At low densities (i.e. banana regime), one finds a first-order phase transition displaying hysteresis; for higher densities (plateau regime) a second-order phase transition pertains. In a later paper [178] the closures used in deriving the above model and its bifurcation properties were verified by examining the behaviour of more fundamental, low-order, mode coupling equations for the turbulence.

The phase-transition model has been developed further, as the edge turbulent layer (ETL) model, by Ossipenko [179]. Solving a Lorenz-like system of equations for velocity shear, turbulent kinetic energy, thermal energy, and the temperature profile, with the incident heat flux and temperature $T_{\rm b}$ (corresponding to a temperature gradient across the turbulent layer) at the core–edge interface given as boundary conditions, a transition from zero plasma flow to a finite flow with reduced turbulence occurs at a critical temperature gradient. The transition in temperature can only occur if the poloidal viscosity varies inversely with temperature, i.e. for the banana regime, $\nu_{*{\rm i}} < 1$. This requires $T > (0.7nqR)^{1/2} Z_{\rm eff}^2 \epsilon^{-3/4} \times 10^{-2}$ keV, typically 0.26 keV. This bifurcation corresponds to the L–H transition and can be expressed as a critical power, $P_{\rm Th} = 1.23\pi^2 n T_{\rm b} R a L_T \nu_{\rm i}$. Modelling $T_{\rm b}$ and L_T, it is found that this can then be fitted by the form

$$P_{\rm Th} \propto nB^2 \left(1 + \frac{c}{Bn}\right) \tag{4.50}$$

where c is a constant. Transition times are $\sim$5–50 ms.

This ETL model itself can be used to provide a boundary condition for a core transport code [180]; the bifurcation happens at a critical value of $T_{\rm b}$ and on a much faster (turbulence)

time scale than τ_E. The code is found to simulate L–H transitions in DIII-D satisfactorily; $P_{\rm Th}$ is found to be linear in n and B and the turbulence and $T_{\rm b}$ respond on different time scales.

5. Other theories for the L–H transition

In this section we consider some remaining theories which do not fall naturally into the classifications used in sections 3 and 4.

One of the earliest explanations for the H-mode was proposed by Ohkawa *et al* [181] who suggested the divertor channel could produce a thermal transport barrier, in much the same way as in a mirror machine. This is a result of the electrostatic potentials associated with an increased plasma density near the divertor target plates due to the ionization of recycled neutrals (typically, this high-density 'accretion region' can occur when $T_{\rm e} \gtrsim 10$ eV and $n \sim 10^{20}$ m^{-3} near the plates and the core plasma density $n \gtrsim 5 \times 10^{19}$ m^{-3}). The electrostatic potential then reflects the electrons, reducing their heat flux to the divertor plates. Furthermore, the higher density near the plates reduces the sheath resistance and the more effective line-tying tends to stabilize modes, reducing turbulent cross-field transport in the SOL. However, this model fails to explain the observation of a transport barrier inside the separatrix.

Another suggestion for the L–H bifurcation based on the divertor region arose from studies of a model for particle, momentum and energy transport in a divertor, coupled to particle transport in the core plasma [182]. This model allows two solutions: a high-recycling one identified with the H-mode and a low-recycling one identified with the L-mode. However, the extremely low densities in the divertor region associated with the L-mode solution have never been observed in a tokamak; indeed L-mode densities there usually exceed those in the H-mode [40].

An early model by Rebut *et al* [183], based on separate electron and ion energy balances, was able to generate an edge electron temperature pedestal inside the separatrix. Taking account of electron and ion thermal conduction and equipartition, they obtained the relation

$$\hat{P} = \hat{q}_{\rm e} + \frac{\hat{q}_{\rm e}}{\hat{q}_{\rm e}^{3/2} + \chi_{\rm e}/\chi_{\rm i}} \tag{5.1}$$

where the normalized power flow $\hat{P} = P/p$ and electron heat flux $\hat{q} = q_{\rm e}/p$, with $p = [n^2 \nu_0 V (nS\chi_{\rm e}/L_T)^{1/2}]^{2/3}$. Here S and V are the surface area and volume of the plasma, L_T a typical temperature scale length near the separatrix and $\nu_0 = \nu_{\rm ei} T^{3/2}/n$. This allows a bifurcation in the electron heat flux above a certain threshold power, provided $\chi_{\rm e} \ll \chi_{\rm i}$, corresponding to a transition from a state in which the ions carry a large fraction of the total heat flux to one in which the electron heat flux becomes significant. This threshold power scales as

$$P_{\rm Th} \propto [n^2 V (nS\chi_{\rm i}/L_T)^{1/2}]^{2/3}. \tag{5.2}$$

For a transport model like the Rebut–Lallia–Watkins (RLW) model, the high magnetic shear associated with a separatrix suppresses anomalous transport, leading to neoclassical levels. Thus $\chi_{\rm e} \ll \chi_{\rm i}$ near the separatrix and the bifurcation can occur, generating a steep electron temperature gradient there. For typical JET conditions, it is found that the RLW transport model predicts that the bifurcation will take place when $P > 5.4$ MW: this corresponds to a transition from a low edge temperature ($\sim$250 eV) with ion transport dominating the power flow, to a high edge temperature ($\sim$1 keV) with electron transport becoming important, generally in accordance with observations on JET. However, as pointed out by Burrell *et al* [40], the condition on $\chi_{\rm e}/\chi_{\rm i}$ for a bifurcation ($\chi_{\rm i}/\chi_{\rm e} > 24$) implies $T_{\rm i}/T_{\rm e} < 1/5$, in conflict with observations on DIII-D.

An early theme for H-mode models was the effect of the presence of a separatrix on neoclassical theory. In the collisionless 'banana' regime, those ions whose pitch angle and energy places them on an orbit which passes beyond a critical radius at the X-point angle are considered to be lost to the divertor. This leads to a 'loss-cone' in velocity space which is repopulated by collisional scattering from the neoclassical ion flux diffusing spatially from the core. With some simplifying geometrical assumptions, Hinton and Chu [184] developed a variational solution of the resulting 'orbit-averaged' drift kinetic equation and showed that a steep gradient in the ion temperature would be generated at the plasma edge

$$\frac{1}{T_\mathrm{i}}\frac{\mathrm{d}T_\mathrm{i}}{\mathrm{d}r} = \frac{-2.2}{\epsilon\rho_\mathrm{pi}} \tag{5.3}$$

comparable to a scale length on the ion banana width ($\sim\epsilon^{1/2}\rho_\mathrm{pi}$) and implying ion temperature gradients of several hundred eV cm^{-1}. This separatrix solution corresponds to an H-mode and would require a sufficient heat flux to produce a hot collisionless edge, i.e. $\nu_{*\mathrm{i}} < 1$; L-modes are associated with high charge exchange losses in a limiter configuration, leading to a cold boundary. The boundary condition (5.3) does not determine T_i, but balancing the collisional scattering into the loss cone against the neoclassical ion heat flux from the core provides a boundary condition for the density in terms of the heat flux. Invoking a similar model for ion particle loss due to ion–ion collisional scattering into the loss cone, one finds that T_i is given by the ratio of heat and particle fluxes at the boundary. This equilibrium is found to be thermally stable [39].

Ohkawa and Hinton [119] also discussed the H-mode energy confinement scaling, assuming that it is controlled by such a neoclassical edge barrier, as well as the role of neutral particles both as a particle source and cause of charge exchange losses; the X-point positions then act as localized heat sinks. In the collisional regime, temperature gradients along the divertor field lines lead to cross-field fluxes through the collisionless heat flux term, as in Pfirsch–Schlüter transport, and their sign therefore depends on the direction of the ion-∇B drift [39]. The consequences depend strongly on the direction of this drift and the details of the separatrix geometry, unlike in the collisionless regime. When the ion-∇B drift is towards (away from) a single null X-point, the heat flux drops (rises) for a fixed T_i', i.e. the confinement improves (deteriorates); with a double null there is no effect. Thus, with the ion-∇B drift towards the X-point, the temperature gradient length L_T decreases to zero when the normalized heat flux

$$\frac{q}{nT_\mathrm{i}\chi_\mathrm{i}} = \Delta_0^{-1} \tag{5.4}$$

where $\Delta_0 = (\pi\chi_\mathrm{i}/5V_\mathrm{Di}) = 2.2(\chi_\mathrm{i}\tau_{\|\mathrm{i}})^{1/2}$ is the neoclassical SOL width. Here χ_i is the Pfirsch–Schlüter cross-field ion thermal diffusivity, $\tau_{\|\mathrm{i}} = (qR)^2/\chi_{i\|}$, where $\chi_{\|\mathrm{i}}$ is the collisional ion thermal diffusivity along the magnetic field, and $V_\mathrm{Di} = T_\mathrm{i}/eBR$ is the ion magnetic drift velocity. The confinement improvement is so strong that the heat flux, q, is exhausted at a finite rate $\sim n_\mathrm{i}T_\mathrm{i}^2$, despite the steep gradient. In the opposite case, when the ion-∇B drift is away from the X-point, the gradient length, Δ, is such that $\Delta \geqslant \Delta_0$: Δ does not need to decrease with q because the heat sink causes a deterioration in confinement. It should be noted that $\Delta_0 \sim (qR/V_{\mathrm{Th}\,\mathrm{i}}\tau_\mathrm{ii})\epsilon\rho_\mathrm{pi}$, i.e. Δ_0 exceeds an untrapped ion orbit width in the collisional regime. These results provide an explanation of why P_Th is lower when the ion-∇B drift is towards the X-point of a single null divertor, rather than away from it. When it is away, H-mode access would need a sufficient heat flux to reach the collisionless regime.

Of course the cross-field losses are not purely neoclassical; Tang and Hinton [185] considered the impact of anomalous losses on the above picture and found it to be essentially

unchanged because an increase in the ion heat flux increases the strength of the sink, in accord with a self-consistent energy balance.

Hinton and Staebler [186] provided a more realistic treatment of the transport in a divertor plasma. Electron and ion radial energy fluxes across the separatrix close to the X-point were calculated taking each to consist of an anomalous component and a neoclassical component, the latter being proportional to the poloidal temperature gradient. This poloidal temperature gradient exists because the temperature is small at the divertor plates and increases away from the plates because of the radial diffusion of heat from the plasma core into the SOL, as illustrated in figure 27. Therefore, this gradient is of opposite sign at the inboard and outboard sides so that the flux is inward on one side and outward on the other. Furthermore, the heat flux is observed experimentally to be larger on the outboard side than on the inboard side, thus enhancing the temperature gradient and leading to a net outflux (influx) of ion energy if the ion-∇B drift is away from (towards) the X-point. In the limit $T_e = T_i$, the classical electron diffusive energy flux is equal in magnitude and opposite in direction to the ion flux, and no net energy would then diffuse across the separatrix. However, because the parallel ion flow is much slower than that of the electrons, the ion poloidal temperature gradient is larger and a net energy flux across the separatrix is predicted. This is further enhanced by the convective energy flux, which is predicted to flow in the same direction as the ion diffusive flux and has the same direction for both electrons and ions. Assuming that the power threshold is proportional to the net total heat flux, Q, from the plasma (upper and lower case symbols are used to distinguish the total, i.e. diffusive plus convective, and diffusive radial heat fluxes, respectively), one can then write

$$P_{\mathrm{Th}} \propto \langle Q_r^{\mathrm{an}} \rangle \pm |\langle Q_r^{\mathrm{cl}} \rangle| \tag{5.5}$$

where the $\pm$ sign corresponds to the ion-∇B drift away from (toward) the X-point. Here an anomalous heat flux, Q^{an}, which is assumed to be independent of the ion-∇B drift direction, has been included. Q^{cl} is the classical heat flux and angled brackets represent a flux surface average. The ratio of the flux surface average of the anomalous flux to that of the classical flux is calculated for a relatively simple model of the divertor geometry, with the result that the ratio

$$\frac{P_{\mathrm{uf}} - P_{\mathrm{f}}}{P_{\mathrm{uf}} + P_{\mathrm{f}}} = \left| \frac{\Delta_1 f}{\Delta_{\mathrm{SOL}}} \right| \frac{\langle q_r^{\mathrm{an}} \rangle}{\langle Q_r^{\mathrm{an}} \rangle}. \tag{5.6}$$

Here f is the ratio of the flux surface average of the electron diffusive heat flux to the amplitude of the poloidally varying component of this flux (i.e. the amplitude of $q_e - \langle q_e \rangle$) and

$$\Delta_1 = \frac{5}{2} \alpha \left(\frac{\chi_B}{\chi_\parallel} \right) \left(\frac{q}{\epsilon} \right)^2 (2\pi a) \frac{B}{B_\phi} \tag{5.7}$$

where α is the coefficient of the thermal force in Ohm's law. The SOL width is denoted by Δ_{SOL} and χ_B and $\chi_\parallel$ are the Bohm and the parallel thermal diffusivities, respectively. The subscripts 'uf' and 'f' indicate the power threshold when the ion-∇B drift is away from and towards the X-point, respectively.

Using related ideas, i.e. accounting for the contribution to the power crossing the edge from the ion-∇B drifts, but incorporating some empirical elements from double-null discharges in DIII-D, Carlstrom *et al* [187] have proposed a non-power-like scaling for the power crossing the separatrix, $P_{\mathrm{Th}}^{\mathrm{Sep}}$,

$$P_{\mathrm{Th}}^{\mathrm{Sep}} = r \left[5.7 \mp \frac{4.35 (P_{\mathrm{Th}}^{\mathrm{Sep}})^{2/7}}{B} \right] \tag{5.8}$$

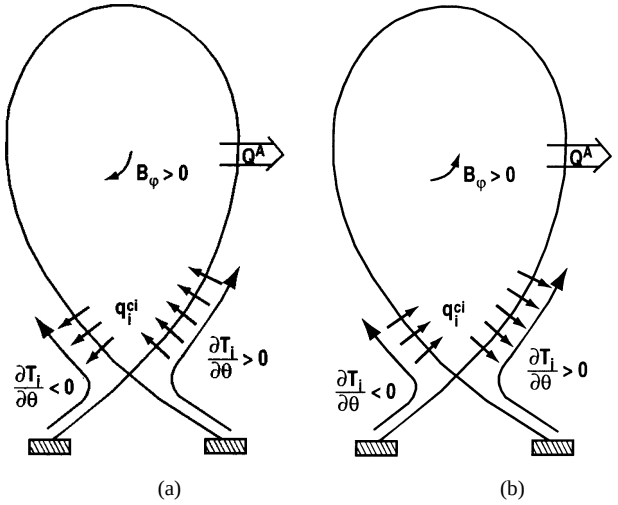

Figure 27. (a) Classical cross-field ion heat flux (q_i^{cl}) for the ion-∇B drift towards the X-point. The anomalous energy flux (Q^{an}) is strongest on the outboard midplane; (b) classical cross-field ion heat flux (q_i^{cl}) for the ion-∇B drift away from the X-point [186].

in units MW, m, T, where $\mp$ correspond to favourable and unfavourable ion-∇B drifts, respectively. This model has been compared with DIII-D data, as shown in figure 28 [187]. It is seen that the curves representing the model saturate with B at large values. For the forward (favourable) direction, P_{Th}^{Sep} approaches zero for low values of B (this is where ohmic H-modes are seen) and increases approximately linearly with B for intermediate values. For the reverse (unfavourable) direction, P_{Th}^{Sep} decreases with B. The presence of sawteeth can affect the comparisons: the sawtooth heat pulse power, P_{ST}, can contribute to P^{Sep} and trigger a transition, lowering the required P_{Th}^{Sep}, as seen in figure 28. Considering only non-sawtooth triggered transitions, there is a weak, but positive, dependence on B, conflicting with the predictions of the simple model. It could be that the direction of $\boldsymbol{B}$ modifies conditions in the divertor region, influencing the poloidal temperature gradient and, perhaps, accounting for the observation. As a direct test of the role of the poloidal temperature gradient, it was increased by heavy gas puffs and by moving the X-point position: the observed trends in P_{Th}^{Sep} were in line with expectations from the model. Equation (5.8) corresponds to collisional transport along the divertor field lines. Thus, these neoclassical ideas could explain a low density threshold: in more collisionless SOL conditions the temperature gradients along field lines are reduced and the neoclassical cross-field fluxes no longer contribute to reducing P_{Th}. Numerical estimates of the neoclassical fluxes in DIII-D show that they are rather small (tens of kW) and that there is little difference between edge gradients for different ion-∇B directions at similar heating power levels [83]. This casts doubts on this mechanism, although it may have a more significant impact on conditions near the X-point. Simulations of coupled core–SOL regions with full X-point geometry using the U-EDGE code [188] do indicate a lower value of P_{Th} for the favourable ion-∇B direction.

Rogister [189–192] has proposed an explanation of the large electric fields associated with the H-mode transport barrier, based on a revised neoclassical theory [193]. This revised theory introduces a re-ordering of the conventional theory so as to account for the steep gradients encountered near the plasma edge. Specifically, it is carried out in the Pfirsch–Schlüter regime and allows balances of gyro- and collisional viscosities and of diamagnetic and parallel heat

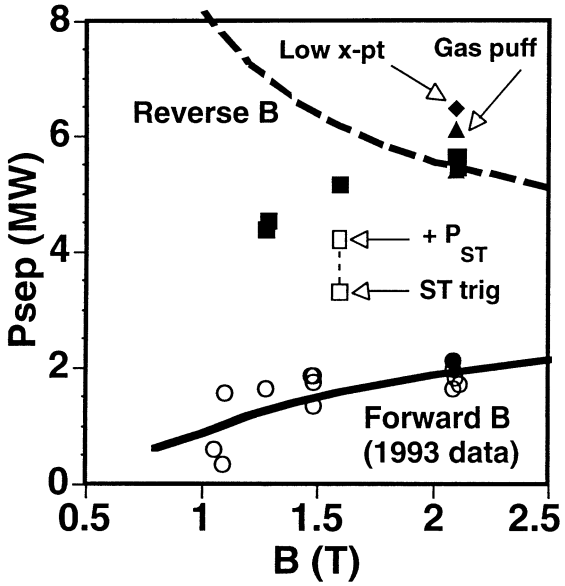

Figure 28. Power flow across the separatrix, P_{Sep}, just before an L–H transition in DIII-D plotted against B [187]. Full symbols, non-sawtooth-triggered transition; open symbols, sawtooth-triggered transition; triangle, heavy gas puff; diamond, low X-point height. The broken curve connecting the two open squares shows the effect of adding an estimate of the sawtooth power to P_{Sep} for this sawtooth-triggered transition. The curves are the ion-∇B drift model. The circles represent the forward B 1993 data, and are shown for reference. Note that almost all of the forward B transitions were triggered by sawteeth.

flows; this means the parameter $\Lambda \sim 1$, where

$$\Lambda \equiv (q^2 R^2 T_{\mathrm{i}})/(reB \mid L_T \mid \chi_{\|\mathrm{i}}). \tag{5.9}$$

Charge exchange losses and momentum sources are also included. The resulting nonlinear equations for the parallel plasma velocity and radial electric field, which follow from the ambipolarity and parallel momentum equations, determine these two quantities fully, and can lead to large values of them in a thin layer near the plasma edge when certain conditions are met. These conditions relate to achieving a sufficient value of the temperature gradient (i.e. a threshold power) and a limit to the charge exchange losses due to neutral particles (thus favouring divertor operations), and can be affected by momentum inputs and the profiles of density and Z_{eff} (e.g. flattening the density and co-injection both ease the conditions). The theory includes an undetermined boundary condition at the LCFS. Independently of this, it predicts a large negative radial electric field at the separatrix, as seen in experiments on DIII-D and ASDEX. The width of this radial electric field structure is

$$\Delta \sim \left(\frac{100}{3}\right) \Lambda^2 L_T \tag{5.10}$$

where Δ is typically $\sim$1 cm. For a particular choice of the undetermined boundary condition, namely one which corresponds to continuity of the flux of parallel momentum across the separatrix, it is found that the structure can be aperiodic or periodic, depending on the various parameters—this transition could describe 'dithering' edge localized modes (ELMs). The large gradients in the electric field layer suppress the cross-field ion thermal transport, leading

to a bifurcation with a transport barrier—sub-neoclassical transport; these gradients can also be expected to reduce anomalous transport by the BDT mechanism.

A treatment of neoclassical theory in the presence of steep gradients, which includes heavy impurities and leads to a transport bifurcation, has been given by Helander [194]. These heavy impurity ions undergo a spontaneous rearrangement on each flux surface, reducing their parallel friction with the bulk ions. Since this is the driving force for the neoclassical particle flux, this flux decreases if the gradients become sufficiently steep, giving rise to the possiblity of a transport bifurcation. Indeed, the relationship between particle flux and gradient is remarkably similar to that postulated by Hinton and Staebler [162] for the anomalous heat flux. The neoclassical heat flux is less influenced than the particle flux by the impurity redistribution, since heat is transported by both ion–ion collisions and ion–impurity collisions but only the latter are affected by the redistribution. However, if $Z_{\rm eff} - 1 \sim {\rm O}(1)$ so that the contributions from these different classes of collisions are comparable, the heat flux is significantly reduced as the contribution from ion–impurity collisions becomes less important. The criterion for such a bifurcation is

$$g \equiv Z^2 \hat{\nu}_{*{\rm i}} \rho_{\rm pi} \left(\frac{1}{L_{n_{\rm i}}} - \frac{1}{2L_{T_{\rm i}}} \right) > 2 \tag{5.11}$$

where Z is the charge of the impurity ion.

An interesting interplay between SOL and core is displayed by the transport code simulations of Leonov [195]. Following an imposed change in the SOL corresponding to that observed between L- and H-modes (i.e. introducing a lower density, narrower SOL width), neutrals penetrate the core more deeply. Transport simulations with the ASTRA code of the changes in plasma density, using a diffusivity $D \propto 1/n$ and following the neutral particle dynamics, led to a density rise in the core. Thus, if there is a mechanism for the L–H transition, involving changes in the SOL, as in section 3.2, then this could explain changes observed in the core.

The canonical profile transport model (CPTM) developed by Dnestrovskij *et al* [196], has a built-in L–H model. A feature of the CPTM model is the presence of terms in the transport fluxes which tend to force the various plasma profiles to relax to certain 'canonical' ones; this model gives a description of L-mode plasmas. However, the model also introduces the idea of a 'forgetting factor': when the deviation of the profiles from the canonical ones exceeds a critical amount, this tendency to relax is weakened (or forgotten!), like a spring passing its elastic limit. The criterion for this to happen to the pressure profile, which occurs first at the plasma edge, is identified with the transition to the H-mode; it takes the form

$$\left(\frac{a}{L_n} + \frac{a}{L_T} \right)_a > Z_{0a} + 3\left(1 - \frac{1}{q_a} \right) \tag{5.12}$$

where Z_0 is the 'forgetting parameter', fitted empirically and taken to be $Z_{0a} \sim$ 6–9 at the plasma edge. This criterion can be combined with the transport model itself to provide an expression for $P_{\rm Th}$

$$P_{\rm Th} = 0.25 R \left(\frac{a}{R} \right)^{0.75} q(a/2) \frac{q(a)}{B} \bar{n} T(a) [T(a/4)]^{1/2} \left(Z_0 + 3\left(1 - \frac{1}{q} \right) - \frac{a}{L_n} \right)_a \tag{5.13}$$

in units MW, m, T, 10^{19} m^{-3}, keV. This is sensitive to edge parameters, such as L_n and T. Because the CPTM model is 'stiff', the transition takes place on a time scale $\tau_{\rm tr} \ll \tau_E$. The model predicts the pedestal width:

$$\frac{\Delta}{a} \propto c \tag{5.14}$$

where $c \sim 0.05$ is a constant; this result is similar to an empirical scaling derived from ITER databases [79]

$$\Delta \sim c' R \qquad c' \simeq 0.05. \tag{5.15}$$

Finally, we note a bifurcation result obtained by Minardi [197] using thermodynamic arguments (based on the statistical mechanics of a model of the plasma as a set of current filaments), together with the empirical ITER89-P energy confinement scaling law. This model predicts a power threshold

$$P_{\mathrm{Th}} = C Z_{\mathrm{eff}}^{0.57} n_{19}^{0.77} B^{0.97} S \tag{5.16}$$

where C($\sim$0.02–0.08) depends on the machine geometry; for instance, it is a factor of two higher in ASDEX Upgrade than JET.

6. Discussion

In the previous sections we have presented a comprehensive review of theories proposed to explain the L–H transition. Where possible, we summarize the predictions of these theories for the conditions for the occurrence of the L–H transition: in table 1 for theories expressed in terms of local edge conditions, in table 2 for those which provide a prediction for the threshold power. These tabulated results are of value for comparison with experimental data. Of course, in the light of subsequent experimental evidence, many of these now no longer appear completely satisfactory candidates as explanations, although they may still contain some relevant elements. A number of reviews, comparing specific theories with particular experimental features, have attempted to discriminate against or support particular theories, or classes of theory: [40–44, 148, 198–201].

In this section we briefly summarize the overall situation concerning the experimental validation of theories, although a number of more detailed points were made when discussing the individual theories in sections 3–5.

The experimental characteristics that theories should aim to explain are:

(i) the general conditions necessary for the L–H transition: in fact it is a robust phenomenon, appearing in many confinement devices and when using different heating schemes, although it appears to be aided by the presence of a separatrix and low particle recycling;
(ii) the empirical behaviour and scalings for P_{Th}, and the issue of hysteresis: generally P_{Th} increases with n, B and R, but can show an increase at low density, or even a low density threshold; P_{Th} is typically a factor of two lower when the ion-∇B drift is towards the X-point; and hysteresis sometimes seems to be related to the H-factor characterizing the H-mode confinement quality;
(iii) the local edge values of the parameters at the transition: there is evidence for a critical temperature (or gradient), scaling positively with B and negatively with n; some evidence for a critical β or ρ_*, but less for a critical $\nu_{*\mathrm{i}}$; and correlations with neutral particle densities inside the separatrix;
(iv) the radial and azimuthal location for initial changes at the L–H transition: changes take place inside the separatrix, and are often initiated at the outboard midplane;
(v) a sharp reduction in fluctuation levels and formation of a transport barrier at the transition: this correlation exists both temporally and spatially;
(vi) the radial width, Δ, of the transport barrier and its scaling with parameters: data supporting $\Delta \propto \rho_{\mathrm{pi}}$, $(\rho_{\mathrm{pi}} R)^{1/2}$ or R have all been cited, as well as $\Delta \propto \ell_{\mathrm{n}}$, the neutral particle penetration length (however, this quantity will tend to shadow the density scale length

Table 1. Local L–H transition criteria expressed in terms of dimensionless variables, and also in the form $T_{\rm crit} = C n^{\alpha_{\rm n}} B^{\alpha_{\rm B}}$.

Theory	Transition criterion	Critical temperature
Connor and co-workers [81, 82, 155]: peeling mode stability	$\frac{\beta q^2}{\epsilon_p} > \alpha_{\rm c}(s)$	$C \propto \frac{\tau}{1+\tau}\frac{\epsilon_p}{q^2}$ $\alpha_{\rm n} = -1, \alpha_{\rm B} = 2$
Drake *et al* [86]: resistive ballooning	$\hat{\nu}_{*{\rm e}} < \left(\frac{m_{\rm i}}{m_{\rm e}}\frac{\epsilon_p}{\epsilon_n^2}\right)^{1/2}\frac{1}{2\pi^2 q_a}\frac{\tau}{1+\tau}$	$C = 0.019 q\sqrt{\frac{1+\tau}{\tau}R\epsilon_n}\left[\frac{1}{\epsilon_p A_{\rm i}}\right]^{1/4}$ $\alpha_n = 1/2, \alpha_B = 0$
Rogers *et al* [88]: drift resistive ballooning, velocity shear, Stringer spin-up	$\frac{\epsilon}{sq\sqrt{\epsilon_p}} > 1$	Geometrical criterion
Rogers *et al* [88]: drift resistive ballooning, velocity shear, $\boldsymbol{E}\times\boldsymbol{B}$ flow	$\rho_{*{\rm s}} > \sqrt{\tau}\frac{s\epsilon_p^{3/2}}{\epsilon}$	$C = 9.58\times 10^4\frac{s^2\epsilon_p^3 R^2\tau}{A_{\rm i}}$ $\alpha_{\rm n} = 0, \alpha_{\rm B} = 2$
Rogers *et al* [90]: ideal and drift resistive ballooning, ion temperature gradient effects	$\beta > 0.5\frac{\epsilon_p}{q^2}$ and $\hat{\nu}_* < \frac{2\sqrt{2}}{9}\left[\frac{m_{\rm i}}{\epsilon_n m_{\rm e}}\right]^{1/2}\frac{1}{q}$	$n_{\rm cr} = 629\left[\frac{\tau}{1+\tau}\right]^{2/3}\frac{\epsilon_p^{2/3}B^{4/3}}{R^{1/3}q^2}\left(\frac{A_{\rm i}}{\epsilon_n}\right)^{1/6}$ $n > n_{\rm cr}$: $C = 0.008 q\sqrt{R}\left(\frac{\epsilon_n}{A_{\rm i}}\right)^{1/4}$ $\alpha_{\rm n} = 1/2, \alpha_{\rm B} = 0$ $n < n_{\rm cr}$: $C = 124\frac{\tau}{1+\tau}\frac{\epsilon_p}{q^2}$ $\alpha_{\rm n} = -1, \alpha_{\rm B} = 2$
Guzdar and Hassam [92]: resistive ballooning, Reynolds stress, Stringer spin-up	$\frac{\hat{\nu}_{*{\rm i}}}{\rho_{*{\rm s}}\beta} < \sqrt{\frac{\tau}{2}}\frac{D}{D_{\rm B}}\frac{q^3}{\epsilon_n^2\epsilon}$	Bohm diffusion: $C = 3.28\frac{\tau^{5/7}}{(1+\tau)^{2/7}}\left(\frac{\epsilon\epsilon_n R}{q}\right)^{4/7}\frac{1}{A_{\rm i}^{1/7}}$ $\alpha_{\rm n} = 0, \alpha_{\rm B} = 6/7$ Gyro-Bohm diffusion: $C = 11.9\frac{\tau^{5/8}}{(1+\tau)^{1/4}}R^{3/4}\left(\frac{\epsilon_n}{q}\right)^{1/2}\frac{\epsilon^{3/4}}{A_{\rm i}^{1/4}}$ $\alpha_{\rm n} = 0, \alpha_{\rm B} = 1$
Zeiler *et al* [93–96]: drift resistive ballooning, 3D nonlinear simulations	See Drake *et al* [86]	
Ohyabu *et al* [98]: microtearing modes	$\hat{\nu}_{*{\rm e}} < \sqrt{\frac{b}{2}\frac{m_{\rm e}}{m_{\rm i}}}\frac{q}{\epsilon_T}$	$b =$ constant: $C = 0.225\sqrt{\epsilon_T R}\left(\frac{A_{\rm i}}{b}\right)^{1/4}$ $\alpha_{\rm n} = 1/2, \alpha_{\rm B} = 0$ $m =$ constant: $C = 3.01\left[\frac{\epsilon_T\epsilon R^2}{m}\right]^{2/5}$ $\alpha_{\rm n} = 2/5, \alpha_{\rm B} = 2/5$
Strauss [101]: low m tearing modes stabilized by drift effects	$\hat{\nu}_{*{\rm e}} < 0.49\left(\frac{m_{\rm i}}{m_{\rm e}}\right)^{1/2}\frac{\beta\tau}{1+\tau}\frac{s\epsilon}{\epsilon_T(r\Delta')}$	$C = 0.21\left(\frac{r\Delta'}{s\epsilon}\right)^{1/3}\frac{(R\epsilon_n q)^{1/3}}{A_{\rm i}^{1/6}}$ $\alpha_{\rm n} = 0, \alpha_{\rm B} = 2/3$
Strauss [101]: low m tearing modes stabilised by sound wave coupling	$\hat{\nu}_{*{\rm e}} < 0.39\frac{q}{s\epsilon_n}\frac{k_y a}{\rho_{*{\rm s}}(a\Delta')^2}\left(\frac{m_{\rm i}}{m_{\rm e}}\right)^{1/2}$ $\times\frac{Z\beta^2\tau^{7/2}}{(1+\tau)^2}$	$C = 0.27\left[\frac{s\epsilon_n}{\epsilon Z}\right]^{2/7}\left[\frac{(a\Delta')^2}{k_y a}\right]^{2/7}\tau^{-3/7}$ $\alpha_{\rm n} = -2/7, \alpha_{\rm B} = 6/7$

Table 1. (Continued)

Theory	Transition criterion	Critical temperature
Scott *et al* [102]: finite β effects on collisional drift wave turbulence	$\beta > \frac{m_e}{m_i}$	$C = 0.135\frac{\tau}{(1+\tau)}\frac{1}{A_i}$ $\alpha_n = -1, \alpha_B = 2$
Kerner *et al* [105]: drift-Alfvén turbulence, $k_\parallel \sim 1/Rq$, $L_p \sim \Delta_{SOL}$	$\sqrt{\frac{m_i}{2m_e}}\frac{\beta q}{\epsilon_\rho} > 1 + \left[\hat{\nu}_{*e}^2\sqrt{\frac{2m_i}{m_e}}\frac{\epsilon_p}{q}\right]^{1/3}$	Collisionless: $C \sim \frac{1}{(Rq)^{4/5}}\frac{1}{A_i^{3/5}}$ $\alpha_n = -7/5, \alpha_B = 2$ Collisional: $C \sim \frac{(Rq)^{2/15}}{A_i^{1/15}}$ $\alpha_n = 1/15, \alpha_B = 2/5$
Rogister [108]: Drift wave instabilities driven by neutral particles	$\rho_{*s} \propto \left(\frac{\ell}{a\hat{\nu}_{*e}}\right)^{1/2}$	$C \propto \frac{A_i q}{\epsilon}$ $\alpha_n = 2, \alpha_B = -2$
Pogutse *et al* [109]: resistive interchange SOL instability, ion-orbit-loss viscosity	$\rho_{*s} > 10\left(\frac{m_i}{m_e}\right)^{1/2}\frac{\Delta_{SOL}^2}{R^2 q\epsilon^{3/2}}\tau$	$C = 1.76\times 10^{10}\frac{\tau^2\Delta_{SOL}^4}{R^2\epsilon q^2}$ $\alpha_n = 0, \alpha_B = 2$
Pogutse *et al* [109]: resistive interchange SOL instability, sheath resistivity dominates	$\rho_{*s} > \frac{31.6}{\epsilon}\left(\frac{\Delta_{SOL}}{R}\right)^{3/2}$	$C = 9.58\times 10^7\frac{\Delta_{SOL}^3}{RA_i}$ $\alpha_n = 0, \alpha_B = 2$
Cordey *et al* [110]: resistive MHD, drift/interchange SOL turbulence	$\rho_{*s} > C_1\frac{\Delta_{SOL}}{\epsilon R}$	$C \propto \frac{\Delta_{SOL}^2}{A_i}$ $\alpha_n = 0, \alpha_B = 2$
Cohen and Xu [115]: electron temperature gradient modes in SOL, incorporating self-consistent calculation of ϵ_{T_e} from [108]	$\beta > \beta_c \propto \rho_{*s}^{2/5}\left(\frac{a}{L_\parallel}\right)^{2/5}\frac{\tau^{2/15}}{A_i^{1/10}}$	$C \propto \frac{\tau^{17/12}}{(1+\tau)^{5/4}}\left(\frac{1}{L_\parallel}\right)^{1/2}A_i^{1/8}$ $\alpha_n = -4/5, \alpha_B = 2$
Chankin [116]: resistive skin effect reduces turbulence length scales in SOL	$\beta > \beta_c \propto \left(\frac{\epsilon}{q}\right)^{2/3}\frac{\hat{\nu}_{*e}}{A_i^{1/2}}\rho_{*s}^{2/3}\left(\frac{1+\tau}{\tau}\right)^{1/2}$	$C \propto \left(\frac{\tau}{1+\tau}\right)^{3/16}\frac{(Rq)^{1/8}}{A_i^{1/16}}$ $\alpha_n = 0, \alpha_B = 1/2$
Shaing and Crume [68]: ion-orbit-loss torque balancing neoclassical poloidal viscous damping	$\nu_{*i} < \nu_c$	$C \propto \frac{\tau}{\epsilon^{3/4}}\sqrt{Rq}$ $\alpha_n = 1/2, \alpha_B = 0$
Itoh and Itoh [69]: ion-orbit-loss, non-ambipolar electron diffusion	$\frac{D}{D_B} \gtrsim \frac{2}{\tau^2}\nu_{*i}\epsilon_n$	Bohm diffusion: $C \propto \sqrt{\frac{Rq\epsilon_n}{\epsilon^{3/2}}}$ $\alpha_n = 1/2, \alpha_B = 0$ Gyro-Bohm diffusion: $C \propto \left(\frac{R^4q^2\epsilon_n^2}{\epsilon A_i}\right)^{1/5}$ $\alpha_n = 2/5, \alpha_B = 2/5$
Itoh and Itoh [69]; Ohkawa and Hinton [119]: more fundamental condition on ion-orbit loss	$\rho_{*s} \gtrsim \frac{\epsilon_n\sqrt{\tau}}{q}$	$C \propto \frac{\epsilon^2R^2\epsilon_n^2\tau}{q^2A_i}$ $\alpha_n = 0, \alpha_B = 2$

Table 1. (Continued)

Theory	Transition criterion	Critical temperature
Itoh *et al* [127]: ion-orbit-loss, CDBM transport model ($T_e = T_i$ assumed)	$\frac{1}{(\epsilon_T R)^2}\left(\frac{c}{\omega_{pe}}\right)^2 \sqrt{\frac{\epsilon}{\epsilon_{T_e}}}\frac{\beta q^2}{\rho_{*s}\hat{\nu}_{*i}} > f(s)$	$C \propto \frac{\epsilon_T}{\epsilon^{3/5}}\frac{R^{4/5}A_i^{1/5}}{q^{2/5}}$ $\alpha_n = 2/5, \alpha_B = 2/5$
Hassam *et al* [70]: Stringer spin-up drive, balanced by neoclassical viscous damping. $2q^2 \gg 1$, for simplicity	$\frac{D}{D_B} \gtrsim \frac{\epsilon\epsilon_n}{\sqrt{\tau}}\frac{\hat{\nu}_{*i}}{q\rho_{*s}}$	Bohm diffusion: $C \propto \epsilon_n^{2/5}\epsilon^{4/5}\tau^{3/5}R^{4/5}A_i^{-1/5}$ $\alpha_n = 2/5, \alpha_B = 2/5$ Gyro-Bohm diffusion: $C \propto \epsilon_n^{1/3}\epsilon\tau^{1/2}RA_i^{-1/3}$ $\alpha_n = 1/3, \alpha_B = 2/3$
Strauss [144] Stringer spin-up, separatrix geometry, dissipative reduced MHD	$\frac{D}{D_B} > \frac{\epsilon_p^2}{\epsilon\tilde{G}q\rho_{*s}}$	Bohm diffusion: $C \propto \frac{R^2\epsilon_p^4}{A_i q^2}$ $\alpha_n = 0, \alpha_B = 2$ Gyro-Bohm diffusion: $C \propto \frac{\epsilon\epsilon_p^2 R^2}{A_i q}$ $\alpha_n = 0, \alpha_B = 2$
Rozhansky *et al* [146, 147]: role of a sheared radial electric field on particle diffusivity	$\rho_* \gtrsim \sqrt{\tau}\frac{\epsilon_n}{q}$	$C \propto \frac{\tau\epsilon^2 R^2\epsilon_n^2}{q^2 A_i}$ $\alpha_n = 0, \alpha_B = 2$
Staebler and Dominguez [161]: ion temperature gradient stabilization and turbulent viscosity	Ion-orbit-loss momentum source ($f =$ fast particle fraction): $\frac{f\sqrt{\nu_{*i}}}{\rho_{*s}}\frac{\epsilon_n^2}{\epsilon^2} > 1$ Neutral beam injection momentum source $P \gtrsim \frac{pV\rho_s c_s}{L_n^2}$	Criterion on f
Transport bifurcation theories, e.g. flow shear suppression of ion-temperature gradient turbulence (equation (2.40)); $0 < \alpha < 1$	$\rho_{*s} > \frac{\epsilon_T^{1+\alpha}}{\epsilon}$	$C \propto \frac{\epsilon_T^{2+2\alpha}R^2}{A_i}$ $\alpha_n = 0, \alpha_B = 2$
Diamond *et al* [167–169]: Generic model system describing flow/turbulence interaction	$\nu_{*i} < 1$: $\nu_{*i} \lesssim \frac{1}{s\tau}\left[\frac{\rho_{*s}q}{\epsilon_n^2}\right]^2$ $\nu_{*i} > 1$: $\rho_{*s} > \frac{\epsilon_n^2\sqrt{s\tau}}{q}$	$C \propto \tau\left(\frac{s}{q}\right)^{1/3}\frac{R\epsilon^{1/6}\epsilon_n^{4/3}}{A_i^{1/3}}$ $\alpha_n = 1/3, \alpha_B = 2/3$ $C \propto \frac{\epsilon_n^4\epsilon^2 R^2\tau s}{q^2 A_i}$ $\alpha_n = 0, \alpha_B = 2$
Helander [194]: effect of heavy impurity ions, charge Ze, on neo-classical transport	$\frac{Z^2}{\sqrt{\tau}}\hat{\nu}_{*i}\frac{\rho_{*s}q}{\epsilon_n}\left(1 - \frac{\epsilon_n}{2\epsilon_T}\right) > 2$	$C \propto \left(\frac{Zq^2}{\epsilon\epsilon_n}\right)^{2/3}\tau A_i^{1/3}\left(1 - \frac{\epsilon_n}{2\epsilon_T}\right)^{2/3}$ $\alpha_n = 2/3, \alpha_B = -2/3$
Dnestrovskij *et al* [196]: CPTM model with 'forgetting factor'	$\frac{\epsilon}{\epsilon_p} > C_D - \frac{3}{q}$ where C_D is a numerical coefficient ∼9–12	

Table 1. (Continued)

Glossary of definitions in table

$\rho_s = 3.23 \times 10^{-3} \frac{\sqrt{A_i T_e}}{B}$	$C_s = 3.10 \times 10^5 \sqrt{\frac{T_e}{A_i}}$	$V_{The} = 1.88 \times 10^7 \sqrt{T_e}$	$V_{Thi} = 4.37 \times 10^5 \sqrt{\frac{T_i}{A_i}}$
$\nu_e = 1.562 \times 10^4 \frac{n_{19}}{T_e^{3/2}}$	$\nu_i = 257.8 \frac{n_{19}}{\sqrt{T_i^3 A_i}}$	$\hat{\nu}_{*e} = 8.30 \times 10^{-4} \frac{n_{19} R q}{T_e^2}$	$\hat{\nu}_{*i} = 5.88 \times 10^{-4} \frac{n_{19} R q}{T_i^2}$
$\hat{\nu}_{*j} = \epsilon^{3/2} \nu_{*j}$	$\tau = \frac{T_e}{T_i}$	$\beta = 4.03 \times 10^{-3} \frac{(1+\tau)}{\tau} \frac{n_{19} T_e}{B^2}$	$\tilde{G} = \frac{R^2 B_p^2}{\langle R^2 B_p^2 \rangle} - 1$
$\epsilon_T = L_T / R$	$\epsilon_n = L_n / R$	$\epsilon_p = L_p / R$	$D_B = \rho_s C_s$
$D_{GB} = D_B \rho_{*s}$	$\rho_{*s} = \frac{\rho_s}{a}$	$b = (k_\theta \rho_s)^2$	$\omega_{pe} = 1.78 \times 10^{11} \sqrt{n_{19}}$

Angled brackets denote flux surface average.

$T_{e,i}$ temperature in keV; n_{19}, density in 10^{19} m^{-3}; B, magnetic field in T; B_p, poloidal component of magnetic field in T; R, major radius in m; a, minor radius in m; ρ_s, ion Larmor radius measured with electron temperature in m; C_s, sound speed in m s^{-1}; q, safety factor, which is defined to be $L_\parallel / R$ in the SOL (where $L_\parallel$ is the distance between divertor target plates along the magnetic field line); $\ln \Lambda = 17$ is taken for both electron and ion collision frequencies.

parameter L_n); one should bear in mind that the region over which the initial L–H transition occurs may well differ from the transport barrier of a fully developed H-mode;

(vii) rapid changes in the edge values of plasma flow velocity and/or the associated radial electric field at the transition: the latter usually becomes more negative;

(viii) the rapid time scale for changes (approximately milliseconds for fast changes, although slow changes, approximately tens of milliseconds, can occur) and causal relationships: for example, between radial electric field changes and confinement changes; the possibility of triggering by biasing experiments.

We now consider these points in relation to the theories in sections 3–5 and draw some general conclusions.

(i) The ubiquity of the L–H transition indicates some robust, 'universal' ingredient, such as the concept of $\boldsymbol{E} \times \boldsymbol{B}$ shear suppression which has been invoked for both internal and the H-mode transport barriers [200]. Of course, many of the theories discussed do involve this feature. It is interesting that the stellarator W7-AS finds H-mode access possible when the magnetic configuration minimizes neoclassical flow damping [202], adding support for flow-based theories. The role of separatrix geometry is suggestive of theories in which the geometry [77, 78] and associated enhanced magnetic shear [97] stabilizes modes or those in which reduced recycling and neutral particles play a role [121, 138, 139, 173, 195]; alternatively the divertor configuration itself may be a key element [115, 119, 181, 188].

(ii) The significance of the parametric scaling of P_{Th} is clouded by the issue of confinement time, τ_E, or edge transport, scalings. Sometimes a theory is 'complete' in that it contains the description of transport within it; often, however, an empirical scaling for τ_E is introduced to deduce a scaling for P_{Th} from the L–H transition criterion. Using dimensional analysis arguments, the empirical scaling (1.7) points to a role for ρ_*, ν_* and β. Alternatively, neutral particles may be involved: indeed Owen *et al* [203] have demonstrated a correlation on DIII-D between P_{Th} and the ratios ν_{cx}/μ, in the transition criterion or edge transport scaling (see figure 29) and a similar correlation of P_{Th} with neutrals has been observed in JT-60U [13]; a response to X-point height and wall conditioning is a signature of this. A number of different theories have predicted scalings for P_{Th} broadly consistent with equation (1.7) as shown in table 2.

The observations of a low density threshold, or increase in P_{Th} at low density, may indicate a role for neutral particles [121, 138, 139, 173], the ratio T_e/T_i [51], magnetic perturbations [130], the collisionless skin depth [116], peeling modes [81, 82] or ion-∇B drifts [184–188].

Table 2. L–H power threshold models.

Theory	Power threshold
Kerner *et al* [107]: threshold in β due to suppression of transport from long wavelength, collisionless drift wave turbulence; converted to power threshold using power balance and Bohm-like edge diffusivity, together with neutral particle source to determine density gradient	Ionization rate inversely proportional to square root of temperature: $P_{\rm Th} \propto \frac{S n_{\rm e}^{3/4} B^{3/2}}{A_{\rm i}}$ Ionization rate independent of temperature: $P_{\rm Th} \propto \frac{S n_{\rm e}^{1/2} B^2}{A_{\rm i}^{5/4}}$
Cordey *et al* [110]: resistive MHD drift/interchange turbulence in SOL, stabilized by steep gradients; SOL energy balance to convert to power threshold	Resistive interchange, collisional (SND): $P_{\rm Th} \propto \frac{n^4 S}{B}\left(\frac{L_\parallel^2}{R}\right)^4$ Resistive interchange, collisional (DND): $P_{\rm Th} \propto n^{8/5} S \left(\frac{L_\parallel^2}{R}\right)^{8/5} \frac{B^{3/5}}{L_\parallel^{2/5}}$ Drift wave, collisionless: $P_{\rm Th} \propto nSB^3 L_\parallel^3$ Drift wave, collisional: $P_{\rm Th} \propto n^{3/2} SB L_\parallel^{3/2}$
Cordey *et al* [112]: effect of parallel current direction in SOL on sheath resistance for interchange modes; $u = j_\parallel / neC_{\rm s}$, the current density $j_\parallel$ is positive when the ion-∇B drift is away from the X-point and $f(u)$ varies by a factor $\sim$2 when u varies from -1 to +1	$P_{\rm Th} \propto [f(u)]^{8/5} n^{8/5} S B^{3/5} q^3 R$
Cohen and Xu [115]: stabilizing effect of polarization current on drift-curvature modes in the SOL ($L_{\rm Pol}$ is the distance around the poloidal circumference)	$P_{\rm Th} \propto A_{\rm i}^{-0.99} B^{0.74} n^{0.75} R L_{\rm Pol}^{0.68}$
Chankin [116]: suppression of drift wave turbulence in SOL when skin depth exceeds perpendicular wavelength ($\gamma = 1.75$ for $k_\perp \sim \rho_{\rm i}^{-1}$ or $\gamma = 1.5$ for $k_\perp \sim 1/\sqrt{(L\rho_{\rm i})}$)	$P_{\rm Th} \propto nBR^\gamma$
Itoh and Itoh [121]: ion-orbit-loss generation of toroidal flow, combined with SOL power balance	$P_{\rm Th} \propto Z^{1.5} B^{1.4} R^{1.2} a^{0.5} n_{19}^{0.5} A_{\rm i}^{-1.2} I^{-0.7}$
Itoh and Itoh [122]: auxiliary heated energetic electron (temperature $T_{\rm h}$) loss due to ripple trapping, balanced against ion-orbit loss, including radial variation in the radial electric field	$P_{\rm Th} \propto 10\epsilon^2 \frac{T_{\rm h}}{T_{\rm i}} \frac{\rho_{\rm pi}}{a} \nu_{\rm i} n_{\rm i} T_{\rm i} V$
Garbet and Waltz [165]: flow shear stabilization of ion temperature gradient modes	$P_{\rm Th} R^{3/4} \propto \rho_*^{-7/2} \beta^{7/4} \nu_*^{-3/4}$
Diamond *et al* [167]: generic 'predator–prey' model of effect of shear flow on turbulence; turbulent diffusion arising from drift wave turbulence (μ is the L-mode viscosity (e.g. neoclassical), n and T are L-mode values)	$P_{\rm Th} \propto \mu n T L_s a R$

Table 2. (Continued)

Sugama and Horton [177]: Reynolds stress arising from electrostatic resistive pressure gradient driven turbulence (D_p is the pressure diffusivity)	$P_{\rm Th} \propto aRD_p \frac{{\rm d}p}{{\rm d}r}$
Ossipenko [179]: system of model equations for flow shear, turbulent kinetic energy, thermal energy and temperature profile evolution; power threshold corresponds to a bifurcation from a low flow state to one of high flow (c is a constant)	$P_{\rm Th} \propto nB^2\left(1+\frac{c}{nB}\right)$
Rebut *et al* [183]: electron–ion energy balance ($\chi_{\rm e} \ll \chi_{\rm i}$)	$P_{\rm Th} \propto \left[n^2 V\left(\frac{nS\chi_{\rm i}}{L_T}\right)^{1/2}\right]^{2/3}$
Carlstrom *et al* [187]: consideration of ion-∇B drifts, incorporating some physical effects ($\pm$ correspond to favourable/unfavourable ion-∇B drift direction), fitted to DIII-D data	$P_{\rm Th} = r\left[5.7 \mp 4.35\frac{P_{\rm Th}^{2/7}}{B}\right]$
Dnestrovskij *et al* [196]: canonical profile transport model; L–H transition when profiles deviate sufficiently far from the canonical ones (Z_0 is the 'forgetting factor', fitted empirically and taken to be $Z_0 \sim 6$–9)	$P_{\rm Th} = 0.25R\left(\frac{a}{R}\right)^{0.75} q(a/2)q(a)$ $\times \frac{\bar{n}T(a)}{B} T^{1/2}(a/4)$ $\times \left(Z_0 + 3\left(1-\frac{1}{q}\right) - \frac{a}{L_n}\right)_a$
Minardi [197]: statistical mechanics model of the plasma as a set of current filaments combined with ITER89-P energy confinement scaling law	$P_{\rm Th} \propto Z_{\rm eff}^{0.57} n^{0.77} B^{0.97} S$
Connor and Wilson (equation (6.1)): $\beta_{\rm N} =$ constant condition for L–H transition, combined with ITER97 L-mode energy confinement scaling law to interpret low density threshold seen on some experiments	$P_{\rm Th} \propto \frac{B^4}{n^{0.8} A_{\rm i}}$

For example, the U-shaped variation of $P_{\rm Th}$ with n in DIII-D correlates with $\nu_{\rm cx}$ and the results in JT-60U agree with the theory of Shaing and Hsu [139]. However, an alternative and simpler argument is to combine a transition criterion such as $\beta_{\rm N} =$ constant ($\beta_{\rm N}$ is the normalized β from MHD stability theory, $\beta_{\rm N} = \beta(\%)a({\rm m})B({\rm T})/I({\rm MA})$), observed on COMPASS-D [18], with the ITER 97 L-mode scaling law [46] to yield (see figure 14)

$$P_{\rm Th} \propto \frac{B^4}{n^{0.8} A_{\rm i}}. \tag{6.1}$$

It is interesting that τ_E introduces a strong isotope effect, observed on JET experiments in H, D and T [20, 156]. This is also consistent with the transport bifurcation theory of Hinton [149], and a number of theories in table 2 [107, 115, 121]. The ubiquitous observation that $P_{\rm Th}$ decreases with favourable ion-∇B drift is consistent with some neoclassically based theories [39, 184–187]. Some of the more detailed consequences of these theories, such as the increase of $P_{\rm Th}$ following reductions of parallel temperature gradients by gas puffing and changes in

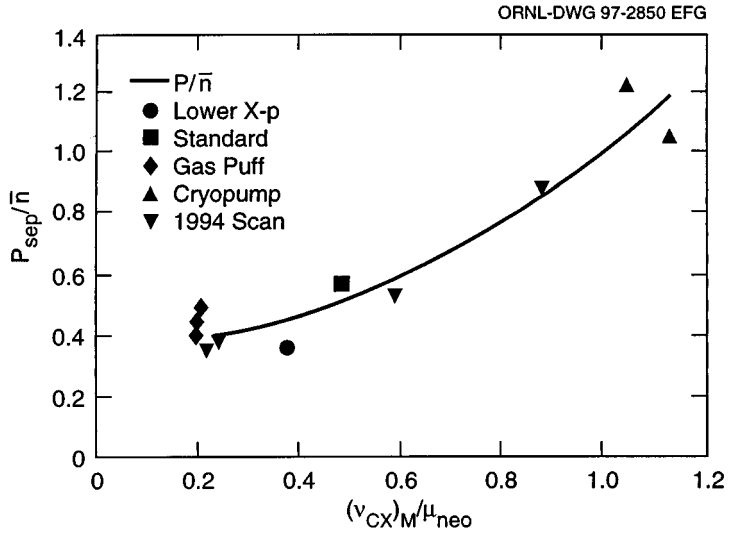

Figure 29. Correlation of threshold power, $P_{\rm sep}$, normalized to the density, $\bar{n}$, with the charge exchange frequency, $\nu_{\rm cx}$, normalized to the neoclassical viscosity, $\mu_{\rm neo}$, on DIII-D [203].

the X-point height, are seen on DIII-D, but the predicted inverse scaling with B when the ion-∇B drift is reversed is not (this may be confused by the effect of B on the sawtooth heat pulse contribution to $P_{\rm Th}$) [187]. The fact that the degree of hysteresis is dependent on the 'quality' of the H-mode confinement suggests that it might arise largely as a trivial result of the differences between L- and H-mode confinement.

(iii) The experimentally observed scaling laws for critical values of edge parameters at the L–H transition (e.g. equation (1.9) for $T_{\rm ecrit}$) are usually more directly meaningful for theories than the scaling law for $P_{\rm Th}$; according to table 1 the theory of [101] offers one of the better fits to (1.9). Recent comparisons of $T_{\rm ecrit}$ data in DIII-D (and their relation to those in ASDEX Upgrade) indicate that it is not a critical parameter for the L–H transition [83]; it should also be noted that $T_{\rm ecrit}$ is a weak function of P in a collisional SOL, as indicated by equation (2.26) for example. It is physically more meaningful to consider dimensionless parameters such as ρ_*, β and ν_*, possibly involving local edge gradient lengths. Similarity experiments on JET and ASDEX Upgrade [204] demonstrate that the transition depends on ρ_*, β and ν_*, and that there is no need to invoke neutral particle effects. Experimental data is generally more supportive of a critical value of ρ_* or β than ν_* [24, 204]. Furthermore, attempts to correlate the transition with $\nu_{*\rm i} \sim 1$ have met with mixed success [205–207]. While ASDEX, PDX and JT-60U [13] show $\nu_{*\rm i} \sim 1$, ASDEX Upgrade finds $\nu_{*\rm i} \sim 5$–15 [8] and DIII-D $\nu_{*\rm i} \sim 2$–17 [208]. This is claimed to count against theories based on ion-orbit loss (section 4.1.1) and the collisionality dependence of poloidal flow damping [143, 167, 177], although the more energetic ions will still be lost: it is possible to invoke a role for energetic ions [129] to explain transitions with $\nu_{*\rm i} \sim 50$ in JFT-2M.

On the other hand, there is more support for theories based on the stabilization of instabilities driven by pressure gradients and edge currents, or suppression of transport with β. The operational diagram proposed by ASDEX Upgrade [8] suggests a role for β, but at a lower value than that for ideal MHD ballooning instability; indeed detailed comparisons with DIII-D and JET argue against such theories [77, 78], but could support ones based on

resistive ballooning modes [86–90] or electromagnetic drift waves [103, 106, 116]; Alcator C-Mod [21] shows interesting agreement with the work of [90]. The response of the transition to current ramps [18, 84, 209] provides evidence for a role for peeling mode theories [81, 82], but could point to a role for magnetic shear stabilization of instabilities [97]. Estimates of the edge density gradients at the transition in DIII-D are consistent with the transport bifurcation theories [149]. An important point to mention in this context is that it may be necessary to distinguish the condition for the onset of flow generation from that for turbulence suppression in theories involving flow shear; the former may well be characterized by a critial ν_*, whereas the latter, which may be more relevant to H-mode onset, could be characterized by a critical value for ρ_* [210]. Another point to bear in mind is that critical parameters involving edge gradients, for example α, may well show a correlation with L- and H-mode regimes; however, this could merely reflect the steeper edge gradients in the H-mode, and be unrelated to the transition. A careful analysis of the role of neutral particles in DIII-D [203] shows that the critical edge temperature is correlated with $\nu_{\rm cx}$, supporting a role for neutral particles in ion-orbit-loss theories [121, 136, 138, 139] or theories involving poloidal flow damping affected by charge exchange losses [173]; however, $\nu_{*\rm i}$ is also correlated with neutral particle densities [13], which could confuse this possibility. Finally, it should be noted that a theory successfully describing the dynamic behaviour of 'dithering' H-modes in ASDEX Upgrade, based on the ion-orbit-loss theory of Itoh and Itoh [69], has been developed by Zohm *et al* [211].

(iv) The fact that the L–H transition appears to take place inside the separatrix argues against theories based on changes in the SOL confinement (section 3.2). However, it is possible these could serve as a trigger for a change in the edge of the core [76, 115, 195]. It has been observed in DIII-D [83] that there is little change in edge parameters when the ion-∇B direction is reversed, but that those in the SOL region are affected; this would point to the SOL as the origin of the trigger. The sensitivity of the transition to details of the X-point position, and plasma conditions there, as observed on DIII-D [83] and JET for example, suggests one should take these into account in L–H transition models, as in [136, 138]. The fact that changes seem to be precipitated at the outer midplane is suggestive of theories based on the stabilization of ballooning modes or suppression of turbulent transport by radial electric field shear, which equation (2.33) shows is most easily achieved there.

(v) Clearly the sharp suppression of turbulent fluctuations, both electrostatic and electromagnetic, in the edge is consistent with theories involving the stabilization or suppression of modes by radial electric field shear; indeed JT-60U observes a correlation of fluctuation suppression with poloidal flow shear on the low field side, where it is most effective according to equation (2.33). Furthermore, the reduction in radial correlation lengths and the creation of a transport barrier is in accord with the BDT theory [34]. It is interesting to note that a sheared radial electric field can generate an inward pinch [212], resulting in an improved edge confinement. Evidence for the presence of magnetic fluctuations could provide support for theories involving turbulent non-ambipolar electron loss [69, 166].

(vi) The scaling of the transport barrier width, Δ, is significant for theories involving the suppression of turbulence by radial electric field shear, since it is related to the region over which the electric field is generated. This can be controlled by:

(a) ion-orbit loss with $\Delta \propto \rho_{\rm pi}$, although orbit squeezing [135] could remove the current scaling from this (but also reduce its magnitude!);
(b) viscosity, so that $\Delta \propto (\mu_\perp/\nu)^{1/2}$, where $\mu_\perp$ is the, possibly turbulent, cross-field viscosity and ν a drag frequency, say poloidal flow damping (this can lead to $\Delta \propto \ell_{\rm n}$, if neutral particle effects dominate $\mu_\perp$ and ν, and $\Delta \propto \rho_{\rm pi}$ for classical collisional processes; but other results can emerge in the case of a turbulent viscosity); the presence of $\mu_\perp$ can also

broaden Δ from that predicted in ion-orbit-loss theories;

(c) the transport processes themselves; for example, for typical ITG transport, $\Delta \propto \rho_{\rm i}^{\alpha} L_T^{1-\alpha}$ [213];

(d) edge fuelling by neutral particles, with $\Delta \propto \ell_{\rm n}$;

(e) Reynolds stress, when Δ is controlled by the mode structure; thus $\Delta \propto \rho_{\rm i}^{\beta} R^{1-\beta}$ with, for example, $\beta = 1$ [72] or $\beta = 2/3$ [154].

The experimental evidence is varied. As shown in figure 4, JT-60U suggests $\Delta \propto \rho_{\rm pi}$ [27] (numerically this may need to be related to fast ions, although this cannot explain JFT-2M observations). Evidence from JFT-2M is more suggestive of a role for $\mu_\perp$ than $\rho_{\rm pi}$ in determining Δ; even though there is a region of high E_r shear, the data does not support an orbit squeezing model [214]. DIII-D does not see a clear scaling with $\rho_{\rm pi}$ [215]; JET suggests a weaker scaling, say weaker than $\Delta \propto (\rho_{\rm pi} a)^{1/2}$ [157, 158], as indicated in figure 30, and a correlation with the fast-ion poloidal radius has been suggested [216]; a multi-machine database favours $\Delta \propto R$ [79]. Thus the evidence is far from conclusive and could be used in particular instances to support any of the classes (a)–(e) listed above; it is interesting that the last result $\Delta \propto R$, is consistent with the CPTM model [196]. A further point is that the H–VH-mode transition in DIII-D could correspond to the increase in Δ with incident flux predicted by Hinton and Staebler [162]. It should also be noted that the velocity shear width tends to narrow in the H-mode: this is consistent with a scaling $\Delta \propto (\mu_\perp/\nu)^{1/2}$ in which the turbulent viscosity reduces in the H-mode, rather than a decrease in the effective poloidal flow damping ν. This observation is counter to theories based on a reduction of neoclassical flow damping or a change in sign of the net damping, as required by Reynolds stress dynamo theory, when anomalous viscosity is included [201].

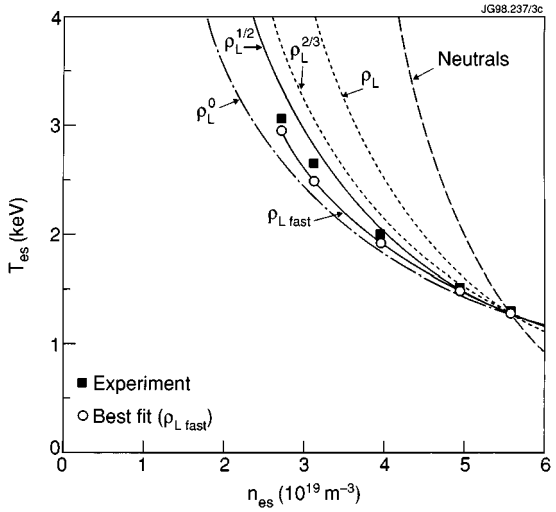

Figure 30. Comparison of the consequences in the edge temperature and density, $T_{\rm es}$ and $n_{\rm es}$, respectively, plane of different models for the dependence of the transport barrier width, Δ, on local plasma parameters ($\Delta =$ constant (ρ_L^0); $\Delta \propto \rho_{\rm fast}$ ($\rho_{L\,fast}$); $\Delta \propto \sqrt{\rho_{\rm i} a}$ ($\rho_L^{1/2}$); $\Delta \propto \sqrt[3]{\rho_{\rm i}^2 a}$ ($\rho_L^{3/2}$); $\Delta \propto \rho_{\rm i}$ (ρ_L); $\Delta \propto \lambda_{\rm ion}$ (neutrals); and ■, experimental data. The open circles represent the best fit, namely $\Delta \propto \rho_{\rm fast}$ [158]).

(vii) The development of radial electric fields observed at the L–H transition reinforces the flow shear paradigm. Remarkably, changes in E_r at the transition were predicted theoretically

[69] before they were observed experimentally; the observation of these has led to their inclusion in many later theories. However, the fact that, experimentally, $E_r < 0$ is difficult to reconcile with the ion-orbit-loss theory of Itoh and Itoh [69] but can be explained by introducing the effects of E_r' [120]. Measurements of impurity flows $V_{\theta z}$ [214] have the correct magnitude for the theory of Shaing and Crume [68], but analysis of the main ion flow shows it to be in the wrong direction. Observations on DIII-D [217] of poloidal flows are inconsistent with ion-orbit-loss or Stringer spin-up theories at the time they are measured (∼3.5 ms after the transition), but may not be so at the transition point itself. These measurements also show that theories need to account for both p' and V_θ dynamics. Measurements of radial electric fields on JET [218] indicate smaller absolute values than on DIII-D. However, according to equations (2.28) or (2.30), the true measure of electric field shear stabilization is in terms of the parameter $R(\mathrm{d}V_\mathrm{E}/\mathrm{d}r)/C_\mathrm{s}$, and this allows smaller values of E_r to have a significant impact in larger devices.

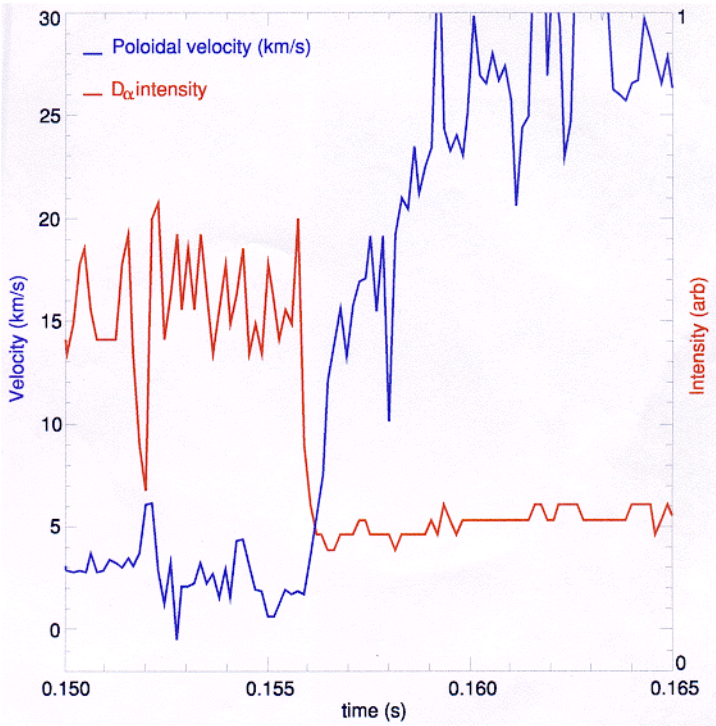

Figure 31. Time evolution of the poloidal velocity in COMPASS-D (in km s^{-1}) at the L–H transition [225]; the D_α intensity is shown for reference.

(viii) A more decisive and stringent test of theories concerns the causal relationships between changes in radial electric field, or plasma flow, and the L–H transition. Observations on DIII-D of the time sequence of changes in E_r and the fluctuations are consistent with $\boldsymbol{E} \times \boldsymbol{B}$ shear causing the change in fluctuations [54]. Both the main ion pressure gradient, p_i', and poloidal flow, $V_{\theta\mathrm{i}}$, are important in determining E_r, with the poloidal flow providing the 'trigger'; thus complete theories must contain the evolution of both p_i' and $V_{\theta\mathrm{i}}$, as in [169]. Furthermore, the sharp onset of fluctuation suppression suggests that a critical E_r is required for this to occur, which also points to models which self-consistently evolve p_i' and $V_{\theta\mathrm{i}}$ [128, 167, 169, 170], rather than those that do not [34, 68]. Fluctuation measurements on

DIII-D show that flow shear stabilization theories need to include multiple fluctuating fields and their relative phases. It should be noted that experimental values of $V_{\theta \mathrm{i}}$ disagree with the predictions of conventional neoclassical theory, questioning theories utilizing such values [149]; this points to the need to elaborate the theory to allow for steep gradients [193, 194] or neutral particle collisions [134]. JFT-2M observes a charge exchange fast ion flux before the H_α rise [219] suggesting this triggers the transition, supporting ion-orbit-loss theories. Observations of changes in E_r on ASDEX Upgrade have given rise to the suggestion that they are too slow to be a trigger for the H-mode [220], but this remains an open question [221]; more conclusive evidence for rapid potential changes in a narrow region has been reported on JFT-2M [222], supporting the theory of [121].

There is some evidence from TFTR [209] that a spin-up of V_θ may precede the transition. Whereas the evidence above is consistent with the picture of turbulence suppression by sheared radial electric fields, that from COMPASS-D [223–225], shown in figure 31, and JET [218] is not so supportive. To the extent that the spatial resolution of the diagnostics allows one to relate the location of measured changes in E_r to the magnetic surface where the L–H transition occurs, these measurements suggest rather that the electric fields build up as a consequence of the steepening pressure gradient resulting from the creation of an edge transport barrier.

Finally, powerful support for features of models based on ion-orbit-loss and neoclassical viscosity and a causal role for E_r is provided by bias experiments [226–228]. Explicit solutions for the radial electric field structure in such situations have been given [229].

Time scales for the transition are also variable: ranging from fast transitions (hundreds of μs), consistent with a 'hard' bifurcation, to slower ones ($\sim$50 ms), particularly near $P \sim P_{\mathrm{Th}}$, reminiscent of 'soft' bifurcations (or second-order phase transitions). Some of these slower transitions may occur when the neutral density is higher and reflect a 'stiff' balance between the effect of neutrals on ion-orbit loss and on poloidal momentum loss [230]. Detailed studies of the temporal evolution of fluctuations and the confinement transition in DIII-D [54] would require a value $\gamma = 2$ for the exponent in equation (2.36), consistent with deductions from bias experiments [227].

7. Conclusions

We have reviewed theoretical models proposed to explain the L–H transition. Identifying a successful model would, apart from giving the satisfaction of understanding this phenomenon, contribute to reducing the uncertainty in predicting P_{Th}, the threshold power for the H-mode, in a Next Step device such as ITER and perhaps enable more efficient access of the H-mode.

After briefly discussing the phenomenology of the L–H transition in section 1, we described general theoretical principles available for understanding the transition in section 2, before systematically reviewing the available models. Thus in section 3 we considered those based on stabilizing specific instabilities, first those in the plasma edge and then those in the SOL. In section 4 we reviewed models involving the generation of sheared radial electric fields and in section 5 a number of other types of theory. The predictions of these theories for critical edge parameters or P_{Th} are summarized in tables 1 and 2, respectively. The discussion in section 6 attempted to marshall experimental observations in order to identify the more promising models. While there is considerable support (but also some reservations) for the paradigm of sheared radial electric field suppression of turbulence as an element of the L–H transition, there is no one theory that accounts for all observations. These observations themselves vary between situations and tokamaks, so there may be a different 'trigger' for the bifurcations playing a part in each case: ion-orbit loss, Reynolds stress, neutral particle effects etc. Improved and more extensive data on causal relationships, scalings of transport barrier

widths and, particularly, critical values of edge plasma parameters for comparison with results in table 1, would help to discriminate between candidate theories. However, to answer the key practical question of the P_{Th} scaling, one also needs a theory of confinement at the plasma edge, including transport simulations to self-consistently treat all the relevant ingredients of models: n, $T_{\mathrm{e,i}}$, E_r, etc. In short, given the range of possible effects and phenomena, the complexities of X-point geometry and the divertor, the role of atomic physics processes, the dominance of different instability mechanisms in different regimes, the interaction of turbulence and transport, one may well need to study the L–H transition using large-scale numerical simulations incorporating all this physics and geometry. From such studies one might hope to identify which of the theoretical concepts or physical ingredients reviewed in this paper dominate in particular situations. In this way, one could build up an understanding of the various experimental results relating to the L–H transition and develop a predictive model.

Acknowledgments

This work is jointly funded by UK DTI and EURATOM. The authors are grateful for valuable comments and insights from Drs B A Carreras, K Itoh and S-I Itoh, to many authors for being so helpful in providing their figures for use in this review and, finally, for the fortitude of Mrs J Bishop in producing the manuscript.

References

[1] Wagner F *et al* 1982 *Phys. Rev. Lett.* **49** 1408
[2] Wagner F *et al* 1991 *Plasma Physics and Controlled Nuclear Fusion Research (Proc. 13th Int. Conf., Washington, 1990)* vol 1 (Vienna: IAEA) p 277
[3] Köppendörfer W *et al* 1996 *Plasma Physics and Controlled Nuclear Fusion Research (Proc. 15th Int. Conf., Seville, 1994)* vol 1 (Vienna: IAEA) p 241
[4] Shimomura Y, Aymar R, Chuyanov V, Huguet M, Parker R and the ITER Joint Central Team and Home Teams 1999 *Nucl. Fusion* **39** 1295
[5] 1998 *Technical Basis for the ITER Final Design Report (ITER EDA Documentation Series No 16)* (Vienna: IAEA)
[6] Thomas D M, Groebner R J, Burrell K H, Osborne T H and Carlstrom T N 1998 *Plasma Phys. Control. Fusion* **40** 707
[7] JET Team (presented by Cordey J G) 1997 *Fusion Energy (Proc. 16th Int. Conf., Montreal, 1996)* vol 1 (Vienna: IAEA) p 603
[8] Ryter F *et al* 1998 *Plasma Phys. Control. Fusion* **40** 725
[9] Kardaun O J W F, Kardaun J W P F, Itoh S-I and Itoh K 1998 *Controlled Fusion and Plasma Physics (Proc. 25th EPS Conf., Prague, 1998)* vol 22C ed P Pavlo (Mulhouse: European Physical Society) p 1975 (paper G100)
[10] ASDEX Team 1989 *Nucl. Fusion* **29** 1959
[11] Wagner F 1994 *Workshop on Transport and Fusion Plasmas* (Gothenburg, Sweden) unpublished
[12] Connor J W and Taylor J B 1977 *Nucl. Fusion* **17** 1047
[13] Fukuda T *et al* 1997 *Nucl. Fusion* **37** 1199
[14] Lackner K 1994 *Comments Plasma Phys. Control. Fusion* **15** 359
[15] Kadomtsev B B 1994 Private communication
[16] Kadomtsev B B 1992 *Tokamak Plasma, a Complex Physical System* (Bristol: IOP Publishing) ch 6
[17] ITER Confinement Database and Modelling Expert Group (presented by Takizuka T) 1997 *Fusion Energy (Proc. 16th Int. Conf., Montreal, 1996)* vol 2 (Vienna: IAEA) p 795
[18] Fielding S J *et al* 1996 *Plasma Phys. Control. Fusion* **38** 1091
[19] Fielding S J *et al* 1998 *Controlled Fusion and Plasma Physics (Proc. 25th EPS Conf., Prague, 1998)* vol 22C ed P Pavlo (Mulhouse: European Physical Society) p 838 (paper B092)
[20] Righi E *et al* 1999 *Nucl. Fusion* **39** 309
[21] Hubbard A E *et al* 1998 *Plasma Phys. Control. Fusion* **40** 689
[22] Righi E *et al* 1997 *Controlled Fusion and Plasma Physics (Proc. 24th EPS Conf., Berchtesgaden, 1997)* vol 21A, ed M Schittenhelm, R Bartiromo and F Wagner (Geneva: European Physical Society) part 1, p 93

[23] The ITER H-mode Threshold Database Working Group (presented by Righi E) 1998 *Plasma Phys. Control. Fusion* **40** 857
[24] Zohm H *et al* 1997 *Fusion Energy (Proc. 16th Int. Conf., Montreal, 1996)* vol 1 (Vienna: IAEA) p 439
[25] Groebner R J and Carlstrom T N 1998 *Plasma Phys. Control. Fusion* **40** 673
[26] The JET Team (presented by Cordey J G) 1999 *Fusion Energy (Proc. 17th Int. Conf., Yokohama, 1998)* CD-ROM (Vienna: IAEA) paper EX7/1; also *Nucl. Fusion* **39** 1763
[27] Hatae T *et al* 1998 *Plasma Phys. Control. Fusion* **40** 1073
[28] Doyle E J *et al* 1993 *Plasma Physics and Controlled Nuclear Fusion Research (Proc. 14th Int. Conf., Würzburg, 1992)* vol 1 (Vienna: IAEA) p 235
[29] Kadomtsev B B 1975 *Fiz. Plasmy* **1** 531 (Engl. Transl. 1975 *Sov. Phys.–J. Plasma. Phys.* **1** 295)
[30] Itoh S-I and Itoh K 1994 *Plasma Phys. Control. Fusion* **36** 1845
[31] Shaing K C *et al* 1989 *Plasma Physics and Controlled Nuclear Fusion Research (Proc. 12th Int. Conf., Nice, 1988)* vol 2 (Vienna: IAEA) p 13
[32] Itoh S-I, Itoh K, Ohkawa T and Ueda N 1989 *Plasma Physics and Controlled Nuclear Fusion Research (Proc. 12th Int. Conf., Nice, 1988)* vol 2 (Vienna: IAEA) p 23
[33] Hassam A B 1991 *Comments Plasma Phys. Control. Fusion* **14** 275
[34] Biglari H, Diamond P H and Terry P W 1990 *Phys. Fluids* B **2** 1
[35] Itoh K 1994 *Plasma Phys. Control. Fusion* **36** A307
[36] Itoh K and Itoh S-I 1996 *Plasma Phys. Control. Fusion* **38** 1
[37] Itoh K, Itoh S-I and Fukuyama A 1999 *Transport and Structural Formation in Plasmas* (Bristol: IOP Publishing)
[38] Wesson J A 1987 *Theory of Fusion Plasmas* ed A Bondeson, E Sindoni and F Troyon (Bologna: Editrice Compositori) p 253
[39] Hinton F L 1985 *Nucl. Fusion* **25** 1457
[40] Burrell K H *et al* 1989 *Plasma Phys. Control. Fusion* **31** 1649
[41] Burrell K H *et al* 1990 *Phys. Fluids* B **2** 1405
[42] Burrell K H *et al* 1992 *Plasma Phys. Control. Fusion* **34** 1859
[43] Burrell K H 1994 *Plasma Phys. Control. Fusion* **36** A291
[44] Carlstrom T N 1996 *Plasma Phys. Control. Fusion* **38** 1149
[45] Luce T C, Petty C C, Balet B and Cordey J G 1997 *Fusion Energy (Proc. 16th Int. Conf., Montreal, 1996)* vol 1 (Vienna: IAEA) p 611
[46] Cordey J G 1997 *Plasma Phys. Control. Fusion* **39** B115
[47] Petty C C *et al* 1996 *Controlled Fusion and Plasma Physics (Proc. 23rd EPS Conf., Kiev, 1996)* vol 20C, ed D Gresillon, A Sitenko and A Zagorodny (Geneva: European Physical Society) part 1, p 211
[48] Perkins F W 1996 *Proc 4th Workshop of the ITER Expert Group on Confinement Databases and Modelling (Moscow, Russia)* unpublished
[49] Fukuda T, Takizuka T, Kamada Y, Tsuchiya K, Mori M and the JT-60 Team 1998 *Plasma Phys. Control. Fusion* **40** 827
[50] Connor J W, Counsell G F, Erents S K, Fielding S J, LaBombard B and Morel K 1999 *Nucl. Fusion* **39** 169
[51] Carreras B A 1997 *Proc. Combined Workshop of the Confinement and Transport and Confinement Modelling and Database ITER Expert Groups (San Diego, USA)* unpublished
[52] Lehnert B 1966 *Phys. Fluids* **9** 1367
[53] Sidikman K L, Carreras B A, Diamond P H and Garcia L 1994 *Phys. Plasmas* **1** 1142
[54] Moyer R A *et al* 1995 *Phys. Plasmas* **2** 2397
[55] Hahm T S 1994 *Phys. Plasmas* **1** 2940
[56] Hahm T S and Burrell K H 1995 *Phys. Plasmas* **2** 1648
[57] Inoue S *et al* 1980 *J. Phys. Soc. Japan* **49** 367
[58] Yoshizawa A and Yokoi N 1998 *Phys. Plasmas* **5** 2902
[59] Hahm T S, Burrell K H, Greenfield C M and Synakowski E J 1998 *Plasma Phys. Control. Fusion* **40** 657
[60] Taylor J B and Wilson H R 1996 *Plasma Phys. Control. Fusion* **38** 1999
[61] Shaing K C, Crume E C Jr and Houlberg W A 1990 *Phys. Fluids* B **2** 1492
[62] Hinton F L 1994 *Theory of Fusion Plasmas* ed E Sindoni, F Troyon and J Vaclavik (Bologna: Editrice Compositori) p 247
[63] Itoh S-I, Itoh K, Fukuyama A and Yagi M 1994 *Phys. Rev. Lett.* **72** 1200
[64] Zhang Y Z and Mahajan S M 1992 *Phys. Fluids* B **4** 1385
[65] Waltz R E, Kerbel G D and Milovich J 1994 *Phys. Plasmas* **1** 2229
[66] Isichenko M B and Diamond P H 1995 *Phys. Plasmas* **2** 2007
[67] Ware A S, Terry P W, Diamond P H and Carreras B A 1996 *Plasma Phys. Control. Fusion* **38** 1343
[68] Shaing K C and Crume E C Jr 1989 *Phys. Rev. Lett.* **63** 2369

[69] Itoh S-I and Itoh K 1988 *Phys. Rev. Lett.* **60** 2276
[70] Hassam A B, Antonsen T M Jr, Drake J F and Liu C S 1991 *Phys. Rev. Lett.* **66** 309
[71] Stringer T E 1969 *Phys. Rev. Lett.* **22** 770
[72] Diamond P H and Kim Y-B 1991 *Phys Fluids* B **3** 1626
[73] Yahagi E, Itoh K and Wakatani M 1988 *Plasma Phys. Control. Fusion* **30** 995
[74] Shaing K C 1984 *Phys Fluids* **27** 1567
[75] Lebedev V B and Diamond P H 1997 *Phys. Plasmas* **4** 1087
[76] Taylor J B, Connor J W and Helander P 1998 *Phys. Plasmas* **5** 3065
[77] Bishop C M 1986 *Nucl. Fusion* **26** 1063
[78] Bishop C M 1987 *Nucl. Fusion* **27** 1765
[79] Igitkhanov Yu *et al* 1998 *Plasma Phys. Control. Fusion* **40** 837
[80] Connor J W, Taylor J B and Turner M F 1984 *Nucl. Fusion* **24** 642
[81] Connor J W, Hastie R J, Wilson H R and Miller R L 1998 *Phys. Plasmas* **5** 2687
[82] Wilson H R, Connor J W, Field A R, Fielding S J, Miller R L, Lao L L, Ferron J R and Turnbull A D 1999 *Phys. Plasmas* **6** 1925
[83] Carlstrom T N, Burrell K H, Groebner R J, Leonard A W, Osborne T H and Thomas D M 1998 Comparison of L–H transition measurements with physics models *General Atomics Report* GA-A22989
[84] Toi K *et al* 1990 *Phys. Rev. Lett.* **64** 1895
[85] Askinazi L G *et al* 1993 *Phys. Fluids* B **5** 2420
[86] Drake J F, Guzdar P N, Novakovskii S, Liu C S, Zeiler A and Biskamp D 1996 *Plasma Physics and Controlled Nuclear Fusion Research (Proc. 15th Int. Conf., Seville, 1994)* vol 3 (Vienna: IAEA) p 483
[87] Drake J F, Lau Y T, Guzdar P N and Hassam A B 1996 *Phys. Rev. Lett.* **77** 494
[88] Rogers B N, Drake J F, Lau Y T, Guzdar P N, Hassam A B and Novakovskii S V 1997 *Fusion Energy (Proc. 16th Int. Conf., Montreal, 1996)* vol 2 (Vienna: IAEA) p 361
[89] Rogers B N and Drake J F 1997 *Phys. Rev. Lett.* **79** 229
[90] Rogers B N, Drake J F and Zeiler A 1998 *Phys. Rev. Lett.* **81** 4396
[91] Field A R, Fielding S J, Helander P, Wilson H R, Ashbourn J M A, Carolan P G, Jones P B and O'Mullane M G 1999 *Controlled Fusion and Plasma Physics (Proc. 26th EPS Conf., Maastricht, 1999)* vol 23J ed B Schweer, G Van Oost and E Vietzke (Mulhouse: European Physical Society) p 273
[92] Guzdar P and Hassam A B 1996 *Phys. Plasmas* **3** 3701
[93] Zeiler A, Biskamp D, Drake J F and Guzdar P N 1996 *Phys. Plasmas* **3** 2951
[94] Zeiler A, Biskamp D and Drake J F 1996 *Phys. Plasmas* **3** 3947
[95] Zeiler A, Drake J F and Biskamp D 1997 *Phys. Plasmas* **4** 991
[96] Zeiler A, Biskamp D, Drake J F and Rogers B N 1997 *Fusion Energy (Proc. 16th Int. Conf., Montreal, 1996)* vol 2 (Vienna: IAEA) p 657
[97] Hahm T S and Diamond P H 1987 *Phys. Fluids* **30** 133
[98] Ohyabu N, Jahns G L, Stambaugh R D and Strait E J 1987 *Phys. Rev. Lett.* **58** 120
[99] Gladd N T, Drake J F, Chang C L and Liu C S 1980 *Phys. Fluids* **23** 1182
[100] Lau Y T 1990 *Nucl. Fusion* **30** 934
[101] Strauss H R 1992 *Phys Fluids* B **4** 934
[102] Scott B, Camargo S and Jenko F 1996 *Fusion Energy (Proc. 16th Int. Conf., Montreal, 1996)* vol 2 (Vienna: IAEA) p 649
[103] Scott B 1998 *Plasma Phys. Control. Fusion* **40** 823
[104] Scott B 1999 *Joint US–EU Transport Task Force Meeting (Portland, USA)* unpublished
[105] Kerner W, Igitkhanov Yu, Janeschitz G and Pogutse O 1998 *Contrib. Plasma Phys.* **38** 118
[106] Pogutse O and Igitkhanov Yu *Czech. J. Plasma Phys.* **48** (Suppl S2) 39
[107] Kerner W, Pogutse O and Igitkhanov Yu 1998 The isotope dependence of the L–H power threshold scaling *JET Report* JET-IR(98)01
[108] Rogister A L 1994 *Plasma Phys. Control. Fusion* **36** A219
[109] Pogutse O, Kerner W, Gribkov V, Bazdenkov S and Osipenko M 1994 *Plasma Phys. Control. Fusion* **36** 1963
[110] Cordey J G, Kerner W and Pogutse O 1995 *Plasma Phys. Control. Fusion* **37** 773
[111] Chankin A V and Stangeby P C 1996 *Plasma Phys. Control. Fusion* **38** 1879
[112] Cordey J G, Kerner W, Pogutse O and Nassigh A 1996 *Plasma Phys. Control. Fusion* **38** 1905
[113] Berk H L, Ryutov D D and Tsidulko Yu 1990 *JETP Lett.* **52** 674
[114] Berk H L, Cohen R H, Ryutov D D, Tsidulko Yu A and Xu X Q 1993 *Nucl. Fusion* **33** 263
[115] Cohen R H and Xu X 1995 *Phys. Plasmas* **2** 3374
[116] Chankin A V 1997 *Plasma Phys. Control. Fusion* **39** 1059
[117] Chankin A V and Saibene G 1999 *Plasma Phys. Control. Fusion* **41** 913

[118] Chankin A V and Matthews G F 1998 *Contrib. Plasma Phys.* **38** 177
[119] Ohkawa T and Hinton F L 1987 *Plasma Physics and Controlled Nuclear Fusion Research (Proc. 11th Int. Conf., Kyoto, 1986)* vol 2 (Vienna: IAEA) p 221
[120] Itoh S-I and Itoh K 1990 *J. Phys. Soc. Japan* **59** 3815
[121] Itoh S-I and Itoh K 1989 *Nucl. Fusion* **29** 1031
[122] Itoh K and Itoh S-I 1992 *Nucl. Fusion* **32** 2243
[123] Itoh K, Itoh S-I and Fukuyama A 1992 *Phys. Rev. Lett.* **69** 1050
[124] Itoh K, Yagi M, Itoh S-I, Fukuyama A and Azumi M 1993 *Plasma Phys. Control. Fusion* **35** 543
[125] Yagi M, Itoh S-I, Itoh K, Fukuyama A and Azumi M 1995 *Phys. Plasmas* **2** 4140
[126] Yagi M, Itoh S-I, Itoh K and Fukuyama A 1997 *Plasma Phys. Control. Fusion* **39** 1887
[127] Itoh S-I, Itoh K, Fukuyama A, Miura Y, Yagi M and Azumi M 1994 *Plasma Phys. Control. Fusion* **36** A261
[128] Fukuyama A, Fuji Y, Itoh S-I, Yagi M and Itoh K 1996 *Plasma Phys. Control. Fusion* **38** 1319
[129] Shaing K C and Christenson P J 1993 *Phys Fluids* B **5** 666
[130] Shaing K C and Zhang Y Z 1995 *Phys. Plasmas* **2** 3243
[131] Hinton F L and Kim Y-B 1994 *Nucl. Fusion* **34** 899
[132] Miyamoto K 1996 *Nucl. Fusion* **36** 927
[133] Krasheninnikov S I and Yushmanov P M 1994 *Phys. Plasmas* **1** 1186
[134] Kim Y-B, Hinton F L, St John H, Taylor T S and Wroblewski D 1994 *Plasma Phys. Control. Fusion* **36** A189
[135] Hinton F L, Kim J, Kim Y-B, Brizard A and Burrell K H 1994 *Phys. Rev. Lett.* **72** 1216
[136] Chang C S 1999 *Combined Meeting of the Core Confinement and Internal Transport Barrier, Confinement Database and Modelling and Edge Pedestal ITER Expert Groups (Garching, Germany)* unpublished
[137] Itoh K and Itoh S-I 1995 *Plasma Phys. Control. Fusion* **37** 491
[138] Toda S, Itoh S-I, Yagi M and Miura Y 1997 *Plasma Phys. Control. Fusion* **39** 301
[139] Shaing K C and Hsu C T 1995 *Phys. Plasmas* **2** 1801
[140] Xiao H, Hazeltine R D and Valanju P M 1995 *Phys. Plasmas* **2** 1996
[141] Hassam A B and Drake J F 1993 *Phys Fluids* B **5** 4022
[142] Hassam A B and Antonsen T M Jr 1994 *Phys. Plasmas* **1** 337
[143] McCarthy D R, Drake J F, Guzdar P N and Hassam A B 1993 *Phys. Fluids* B **5** 1188
[144] Strauss H R 1995 *Phys. Plasmas* **2** 1229
[145] Rozhansky V and Tendler M 1992 *Phys Fluids* B **4** 1877
[146] Rozhansky V, Tendler M and Voskoboinikov S 1997 *Fusion Energy (Proc. 16th Int. Conf., Montreal, 1996)* vol 2 (Vienna: IAEA) p 551
[147] Rozhansky V, Tendler M and Voskoboinikov S 1996 *Plasma Phys. Control. Fusion* **38** 1327
[148] Tendler M 1997 *Plasma Phys. Control. Fusion* **39** B371
[149] Hinton F L 1991 *Phys Fluids* B **3** 696
[150] Hasegawa A and Wakatani M 1987 *Phys. Rev. Lett.* **59** 1581
[151] Yoshizawa A 1990 *Phys Fluids* B **2** 1589
[152] Carreras B A, Lynch V E and Garcia L 1991 *Phys. Fluids* B **3** 1438
[153] Hidalgo C *et al* 1999 *Phys. Rev. Lett.* **83** 2203
[154] Wilson H R and Connor J W 1997 *Controlled Fusion and Plasma Physics (Proc. 24th EPS Conf., Berchtesgaden, 1997)* vol 21A, ed M Schittenhelm, R Bartiromo and F Wagner (Geneva: European Physical Society) part 1, p 289
[155] Wilson H R, Connor J W, Field A R, Fielding S J, Hastie R J, Miller R L and Taylor J B 1999 *Fusion Energy (Proc. 17th Int. Conf., Yokohama, 1998)* CD-ROM (Vienna: IAEA) paper TH3/2; *Nucl. Fusion* to be published
[156] Keilhacker M 1997 *Plasma Phys. Control. Fusion* **39** B1
[157] Breger P, Flewin C, Zastrow K-D and Davies S J 1998 *Plasma Phys. Control. Fusion* **40** 347
[158] Parail V V, Guo H Y and Lingertat J 1999 *Nucl. Fusion* **39** 369
[159] Waltz R E, Staebler G M, Dorland W, Hammett G W, Kotschenreuther M and Konings J A 1997 *Phys. Plasmas* **4** 2482
[160] Staebler G M and Dominguez R R 1991 *Nucl. Fusion* **31** 1891
[161] Staebler G M and Dominguez R R 1993 *Nucl. Fusion* **33** 77
[162] Hinton F L and Staebler G M 1993 *Phys. Fluids* B **5** 1281
[163] Staebler G M *et al* 1994 *Phys. Plasmas* **1** 909
[164] Hinton F L, Staebler G M and Kim Y-B 1994 *Plasma Phys. Control. Fusion* **36** A273
[165] Garbet X and Waltz R E 1996 *Theory of Fusion Plasmas* ed J W Connor, E Sindoni and J Vaclavik (Bologna: Editrice Compositori) p 171
[166] Vojtsekhovich L A, Dnestrovskij A Yu and Parail V V 1995 *Nucl. Fusion* **35** 631

[167] Diamond P H, Liang Y-M, Carreras B A and Terry P W 1994 *Phys. Rev. Lett.* **72** 2565
[168] Diamond P H *et al* 1996 *Plasma Physics and Controlled Nuclear Fusion Research (Proc. 15th Int. Conf., Seville, 1994)* vol 3 (Vienna: IAEA) p 323
[169] Carreras B A, Diamond P H, Liang Y-M, Lebedev V and Newman D 1994 *Plasma Phys. Control. Fusion* **36** A93
[170] Carreras B A, Newman D, Diamond P H and Liang Y-M 1994 *Phys. Plasmas* **1** 4014
[171] Newman D E, Carreras B A and Diamond P H 1995 *Phys. Plasmas* **2** 3044
[172] Diamond P H, Lebedev V B, Newman D E and Carreras B A 1995 *Phys. Plasmas* **2** 3685
[173] Carreras B A, Diamond P H and Vetoulix G 1996 *Phys. Plasmas* **3** 4106
[174] Lebedev V B, Diamond P H, Carreras B A and Newman D E 1997 *US-EU Transport Task Force Workshop (Madison, USA)* unpublished
[175] Carreras B A, Lynch V E, Garcia L and Diamond P H 1995 *Phys. Plasmas* **2** 2744
[176] Lebedev V B, Yushmanov P, Diamond P H, Novakovskii S V and Smolyakov A I 1996 *Phys. Plasmas* **3** 3023
[177] Sugama H and Horton W 1995 *Plasma Phys. Control. Fusion* **37** 345
[178] Horton W, Hu G and Laval G 1996 *Phys. Plasmas* **3** 2912
[179] Ossipenko M V 1997 *Plasma Phys. Rep.* **23** 837
[180] Dnestrovskij Yu N, Ossipenko M V and Tsaun S V 1997 *Proc. Combined ITER Expert Groups Workshop on Confinement and Transport and Confinement Databases and Modelling (Garching, Germany)* unpublished
[181] Ohkawa T, Chu M S, Hinton F L, Liu C S and Lee Y C 1983 *Phys. Rev. Lett.* **51** 2101
[182] Saito S, Kobayashi T, Sugihara M, Hirayama T and Fujisawa N 1985 *Nucl. Fusion* **25** 828
[183] Rebut P H, Watkins M L and Lallia P P 1988 *Plasma Phys. Control. Fusion (Proc. 15th EPS, Dubrovnick, 1988)* vol 12B, ed S Pesic and J Jacquinot (Geneva: European Physics Society) part 1, p 247
[184] Hinton F L and Chu M S 1985 *Nucl. Fusion* **25** 345
[185] Tang W and Hinton F L 1988 *Nucl. Fusion* **28** 443
[186] Hinton F L and Staebler G M 1989 *Nucl. Fusion* **29** 405
[187] Carlstrom T N, Burrell K H and Groebner R J 1998 *Plasma Phys. Control. Fusion* **40** 669
[188] LoDestro L L *et al* 1998 *Fusion Energy (Proc. 17th Int. Conf., Yokohama, 1998)* CD-ROM (Vienna: IAEA) paper THP2/04
[189] Rogister A L 1997 *Fusion Energy (Proc. 16th Int. Conf., Montreal, 1996)* vol 2 (Vienna: IAEA) p 573
[190] Rogister A L 1998 *Plasma Phys. Control. Fusion* **40** 817
[191] Rogister A L 1998 *Phys. Rev. Lett.* **81** 3663
[192] Rogister A L 1999 *Phys. Plasmas* **6** 200
[193] Rogister A L 1994 *Phys. Plasmas* **1** 619
[194] Helander P 1998 *Phys. Plasmas* **5** 3999
[195] Leonov V M 1994 *Plasma Phys. Rep.* **20** 341
[196] Dnestrovskij Yu N, Lysenko S E and Tarasyan K N 1995 *Nucl. Fusion* **35** 1047
[197] Minardi E 1996 *EU–US Workshop on Transport in Fusion Plasmas (Varenna, Italy)* unpublished
[198] Ward D J 1996 *Plasma Phys. Control. Fusion* **38** 1201
[199] Ossipenko M V 1995 *ITER Expert Group Workshop on Confinement and Transport (San Diego, USA)* unpublished
[200] Burrell K H 1997 *Phys. Plasmas* **4** 1499
[201] Staebler G M 1998 *Plasma Phys. Control. Fusion* **40** 569
[202] Hirsch M, Amadeo P, Anton M and Baldzuhm J 1998 *Plasma Phys. Control. Fusion* **40** 631
[203] Owen L W, Carreras B A, Maingi R, Mioduszewski P K, Carlstrom T N and Groebner R J 1998 *Plasma Phys. Control. Fusion* **40** 717
[204] Ryter F *et al* 1998 *Fusion Energy (Proc. 17th Int. Conf., Yokohama, 1998)* CD-ROM (Vienna: IAEA) paper EXP2/03
[205] Groebner R J, Allen S L, Baker D R and Brooks N H 1994 *Plasma Phys. Control. Fusion* **36** A13
[206] Mori M, JT-60 Team and JFT-2M Team 1994 *Plasma Phys. Control. Fusion* **36** A39
[207] Hawkes N C and Thomas P J 1993 *Controlled Fusion and Plasma Physics (Proc. 20th EPS Conf., Lisbon, 1993)* vol 17C, ed J Costa *et al* (Geneva: European Physical Society) part 1, p 7
[208] Groebner R J, Carlstrom T N, Burrell K H and Coda S 1997 *Fusion Energy (Proc. 16th Int. Conf., Montreal)* vol 1 (Vienna: IAEA) p 867
[209] Bush C E, Bretz N, Budny R and Synakowski E J 1994 *Plasma Phys. Control. Fusion* **36** A153
[210] Carreras B A 1999 Private communication
[211] Zohm H *et al* 1994 *Plasma Phys. Control. Fusion* **36** A129
[212] Itoh S-I 1990 *J. Phys. Soc. Japan* **59** 3431
[213] Romanelli F 1997 Private communication

[214] Ida K, Miura Y, Itoh K, Itoh S-I, Fukuyama A and JFT-2M 1994 *Plasma Phys. Control. Fusion* **36** A279
[215] Osborne T H *et al* 1998 *Plasma Phys. Control. Fusion* **40** 845
[216] Lingertat J, Bhatnagar V, Conway G D and Eriksson L-G 1999 *J. Nucl. Mater.* **266–269** 124
[217] Burrell K H *et al* 1994 *Phys. Plasmas* **1** 1536
[218] Hawkes N C *et al* 1996 *Plasma Phys. Control. Fusion* **38** 1261
[219] Miura Y *et al* 1994 *Plasma Phys. Control. Fusion* **36** A81
[220] Herrmann W, Heikkinen J A, Kurki-Suonio T and the ASDEX Upgrade Team 1998 *Plasma Phys. Control. Fusion* **40** 683
[221] Herrmann W and the ASDEX Upgrade Team 1998 *Rev. Sci. Instrum.* **69** 3165
[222] Hamada Y, Ido T, Kamiya K, Nishizawa A and Kawasumi Y 1999 *Fusion Energy (Proc. 17th Int. Conf., Yokohama, 1998)* CD-ROM (Vienna: IAEA) paper EXP2/14
[223] Carolan P G, O'Connell R, Conway N J, Bamford R A, Hugill J and Melnich I M 1995 *Controlled Fusion and Plasma Physics (Proc. 22nd EPS Conf., Bournemouth, 1995)* vol 19C, ed B E Keen, P E Stott and J Winter (Geneva: European Physical Society) part 2, p 133
[224] O'Connell R 1996 Impurity fluid investigations on the COMPASS-D tokamak *PhD Thesis* University College of Dublin
[225] Carolan P G *et al* 1998 *Bulletin of American Physical Society (Programme of 40th Annual Meeting of Division of Plasma Physics, New Orleans, November 1998)* vol 43 (Woodbury, NY: AIP) p 1867
[226] Taylor R J, Brown M L, Fried B D, Grote H, Liberati J R, Morales G J and Pribyl P 1989 *Phys. Rev. Lett.* **63** 2365
[227] Weynants R R, Jachmich S and Van Oost G 1998 *Plasma Phys. Control. Fusion* **40** 635
[228] Cornelis J, Sporken R, Van Oost G and Weynants R R 1998 *Nucl. Fusion* **34** 171
[229] Itoh K, Itoh S-I, Yagi M and Fukuyama A 1998 *Phys. Plasmas* **5** 4121
[230] Stambaugh R 1999 *Combined Meeting of the Core Confinement and Internal Transport Barrier, Confinement Database and Modelling and Edge Pedestal ITER Expert Groups (Garching, Germany)* unpublished